PDEδ interference impedes the proliferation and survival of oncogenic KRas expressing human cancer cell lines

Dissertation

zur Erlangung des akademischen Grades eines Doktors der Naturwissenschaften der Fakultät für Chemie und Chemische Biologie der Technischen Universität Dortmund

vorgelegt von

Christian H. Klein

geboren in Hamm

Dezember, 2018

The work presented in this thesis was performed under the supervision of Prof. Dr. Philippe I. H. Bastiaens in his department of Systemic Cell Biology at the Max Planck Institute of Molecular Physiology in Dortmund, Germany, in the time from December 2014 to December 2018.

1st Examiner:

Prof. Dr. Philippe I. H. Bastiaens

Department of Systemic Cell Biology
Max Planck Institute of Molecular Physiology, Dortmund;
Faculty of Chemistry and Chemical Biology, TU Dortmund

2nd Examiner:

PD. Dr. Leif Dehmelt

Department of Systemic Cell Biology
Max Planck Institute of Molecular Physiology, Dortmund;
Faculty of Chemistry and Chemical Biology, TU Dortmund

Eidesstattliche Versicherung (Affidavit)

Name, Vorname
(Surname, first name)

Matrikel-Nr.
(Enrolment number)

Belehrung:

Wer vorsätzlich gegen eine die Täuschung über Prüfungsleistungen betreffende Regelung einer Hochschulprüfungsordnung verstößt, handelt ordnungswidrig. Die Ordnungswidrigkeit kann mit einer Geldbuße von bis zu 50.000,00 € geahndet werden. Zuständige Verwaltungsbehörde für die Verfolgung und Ahndung von Ordnungswidrigkeiten ist der Kanzler/die Kanzlerin der Technischen Universität Dortmund. Im Falle eines mehrfachen oder sonstigen schwerwiegenden Täuschungsversuches kann der Prüfling zudem exmatrikuliert werden, § 63 Abs. 5 Hochschulgesetz NRW.

Die Abgabe einer falschen Versicherung an Eides statt ist strafbar.

Wer vorsätzlich eine falsche Versicherung an Eides statt abgibt, kann mit einer Freiheitsstrafe bis zu drei Jahren oder mit Geldstrafe bestraft werden, § 156 StGB. Die fahrlässige Abgabe einer falschen Versicherung an Eides statt kann mit einer Freiheitsstrafe bis zu einem Jahr oder Geldstrafe bestraft werden, § 161 StGB.

Die oben stehende Belehrung habe ich zur Kenntnis genommen:

Official notification:

Any person who intentionally breaches any regulation of university examination regulations relating to deception in examination performance is acting improperly. This offence can be punished with a fine of up to EUR 50,000.00. The competent administrative authority for the pursuit and prosecution of offences of this type is the chancellor of the TU Dortmund University. In the case of multiple or other serious attempts at deception, the candidate can also be unenrolled, Section 63, paragraph 5 of the Universities Act of North Rhine-Westphalia.

The submission of a false affidavit is punishable.

Any person who intentionally submits a false affidavit can be punished with a prison sentence of up to three years or a fine, Section 156 of the Criminal Code. The negligent submission of a false affidavit can be punished with a prison sentence of up to one year or a fine, Section 161 of the Criminal Code.

I have taken note of the above official notification.

Ort, Datum
(Place, date)

Unterschrift
(Signature)

Titel der Dissertation:
(Title of the thesis):

Ich versichere hiermit an Eides statt, dass ich die vorliegende Dissertation mit dem Titel selbstständig und ohne unzulässige fremde Hilfe angefertigt habe. Ich habe keine anderen als die angegebenen Quellen und Hilfsmittel benutzt sowie wörtliche und sinngemäße Zitate kenntlich gemacht.
Die Arbeit hat in gegenwärtiger oder in einer anderen Fassung weder der TU Dortmund noch einer anderen Hochschule im Zusammenhang mit einer staatlichen oder akademischen Prüfung vorgelegen.

I hereby swear that I have completed the present dissertation independently and without inadmissible external support. I have not used any sources or tools other than those indicated and have identified literal and analogous quotations.

The thesis in its current version or another version has not been presented to the TU Dortmund University or another university in connection with a state or academic examination.*

*Please be aware that solely the German version of the affidavit ("Eidesstattliche Versicherung") for the PhD thesis is the official and legally binding version.

Ort, Datum
(Place, date)

Unterschrift
(Signature)

II Abstract

Ras proteins, most notably isoform KRas4B are frequently mutated oncogenes in numerous human cancers and associated with poor prognosis. Despite ambitious research affords since the discovery of Ras proteins as human oncogenes in 1982, no pharmacological therapy approach reached the clinic yet and Ras is still viewed as “undruggable” protein. For signal propagation, Ras proteins have to be localized at the plasma membrane. Enrichment there is facilitated by spatial cycles that utilize the prenyl binding protein PDEδ as solubilizing factor. Thus, instead of targeting Ras proteins directly, interference with its spatial organization by targeting PDEδ was studied as promising alternative. First generations of small molecule inhibitors of PDEδ were reported to selectively affect proliferation of oncogenic KRas-dependent human pancreatic ductal adenocarcinoma cell lines.

Here, we characterize the activity of a new small molecule inhibitor chemotype called Deltasonamide in cells. We show that Deltasonamide administration leads to a depletion of KRas from the plasma membrane and report enhanced anti-proliferative effects of the high affinity inhibitor in oncogenic KRas-dependent human pancreatic ductal adenocarcinoma cell lines, for the first time at sub-micromolar concentrations.

Furthermore, we demonstrate that PDEδ inhibition is also an applicable tool to interfere with aberrant KRas signaling in human colorectal cancer cell lines. Both PDEδ knock down and small molecule inhibition selectively reduced proliferation and viability of colorectal cancer cell lines harboring oncogenic KRas mutations, whereas cell lines expressing only wild type KRas were not affected by interference with PDEδ. Moreover, we report an interdependence of oncogenic KRas activity and PDEδ’s solubilizing function that is manifested in the correlation of both proteins within the cell lines and well reflected in the distinct survivability after PDEδ interference.

Together, our results show that PDEδ is a valid therapeutic target in both pancreatic ductal adenocarcinoma and colorectal cancer harboring oncogenic KRas mutations.

III Zusammenfassung

Ras Proteine, vor allem Isoform KRas4B, sind häufig mutierte Onkogene in vielen menschlichen Krebserkrankungen und werden mit schlechten Überlebenschancen assoziiert. Trotz ambitionierter Forschungsbestrebungen seit der Entdeckung von Ras Proteinen als menschliche Onkogene im Jahr 1982 gibt es bisher keine klinisch zugelassenen Therapeutika und Ras Proteine werden immer noch als „undruggable“ angesehen. Für die Weiterleitung von Signalen müssen Ras Proteine an der Plasmamembran lokalisiert sein. Die dortige Anreicherung wird durch räumliche Zyklen ermöglicht, die auf der Nutzung des Prenyl-bindenden Proteins PDEδ als Löslichkeitsfaktor basieren. Deshalb wurde anstelle Ras direkt zu attackieren das Interferieren mit der räumlichen Organisation von Ras durch attackieren von PDEδ als mögliche Alternative untersucht. Erste Genrationen von PDEδ Inhibitoren verringerten selektiv das Wachstum von onkogenen KRas abhängigen menschlichen pankreatischen Adenokarzinoma Zelllinien.

Hier charakterisieren wir die Aktivität von einem neuen Inhibitor basierend auf einem neuen Chemotyp, genannt Deltasonamide, in Zellen. Wir zeigen, dass die Administration von Deltasonamide zu einer Delokalisierung von KRas von der Plasmamembran führt. Außerdem demonstrieren wir verbesserte wachstums-verringernde Effekte in von onkogenem KRas abhängigen menschlichen pankreatischen Adenokarzinoma Zelllinien, zum ersten Mal unterhalb mikromolarer Konzentrationen.

Weiterhin demonstrieren wir, dass die Inhibierung von PDEδ auch angewandt werden kann, um krankhafte KRas Aktivität in menschlichen Darmkrebs Zelllinien zu unterbinden. Sowohl „knock down“ als auch pharmakologische Inhibierung von PDEδ reduzierten selektiv das Wachstum und die Vitalität von Darmkrebs Zelllinien, die onkogenes KRas exprimieren, wohingegen Zelllinien die nur normales KRas exprimieren nicht durch die Interferenz mit PDEδ beeinträchtigt wurden. Darüber hinaus berichten wir eine Interdependenz zwischen der Aktivität von onkogenem KRas und der Löslichkeits-Funktion von PDEδ, die sich in der Korrelation der

Expressions-Level beider Proteine manifestiert und sich in der unterschiedlichen Vitalität nach PDEδ Interferenz wiederspiegelt.

Zusammengenommen zeigen unsere Resultate, dass PDEδ ein valides therapeutisches Ziel sowohl in pankreatischen Adenokarzinoma Zelllinien als auch in Darmkrebs Zelllinien, die onkogenes KRas exprimieren, darstellt.

Table of Content

1. Abbreviations

%	percent
°C	degree Celsius
µg	microgram
µl	microliter
µM	micromolar
7-AAD	7-aminoactinomycin D
ANOVA	analysis of variance
APC	adenomatous polyposis coli
APT1	acyl protein thioesterase 1
Arl2	ADP ribosylation factor-like protein 2
Arl2	Arf-like protein 2
ATCC	American Type Culture Collection
BCA	bicinchoninic acid
BRaf	serine/threonine-protein kinase
BSA	bovine serum albumin
CIAP	calf intestinal alkaline phosphatase
cm	centimeter
CO_2	carbon-dioxide
CRC	colorectal cancer
CT	cycling time
Cyp B	Cyclophilin B
DMEM	Dulbecco's Modified Eagle's Medium
DMSO	dimethyl-sulfoxide
DNA	deoxyribonucleic acid
dNTP	deoxy nucleoside triphosphate
dox	doxycycline
DR	Deltarasin
DS2	Deltasonamide 2
E. *coli*	Escherichia *coli*
EC_{50}	half maximal effective concentration
EDTA	ethylenediaminetetraacetic acid
EGF	epidermal growth factor
EGFR	epidermal growth factor receptor
ER	Endoplasmic reticulum
Erk	extracellular regulated kinase
FACS	fluorescent activated cell sorting
FCS	fatal calf serum
FLIM	fluorescence lifetime imaging microscopy
FRET	Förster resonance energy transfer
FTI	farnesyl transferase inhibitor

g	gravitation constant
GAP	GTPase activating proteins
GAPDH	glyceraldehyde 3-phosphate dehydrogenase
GDP	guanosine di-phosphate
GEF	guanosine nucleotide exchange factor
GST	glutathione S-transferase
GTP	guanosine tri-phosphate
h	hour
H-bond	hydrogen bond
hPDAC	human pancreatic ductal adenocarcinoma
HRas	Harvey rat sarcoma
HVR	hyper variable region
ICMT	isoprenylcysteine carboxylmethyl-transferase
IPTG	isopropyl β-D-1-thiogalactopyranoside
K_D	dissociation constant
k_{off}	off-rate
KRas	Kirsten rat sarcoma
MAPK	mitogen activated protein kinase
MDCK	Madin-Darby canine kidney
min	minute
ml	milliliter
mM	millimolar
mRNA	messenger ribonucleic acid
mTOR	mammalian target of rapamycin
NEAA	non-essential amino acids
ng	nanogram
nM	nanomolar
NRas	Neuroblastoma rat sarcoma
PAT	palmitoyl acyl transferases
PBS	phosphate buffered saline
PCR	polymerase chain reaction
PDAC	pancreatic ductal adenocarcinoma
PDE6D	gene encoding PDEδ
PDEδ	subunit delta of phosphodiesterase 6
pErk	phosphor-Erk
PFA	paraformaldehyde
PI3K	phosphatidylinositol-3-kinases
PIP3	3-phosphatidylinositol 3,4,5 triphosphate
pM	pico-molar

PM	plasma membrane
PVDF	polyvinylidene fluoride
Raf	rapidly accelerated fibrosacroma
Ras	rat sarcoma
RBD	Ras-binding domain
RCE1	Ras converting enzyme 1
RE	recycling endosome
Rheb	Ras homologous enriched in brain
RNA	ribonucleic acid
ROI	region of interest
rpm	rounds per minute
RT	room temperature
RTCA	real-time cell analysis
RTK	receptor tyrosine kniase
RT-qPCR	real-time quantitative PCR
s	seconds
s.d.	standard deviation
s.e.m.	standard error of the mean
scr	scrambled
SDS	sodium dodecyl sulfate
shRNA	short hairpin ribonucleic acid
SOC	super optimal broth
SOS	son of sevenless
STR	short-tandem repeats
TB	terrific broth
TBS	tris buffered saline
TBS-T	tris buffered saline with 0.1 % Tween-20
TCGA	The Cancer Genome Atlas
tErk	total-Erk
V	volt
WCL	whole cell lysate
wt	wild type
α	molar interacting fraction alpha

2. Introduction

2.1 Characteristics of cancer

In multicellular organisms, tissue homeostasis is maintained by cells communicating with each other. Thereby, critical processes like proliferation, differentiation and survival are strictly regulated. One hallmark of cancer is uncontrolled proliferation, independent from contact inhibition or other mechanisms that normally attenuate proliferation (Hanahan and Weinberg 2011). However, the replication capability of cells is not infinite but rather limited by telomere shortening, exempt in stem cells that express low levels of telomerase. It is therefore likely that only accumulated mutations in stem cells result in cancer, whereas oncogenic mutations in somatic cell are neglectable due to their limited proliferation capacity (Gunes and Rudolph 2013). Moreover, a recent study demonstrated that most mutations are randomly acquired before the cancer initiating mutation rather than a consequence of genomic instability after cancer initiation (Welch et al. 2012). This initiating mutation can either be a gain-of-function mutation of a gene involved in proliferation or survival (oncogene) or a loss-of-function mutation of a gene involved in DNA damage response or apoptosis regulation (tumor suppressor) (Weinberg 1994). Further acquired mutations lead to heterogenic subpopulations within the tumor, forming their own microenvironment that also affects surrounding stroma cells (Feig et al. 2012).

Together, this emphasizes that the progression of cancer is characterized by the accumulation of many mutations and not alone based on one driver oncogene. However, an initiating oncogenic mutation or a loss-of-function mutation of a tumor suppressor gene are the originators of cancer. The most frequent oncogenes in human cancers are Ras proteins, which are mutated in approximately 30 % of all tumors (Forbes et al. 2011).

2.2 Ras family of small GTPases

The Ras superfamily of small GTPases describes a protein class consisting of more than 150 proteins that all share a catalytic G domain. The Ras superfamily can be

divided in several subfamilies, among them the subfamilies of Ras, Rho, Rab and Arf small GTPases (Wennerberg et al. 2005).

The most notable members of the Ras subfamily are four ubiquitously expressed proteins that are encoded by three distinct genes and that exhibit a high homology. While the HRAS and NRAS gene only encode for one protein, the KRAS gene can be spliced into two distinct variants that differ in exon 4 and result in either KRas4A or KRas4B (Capon et al. 1983). Since splice variant KRas4B is more abundant, the term KRas mostly refers to this isoform. All four isoforms share the G domain that is common for all small GTPases and show overall a high sequence identity of around 80 % (Wennerberg et al. 2005). However, the last 24 amino acids at the C-terminus only exhibit 8 % homology, wherefore it is called hyper-variable region (HVR).

2.3 Posttranslational modifications of Ras proteins

All Ras isoforms share a C-terminal CAAX-motif in the HVR, whereas C is a cysteine, A must be an aliphatic amino acid and X can be any amino acid. The CAAX-motif results in a sequence of three consecutive posttranslational modifications of the Ras proteins. First, the cysteine residue is irreversibly farnesylated, catalyzed by the cytosolic enzyme farnesyl transferase. This farnesylation increases membrane affinity due to hydrophobic interactions and enables localization to the endoplasmic reticulum (ER). There, the three terminal amino acids AAX are removed by the Ras-converting enzyme RCE1. Subsequently, the enzyme isoprenylcysteine carboxylmethyl-transferase (ICMT) catalyzes the methylation of the now terminal farnesylated cysteine residue (Wright and Philips 2006).

Depending on the Ras isoform, additional posttranslational modifications take place to further increase membrane affinity (Figure 1). Both NRas and KRas4A contain one additional cysteine residue in their HVR that can be reversibly S-palmitoylated at the Golgi apparatus. The isoform HRas exhibits even two additional cysteine residues that can be palmitoylated. In contrast, KRas4B lacks further cysteine residues and is not additionally modified. Instead, the HVR contains a so-called polybasic stretch

consisting of six consecutive lysine residues (Hancock et al. 1989, Hancock et al. 1990). Under physiological pH, lysine residues are positively charged, thereby enhancing affinity to membranes that exhibit a high density of negatively charged lipids. Such lipid compartments are the inner leaflet of the plasma membrane (PM) and the recycling endosome (RE) (Schmick et al. 2014).

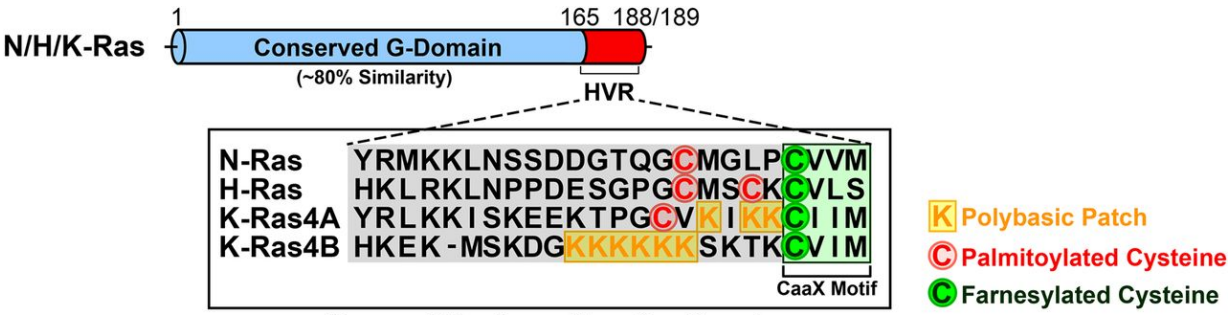

Figure 1: Ras isoforms and corresponding post translational modifications. All Ras isoforms comprise a highly conserved G domain (80 % sequence identity) and a C-terminal hypervariable region with low homology. All isoforms traverse a triad of irreversible posttranslational modifications at the C-terminal CAAX motif. KRas4B contains an additional polybasic patch of six consecutive lysine residues (yellow). The other three isoforms can be reversible S-palmitoylated at the cysteine residues depicted in red (Adapted from Lin et al. 2017).

2.4 Ras activity cycle

All Ras isoforms share a G domain that catalyzes the hydrolysis of guanosine tri-phosphate (GTP) to guanosine di-phosphate (GDP). Ras proteins can cycle between an active and an inactive conformation, which is dependent on the nucleotide bound. If Ras is GTP-bound, it engages the active conformation whereas Ras is inactive when GDP is bound. Both nucleotides are bound with a similar affinity (Vetter and Wittinghofer 2001). However, due to the 10-fold excess of GTP in the cell, GTP binding is favored (Traut 1994). This is further potentiated by the low intrinsic GTPase activity.

In the active, GTP bound conformation, Ras can interact with Ras binding domains (RBD) of effectors. This interaction cannot be formed when Ras is in its inactive, GDP bound conformation. The conformational changes in the G domain are most

pronounced in the so-called switch regions, “switch I” and “switch II”, by formation of hydrogen bonds to the γ-phosphate of GTP. This results in an ordered structure of these otherwise unstructured regions, enabling effector binding. In contrast, no hydrogen bonds can be formed if GDP is bound, rendering the switch regions flexible and unable to bind effector domains (Vetter and Wittinghofer 2001). Because of the constant cycling between an “on” and an “off” state, Ras proteins are thought of as binary switches within the cell. However, both the intrinsic hydrolysis rate as well as the GDP-GTP exchange rate are too slow to enable the actual rapid switching between both states. To overcome these limitations, Ras regulatory proteins, called GTPase activating proteins (GAPs) and guanine nucleotide exchange factors (GEFs) catalyze the respective processes (Figure 2).

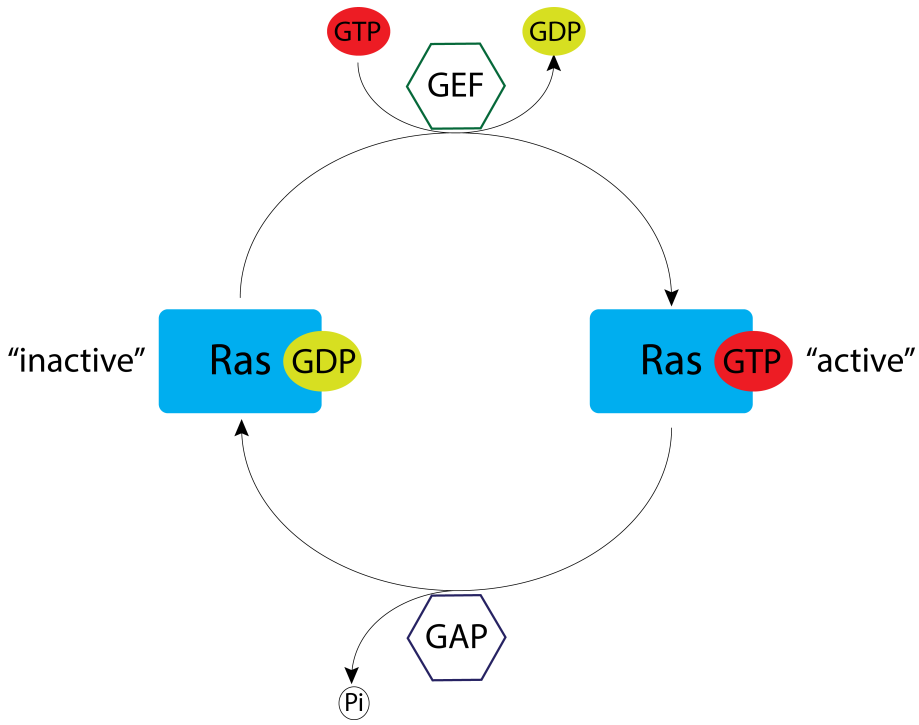

Figure 2: GTPase cycle of Ras. Small GTPases of the Ras family can cycle between a GDP-bound, inactive and a GTP-bound, active state. The intrinsic hydrolysis from GTP to GDP is catalyzed by GTPase activating proteins (GAPs). The exchange from GDP to GTP is facilitated by guanine nucleotide exchange factors (GEFs).

2.4.1 Ras activity regulating proteins

The intrinsic GDP-GTP exchange rate is slow due to the nanomolar affinity with which GDP is bound, resulting in slow dissociation (John et al. 1990). Guanine nucleotide exchange factors enhance dissociation of GDP from the G domain by a three-step process. First, the GEF binds to the GDP-bound protein resulting in an unstable trimer. In this complex, GDP dissociation is facilitated by a conformational change of the G domain. The now empty nucleotide binding site will bind GTP due to the 10-fold excess over GDP within cells. GTP binding in turn promotes the release of the GEF, resulting in active, GTP-bound Ras that can interact with effectors (Bos et al. 2007).

As stated above, the intrinsic hydrolysis rate of small GTPases is too slow to enable rapid transition from the active to the inactive state. However, the effective hydrolysis rate is 100,000-fold increased by interaction with GTPase activating proteins (Gideon et al. 1992). This is possible through an arginine-finger motif of the GAPs that stabilizes a glutamine residue in the “switch II” region that is necessary to coordinate a water molecule needed for the nucleophilic attack to hydrolyze GTP (Bos et al. 2007).

While the interplay of GEFs and GAPs enable rapid cycling between the two nucleotide bound states of Ras proteins, the activities of the regulatory proteins themselves have to be controlled. This will be illustrated below by means of the Ras-GEF Sos (son of sevenless).

2.5 Ras signaling

Ras proteins are involved in many cellular signaling processes, among them proliferative and survival signaling (Figure 3). Usually, Ras proteins can be activated by extracellular signals that are integrated by transmembrane receptors, for example receptor tyrosine kinases (RTK) (Lemmon and Schlessinger 2010). One well-studied RTK is the epidermal growth factor receptor (EGFR). Binding of a ligand, here EGF, to the extracellular domain of EGFR leads to receptor dimerization and in turn to autophosphorylation of tyrosine residues at the intracellular domain (Yarden and

Schlessinger 1987). Activated receptor dimers can recruit adaptor proteins like Grb2 by SH2-domain binding to the phosphorylated tyrosine residue (Batzer et al. 1994), which can in turn recruit the Ras-GEF Sos (Bowtell et al. 1992). This leads to increased concentration of GEF at the plasma membrane, resulting in enhanced ratio of GDP to GTP exchange of Ras and thereby increased Ras activity (Iversen et al. 2014). Moreover, Ras proteins can also be activated by other proteins for example members of Src family kinases (van der Geer et al. 1996).

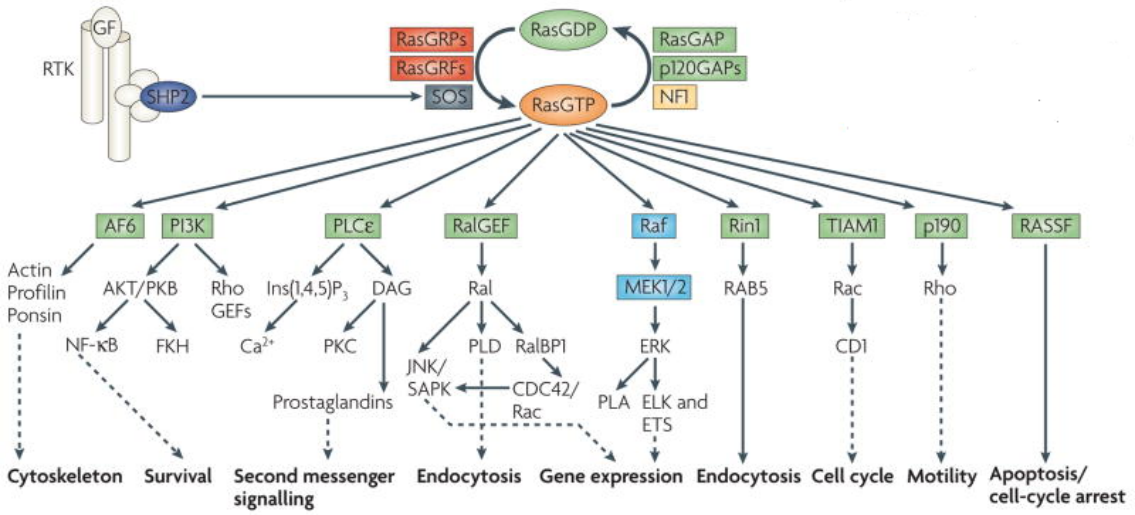

Figure 3: Ras signaling networks. Receptor tyrosine kinases can activate Ras by recruiting Ras-GEFs to the plasma membrane. Active, GTP-bound Ras can interact with the Ras binding domain of numerous downstream effectors, resulting in the initiation of diverse cellular processes. Only key notes of each signaling network are shown (Adapted from Karnoub and Weinberg 2008).

The most extensively studied signaling network Ras proteins are engaged in is the mitogen activated protein kinase (MAPK) cascade (Seger and Krebs 1995). Here, active Ras leads to a recruitment of Raf proteins (MAPKKK) to the plasma membrane, which interact with GTP-bound Ras proteins with their Ras-binding domain. Instead of activating Raf directly, the recruitment equals a dimension reduction from a 3D volume to a 2D surface, whereby probability of dimerization of Raf molecules is dramatically enhanced. Moreover, the Raf-Ras heterodimers possess reduced diffusion speed compared to Raf monomers (Kholodenko et al. 2000). Dimerized Raf proteins are activated by trans-phosphorylation and can then

phosphorylate and thereby activate the MAP kinase kinase Mek (MAPKK). Active Mek in turn can phosphorylate and activate the extracellular regulated kinase (Erk; MAPK), which either interacts with cytosolic effectors or translocates into the nucleus where it can induce gene expression by activation of transcription factors (Canagarajah et al. 1997, Khokhlatchev et al. 1998).

Besides the MAK signaling network, Ras proteins are involved in a multitude of other signaling networks (Figure 3). Active Ras can for example interact with phosphatidylinositol-3-kinases (PI3K), which then recruits and activates Akt by generating increased levels of 3-phosphatidylinositol 3,4,5 triphosphate (PIP3). Finally, this results in the activation of the mammalian target of rapamycin (mTOR), which is involved in metabolism as well as survival signaling (Mendoza et al. 2011).

2.6 Spatial organization

For proper signaling, Ras proteins have to be localized at the plasma membrane, because their activators and effectors are either located or recruited there. PM localization is facilitated by an irreversible farnesylation that is present in all isoforms and an additional secondary membrane localization motif, either S-palmitoylation or a polybasic stretch (Hancock et al. 1990). However, PM enrichment is countered by entropy driven redistribution to the much larger endomembrane surface as well as constant endocytosis (Schmick et al. 2014, Schmick et al. 2015). Furthermore, palmitoylated Ras isoforms are constantly de-palmitoylated by acyl protein thioesterase 1 (APT1), decreasing their affinity to membranes. To counteract this depletion and maintain PM enrichment, spatial cycles that transport Ras molecules to the PM by an energy-driven process are executed (Figure 4).

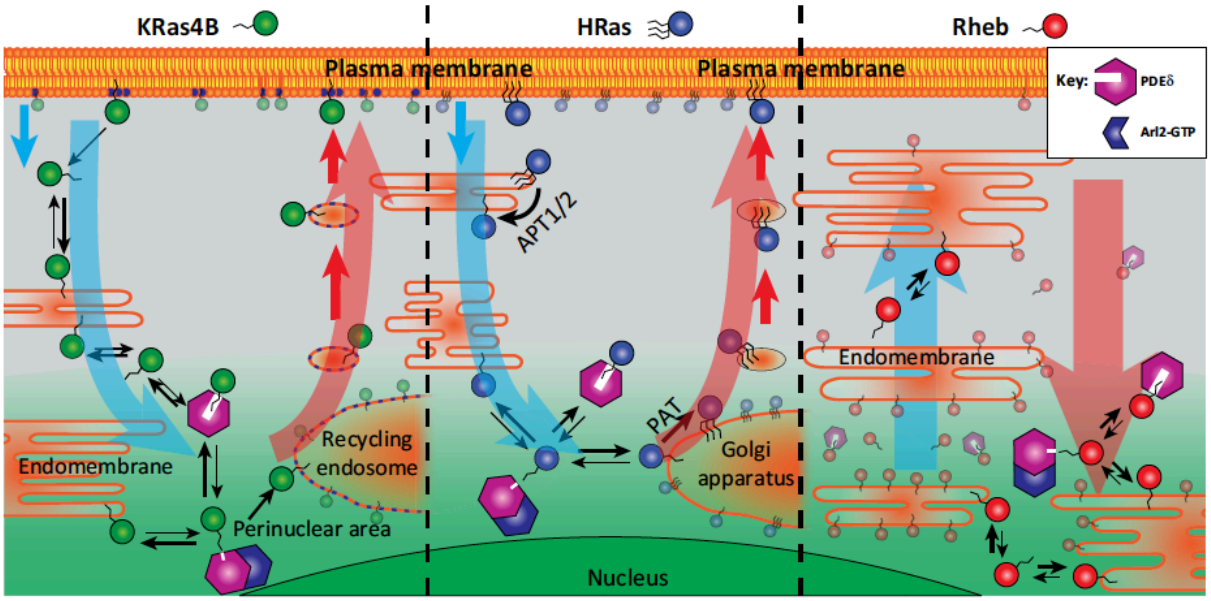

Figure 4: Spatial cycle of distinct Ras proteins mediated by PDEδ and Arl2. Both KRas4B and HRas are depleted from the plasma membrane (PM) by entropic redistribution to the abundant endomembrane surface as well as endocytosis. PDEδ sequesters un-palmitoylated Ras proteins from endomembranes and enhances their diffusion speed within the cytosol. After Arl2-GTP mediated local release in the perinuclear area, KRas4B is enriched at the recycling endosome and HRas at the Golgi apparatus, respectively. Both proteins are then transported back to the PM by directed vesicular transport from their respective trapping compartment. The small GTPase Rheb (Ras homologous enriched in brain) contains no secondary localization motif and is consequently not enriched at the PM (Adapted from Schmick et al. 2015)

The C-terminal farnesylation of Ras proteins increases their affinity to membranes and decreases the diffusion speed within the cytoplasm. Hence, an additional factor is necessary to both enhance diffusion speed and shield the farnesyl-tail to prevent membrane association. This function is executed by the guanine nucleotide dissociation inhibitor (GDI-) like solubilization factor PDEδ (Chandra et al. 2011, Schmick et al. 2014). PDEδ, named after its discovery as delta-subunit of the phosphodiesterase 6, is an ubiquitous expressed protein that exhibits a hydrophobic binding pocket, which can bind farnesylated cargo (Nancy et al. 2002). For KRas4B, depletion from the PM during endocytosis is more crucial compared to other Ras isoforms due to the lost negatively charged lipids during this process. Therefore, the

off-rate of KRas4B from the PM is higher. This implies that the solubilizing functionality of PDEδ is more important for KRas4B than for other Ras isoforms.

However, the solubilizing factor PDEδ alone is still not sufficient to maintain PM enrichment of Ras proteins. Plasma membrane enrichment is facilitated through localized release of Ras molecules by the small GTPase Arl2 (Arf-like protein 2). Arl2 can bind to loaded PDEδ at an allosteric binding site in a GTP-dependent manner. This interaction leads to a conformational change, resulting in cargo release from PDEδ (Hanzal-Bayer et al. 2002, Ismail et al. 2011). Since Arl2 is active in the perinuclear region of the cell, Ras proteins are also enriched there and start to repopulate the different endomembrane compartments (Schmick et al. 2014). For Ras isoforms that can be S-palmitoylated, the Golgi apparatus, where palmitoyl acyl transferases (PAT) are located, serves as kinetical trap, since the membrane affinity is considerably enhanced by the palmitoylation. From the Golgi apparatus, HRas, NRas and KRas4A are transported to the PM via directed vesicular transport (Rocks et al. 2005, Lorentzen et al. 2010).

Since KRas4B is not palmitoylated it cannot be trapped at the Golgi apparatus. However, an analogous mechanism that creates a localized pool of KRas4B molecules that can be directed back to the PM is necessary to maintain the enrichment there. In contrast to palmitoylated isoforms, KRas4B exhibits a polybasic stretch in its hypervariable region. Therefore, KRas4B is enriched at the recycling endosome, an endomembrane compartment that exhibits a high density of negatively charged lipids. From there, KRas is transported back to the PM by directional vesicular transport (Schmick et al. 2014).

2.7 Aberrant Ras signaling in cancer

Signals emanating from active Ras are essential for cells but aberrant signaling can have severe consequences. One single point mutation is sufficient to retain Ras proteins in a GTP-bound conformation resulting in constitutive signaling independent of extracellular signaling input. Most common sites of mutations are the glycine

residues in position 12 and 13 that are located in the P-loop or the glutamine at position 61 (located in the “switch II” region). Further, GAP activity can no longer catalyze hydrolysis in order to convert the active into the inactive state (Wittinghofer 1998, Prior et al. 2012). Thereby, cells receive continuous proliferative and survival signals, leading to uncontrolled cell growth, which is one of the hallmarks of cancer (Hanahan and Weinberg 2011). In addition to activating point mutations, a miss regulation of Ras regulatory proteins, either a hyperactivation of GEFs or a downregulation of GAP activity, can also result in sustained Ras signaling (Vigil et al. 2010).

Ras proteins are abundant oncogenes in many human cancers and often act as a driver oncogene in early cancer development. Considering all types of cancer, the most commonly mutated isoform is KRas. Yet, the mutated isoform is strongly dependent on the cancer type. While oncogenic KRas mutations are characteristic for pancreatic ductal adenocarcinoma (PDAC), activating mutations of NRas are for example dominant in skin melanoma (Forbes et al. 2011).

In pancreatic ductal adenocarcinoma, 90 % of all tumors exhibit an activating KRas mutation that is already present in early stages (Rozenblum et al. 1997, Cox et al. 2014). Later, loss-of-function mutations of tumor suppressor genes like p53 are acquired, amplifying disease progression (Olive et al. 2004, Hingorani et al. 2005, Morton et al. 2010). Another tumor class that harbors predominantly oncogenic KRas mutations is colorectal cancer (CRC). In CRC progression, a loss-off-function mutation of the tumor suppressor protein adenomatous polyposis coli (APC) is reported as the initiating mutation (Fodde 2002). However, 45 % of CRC cancers exhibit also activating KRas mutations, which are associated with poor prognosis (Cox et al. 2014).

2.8 Targeting oncogenic Ras

Ras proteins were the first described human oncogenes in 1982 (Der et al. 1982, Parada et al. 1982). The discovery of oncogenes in humans led to tremendous

research affords to develop new drugs to overcome the poor median survival rates associated with most cancers. Despite ongoing Ras-centric research, no approved drug to treat cancers harboring oncogenic Ras has reached the clinic yet (Papke and Der 2017). However, a multitude of distinct targeting strategies have been applied that can be grouped into five major categories (Figure 5).

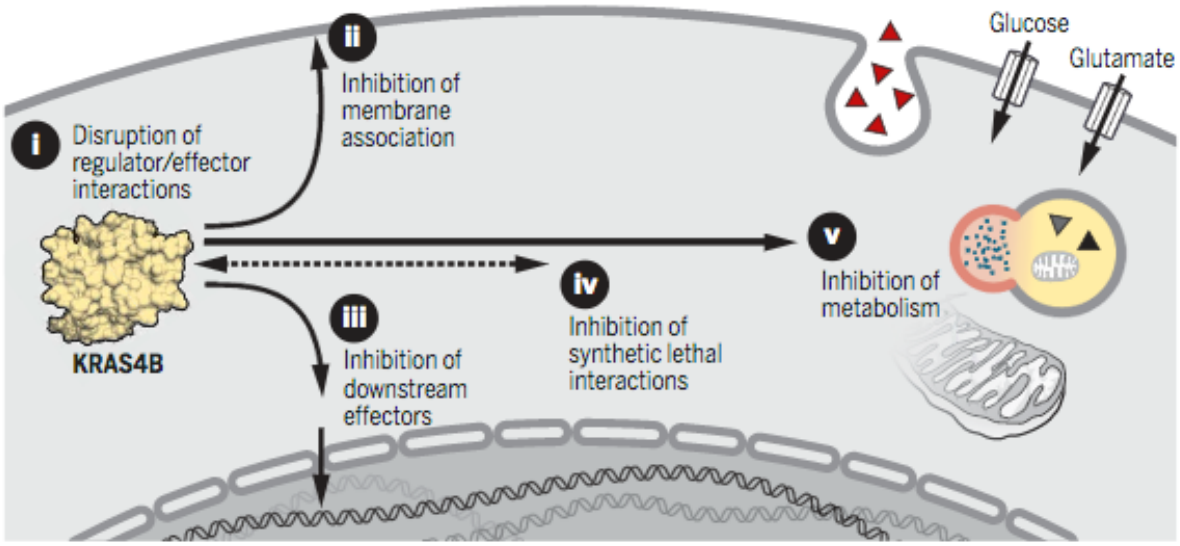

Figure 5: Distinct strategies for targeting aberrant Ras signaling. i Direct targeting of Ras can hinder binding to effector proteins like Raf or impede the interaction with regulator proteins like GEFs. **ii** Interference with Ras spatial organization can result in reduced signaling activity. **iii** Direct targeting of downstream effectors, for example kinases of the MAP kinase cascade, can hinder signal progression of oncogenic Ras. **iv** Identification and targeting of synthetic lethal interaction partners enables selective interference with oncogenic Ras harboring cells. **v** Uncontrolled proliferating cancer cells require more energy und nutrients. Therefore, up-regulated metabolic processes provide an indirect point of attack (Adapted from Papke and Der, 2017).

The majority of these strategies have in common that they target Ras indirectly, for example by interference with downstream effectors or by targeting the spatial organization of Ras. Two strategies of spatial interference will be discussed in more detail in 2.8.1.

One more recent strategy to impair oncogenic KRas signaling has been the identification and targeting of synthetic lethal interaction partners. Most of the potential synthetic lethal proteins have been identified by shRNA-mediated genome wide screenings in isogenic cell lines that presumably only differ in their KRas mutation status (Luo et al. 2009, Singh et al. 2009). While these screens have revealed a lot of false positive lethal interaction partners, some of them, for example TAK1 in KRas dependent colorectal cancer cell lines that also harbor APC loss-of-function mutations, could be identified (Singh et al. 2012). However, synthetic lethal interaction partners seem to be highly context-dependent and did not result in advanced drugs yet.

2.8.1 Therapy approaches targeting spatial cycles of Ras proteins

Another point of attack arises from the inevitable spatial organization of Ras within the cell. As elucidated before, Ras has to be localized at the PM for signal propagation. A delocalization of Ras from the plasma membrane results in impaired signaling. To date, two distinct strategies to disturb the PM enrichment of Ras proteins have been explored in depth. In the 1990's, many efforts were taken to develop inhibitors of farnesyl transferases (Basso et al. 2006). More recently, the chaperon PDEδ gained increased interest as an indispensable solubilizing factor for farnesylated Ras proteins.

2.8.1.1 Farneysl transferase inhibitors

Newly synthesized Ras proteins are soluble and would remain in the cytosol without further posttranslational modifications. Subsequently after translation, all Ras isoforms are prenylated at the cysteine of the C-Terminal CAAX motif, increasing membrane affinity. It has been shown that this irreversible farnesylation is essential for membrane interaction and thereby for aberrant KRas signaling (Jackson et al. 1990). This led to the development of several distinct farnesyl transferase inhibitors (FTIs) based on the concept that by inhibiting farnesyl transferase activity, Ras proteins would remain soluble and never reach the plasma membrane.

FTIs have been shown to effectively prevent farnesylation of HRas, accompanied with a redistribution of HRas into the cytosol (Bishop et al. 1995, Whyte et al. 1997). However, for the NRas and KRas isoforms, the inhibition of farnesylation could be compensated by geranylgeranyl modification catalyzed by the geranylgeranyl transferase 1 (GGT1) in cells treated with FTIs (Whyte et al. 1997). Thereby, plasma membrane enrichment of N- and KRas were not impaired by FTI treatment. This failure reduced the interest of the pharmaceutical industry in further development of Ras inhibitors, especially inhibitors of its spatial organization, for over a decade.

2.8.1.2 Small molecule PDEδ inhibitors

Another opportunity to interfere with the spatial localization of Ras arose with the discovery of the GDI-like solubilization factor PDEδ (Hanzal-Bayer et al. 2002, Nancy et al. 2002). As discussed in chapter 2.5, the sequestration of Ras molecules from endomembranes and the enhanced diffusion within the cytoplasm as well as the localized release of cargo from PDEδ by the small GTPase Arl2 are essential to maintain the plasma membrane enrichment of Ras (Schmick et al. 2014, Schmick et al. 2015). It could be shown that RNAi-mediated interference with PDEδ leads to a redistribution of all Ras isoforms from the PM to endomembranes. Moreover, PDEδ-mediated delocalization of Ras from the PM results in impaired down-stream signal progression in the MAPK network (Chandra et al. 2011).

These results have motivated a novel strategy to target aberrant Ras signaling. Since PDEδ binds to the farnesyl-tail of Ras proteins, occupying the prenyl binding pocket of PDEδ by competitive small molecule inhibitors has been thought to phenocopy the RNAi-induced knock down of PDEδ. The first described small molecule inhibitor of the Ras-PDEδ interaction was Deltarasin in 2013 (Zimmermann et al. 2013). Since then, enhancement and validation of small molecule PDEδ inhibitors is an ongoing line of research that may lead to clinically relevant drugs in the future.

3. Objectives

Ras proteins are important signaling hubs within cells that cycle between an active and an inactive state. Oncogenic mutations retain Ras proteins in their active conformation, leading to aberrant signaling. Since most effectors of Ras proteins are recruited to the plasma membrane where Ras is normally enriched, the spatial organization of Ras proteins represents an alternative to direct targeting of oncogenic Ras. It could be shown that interference with the solubilizing functionality of PDEδ depletes KRas from the plasma membrane and thus reduces KRas signal propagation. This finding gave rise to the development of distinct small-molecule inhibitors that competitively bind in the prenyl binding pocket of PDEδ. While these inhibitors selectively affected proliferation of oncogenic KRas bearing pancreatic ductal adenocarcinoma cell lines, the effective concentrations were much higher than anticipated from the corresponding *in vitro* and "in cell" K_D's.

Therefore, further chemotypes have to be screened and potential hits have to be optimized to develop more potent inhibitors. To facilitate development of inhibitors that, in the end, may become clinical relevant, the biological activity of those inhibitors has to be thoroughly validated, starting in two-dimensional cell culture model systems. In addition to the focus on increased potency, the bioavailability of the inhibitors needs to be monitored and weighted against the increased potency.

To date, the strategy of spatial interference with aberrant KRas signaling by means of PDEδ inhibition has only been explored in the background of pancreatic ductal adenocarcinoma. Therefore, this strategy has to be transferred to other types of cancer that harbor predominantly oncogenic KRas mutations. One of these cancer types is colorectal cancer. While in general one of the best treatable forms of cancer, oncogenic KRas mutations render standard therapy approaches for CRC ineffective. Thus, PDEδ interference needs to be investigated as alternative strategy for these cases. Moreover, we questioned, if oncogenic KRas activity is correlated with PDEδ expression in CRC and could be of prognostic relevance.

4. Results

4.1 Characterization of a novel chemotype of PDEδ inhibitors

The development of the first inhibitor of the Ras-PDEδ interaction in 2013 represented a milestone in targeting oncogenic KRas signaling. This small molecule inhibitor, called Deltarasin (Zimmermann et al. 2013), was based on the concept that instead of targeting the "undruggable" small GTPase Ras itself, interfering with the spatial organization of Ras could be sufficient to interfere with aberrant signaling. Indeed, Deltarasin, as well as the second generation inhibitor Deltazinone 1 (Papke et al. 2016), showed anti-proliferative effects in oncogenic KRas-dependent human pancreatic ductal adenocarcinoma cells (hPDACs). However, a big discrepancy between the determined nM binding affinities *in vitro* as well as in cells and the required micromolar concentrations to affect cell growth was evident for both compounds. Thus, further development of new inhibitor classes was necessary to overcome this limitation and resulted in the new chemotype called Deltasonamide. While Deltarasin is based on a benzimidazole scaffold, Deltasonamide exhibit two sulfonamide groups. Both inhibitor chemotypes competitively bind to the hydrophobic binding pocket of PDEδ through hydrogen bonds (H-bonds). However, the first generation PDEδ inhibitor Deltarasin engages only in 3 H-bonds resulting in a moderate affinity (K_D= 38 ± 16 nM) (Zimmermann et al. 2013). In contrast, Deltasonamide 1 and 2 both engage the PDEδ binding pocket with 7 H-bonds and exhibit a corresponding higher *in vitro* affinity of K_D= 203 ± 31 pM and K_D= 385 ± 52 pM (Martin-Gago et al. 2017), respectively (Figure 6).

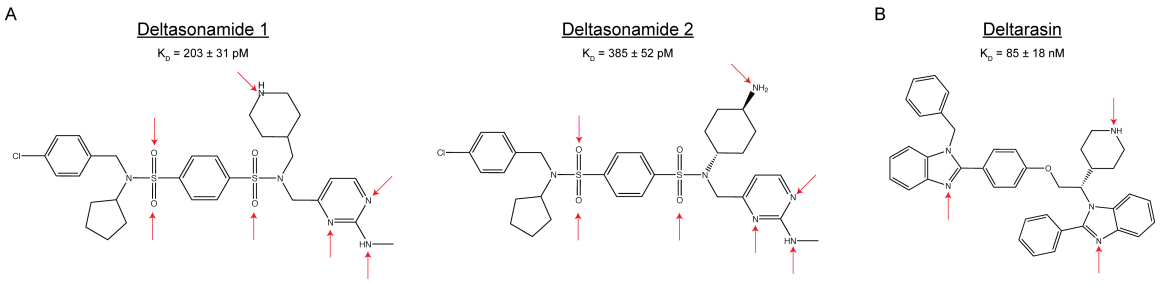

Figure 6: Chemical structures and *in vitro* binding affinities of PDEδ inhibitors. Chemical structures of Deltasonamide 1 and 2 (A) as well as of Deltarasin (B). Formed hydrogen bonds to the PDEδ binding pocket are indicated by red arrows. The shown *in vitro* K_D's were determined by competitive fluorescence polarization assays as described in (Martin-Gago et al. 2017).

4.1.1 Deltasonamides suppress the Ras - PDEδ interaction inside cells

To address if the new inhibitor class affects the interaction between PDEδ and farnesylated Ras proteins in living cells, fluorescence lifetime imaging microscopy measurements based on Förster resonance energy transfer (FLIM-FRET) were performed. For this, mCitrine-Rheb and mCherry-PDEδ were transiently transfected into Madin-Darby canine kidney (MDCK) cells. The low membrane affinity of farnesylated Rheb that, in contrast to other Ras proteins, lacks a secondary localization motif, accounts for an enhanced cytosolic fraction of mCitrine-Rheb interacting with mCherry-PDEδ (Zimmermann et al. 2013, Papke et al. 2016). Further, a 1:3 Rheb:PDEδ transfection ratio was chosen to ensure a maximized fraction of solubilized Rheb. Together, this enabled a robust detection of small molecule inhibition on the Rheb-PDEδ complex formation. The homogenous fluorescence patterns of both proteins in the absence of inhibitor indicated the solubilization of mCitrine-Rheb by mCherry-PDEδ (Figure 7), which was also reflected in the high molar fraction α of interacting mCitrine-Rheb and mCherry-PDEδ molecules derived from a global analysis of the FLIM data (Grecco et al. 2009). Treatment with increasing concentrations of Deltasonamide inhibitors resulted in relocalization of Rheb to endomembranes, accompanied with a reduced interacting fraction α of mCitrine-Rheb with mCherry-PDEδ. Fitting of the dose-dependent measurements to an equilibrium model (Zimmermann et al. 2013, Papke et al. 2016) yielded an 'in-cell'

K_D of 85 ± 18 nM for Deltasonamide 1 (Figure 7 A) and 61 ± 5 nM for Deltasonamide 2 (Figure 7 B).

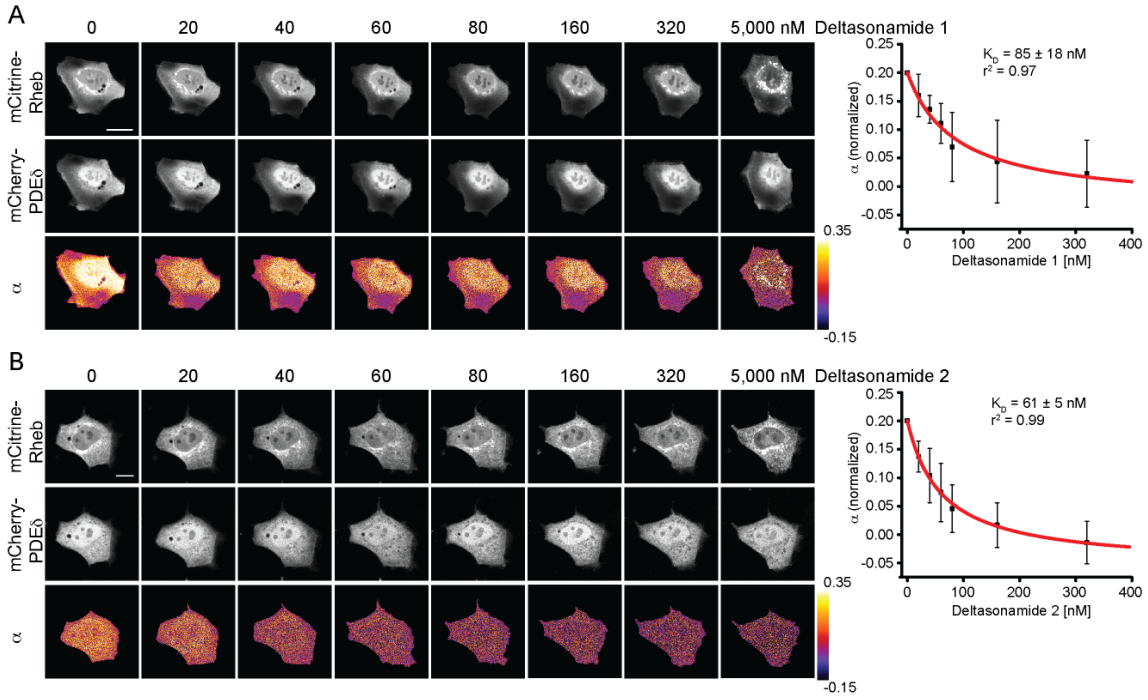

Figure 7: **In-cell measurement of the effect of Deltasonamide 1 and 2 on the interaction between Rheb and PDEδ. A, B** Left panels: FLIM measurements of the inhibitor dose-dependent interacting molar fraction α between mCitrine-Rheb and mCherry-PDEδ. Upper and middle rows show fluorescence intensity of mCitrine-Rheb and mCherry-PDEδ, respectively. Lower rows show molar fraction α of mCitrine-Rheb with mCherry-PDEδ. Inhibitor concentrations are indicated above each image in nM. Right panels: Fit of averaged dose-response ± s.e.m of five independent experiments to a binding model (see methods) yielded an 'in cell KD' of 85 ± 18 nM for Deltasonamide 1 and 61 ± 5 nM for Deltasonamide 2. Scale bars: 10 µM.

4.1.2 Deltasonamide administration counters PM enrichment of KRas

To examine if the new inhibitor chemotype also interferes with the localization of KRas, MiaPaCa-2 cells ectopically expressing mCitrine-KRas were treated with 5 µM Deltasonamide 2 and the KRas localization was monitored over a time course of 90 min. As apparent from the confocal micrographs (Figure 8 A) as well as the corresponding quantification (Figure 8 B, C), Deltasonamide 2 administration led to a loss of plasma membrane localization of KRas over time, paralleled by an increased

fraction of KRas within the cell's interior. Analysis of variance showed a significant loss of PM localization starting 30 min after Deltasonamide 2 administration, which matches with the effective dissociation rate of KRas from the PM (Schmick et al. 2014).

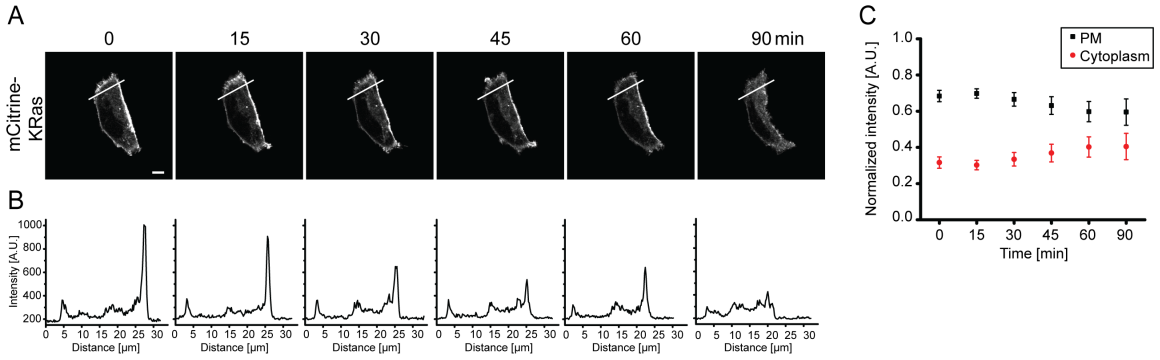

Figure 8: Deltasonamide 2 administration counters the PM enrichment of KRas. A Representative time series of mCitrine-KRas redistribution upon administration of 5 µM Deltasonamide 2 in MiaPaCa-2 cells. The time is indicated above each image in min. **B** Intensity profiles of mCitrine-KRas fluorescence within the corresponding ROIs indicated in (A). **C** Normalized KRas mean intensity ± s.d. at the PM (black) and inside the cell (red) over time (n= 8 cells). Scalebar: 10 µM.

4.1.3 Deltasonamides impede proliferation of K-Ras dependent hPDAC cells

To determine, if the new inhibitor chemotype affects proliferation, impedance-based real time cell analyzes (RTCA) measurements were performed in four human pancreatic ductal adenocarcinoma cell lines. Both MiaPaCa-2 (Yunis et al. 1977) and PANC-Tu-1 (Elsasser et al. 1993) cell lines exhibit an oncogenic KRas mutation and were reported to be dependent on oncogenic KRas signaling (Singh et al. 2009, Babij et al. 2011). In contrast, the PANC-1 cell line (Lieber et al. 1975) is not dependent on oncogenic KRas signaling despite harboring an oncogenic KRas allele (Singh et al. 2009, Babij et al. 2011), while BxPC-3 cells (Tan et al. 1986) are homozygote for wild type KRas (Babij et al. 2011).

Both Deltasonamide 1 (Figure 9) and Deltasonamide 2 (Figure 10) reduced the proliferation of oncogenic KRas dependent MiaPaCa-2 and PANC-Tu-1 cell lines.

However, the inhibitor Deltasonamide 2 showed a stronger anti-proliferative effect at lower doses and even exhibited a sub-micromolar EC_{50} in MiaPaCa-2 cells. Strikingly, the growth rates of oncogenic KRas independent PANC-1 and KRas wild type bearing BxPc-3 cells were affected to a much lesser extend by both inhibitors.

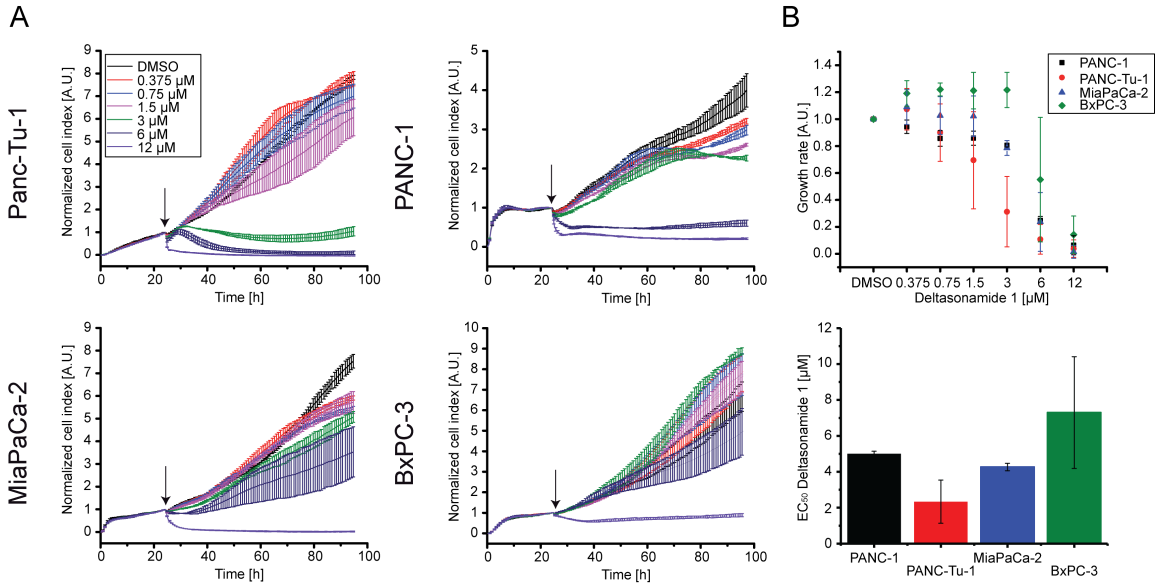

Figure 9: Deltasonamide 1 decreases proliferation of human pancreatic cancer cell lines. A Representative real-time cell analysis (RTCA) profiles (N=3) of hPDAC cell lines with distinct KRas mutation status. Cell indices ± s.d. were measured in duplicates and normalized to the time point of drug administration (arrow). **B** Upper graph: Growth rate ± s.d. in dependence of Deltasonamide 1 dose. The growth rates were determined by integration of the area below the RTCA curves over 60 h after drug administration and normalized to the respective DMSO control. Lower bar graph: EC_{50} ± s.d. for Deltasonamide 1 in distinct hPDAC cell lines. EC_{50} values were determined by sigmoidal curve fit of the growth rates depicted above.

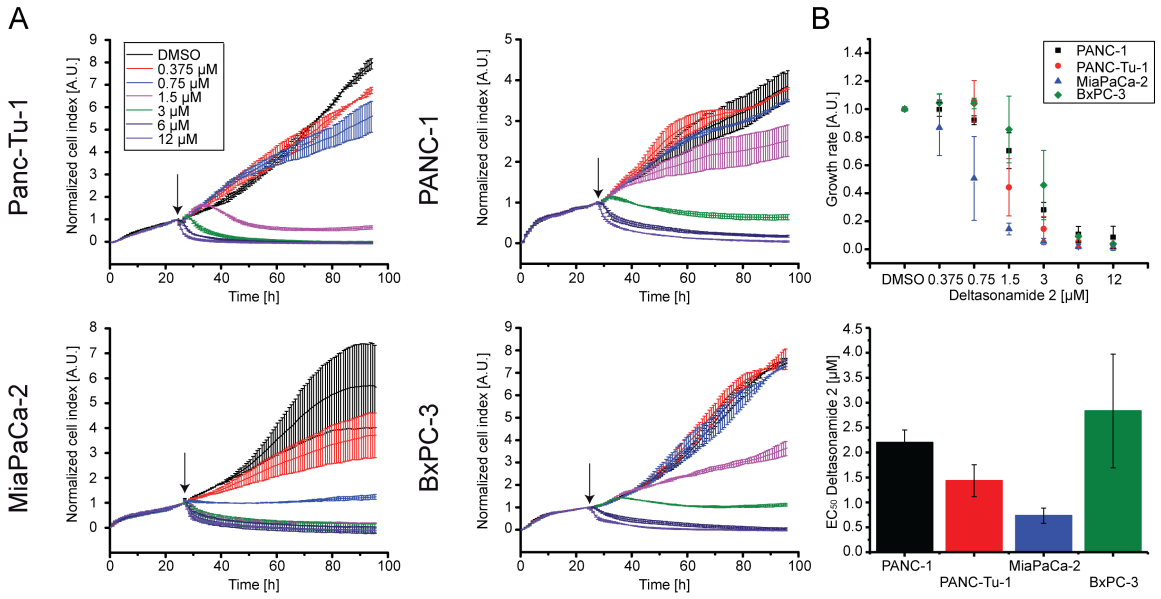

Figure 10: Deltasonamide 2 decreases proliferation of human pancreatic cancer cell lines. A Representative real-time cell analysis (RTCA) profiles (N=3) of hPDAC cell lines with distinct KRas mutation status. Cell indices ± s.d. were measured in duplicates and normalized to the time point of drug administration (arrow). **B** Upper graph: Growth rate ± s.d. in dependence of Deltasonamide 2 dose. The growth rates were determined by integration of the area below the RTCA curves over 60 h after drug administration and normalized to the respective DMSO control. Lower bar graph: EC_{50} ± s.d. for Deltasonamide 2 in distinct hPDAC cell lines. EC_{50} values were determined by sigmoidal curve fit of the growth rates depicted above.

Compared to the first- and second-generation of small molecule PDEδ inhibitors Deltarasin (Zimmermann et al. 2013) and Deltazinone 1 (Papke et al. 2016), the new chemotype Deltasonamide reduced cell proliferation of KRas-dependent human pancreatic ductal adenocarcinoma cells at substantially lower doses, whereas the proliferation of KRas-independent PANC-1 cells and wild type KRas harboring BxPc-3 cells were still affected albeit to a lesser extent. However, the effectiveness of PDEδ inhibitors on stalling aberrant KRas signaling was so far only investigated in hPDACs. Therefore, we wanted to expand the strategy of pharmacological PDEδ interference to colorectal cancer (CRC), another tumor class that exhibits a high frequency of oncogenic KRas mutations (Cox et al. 2014).

4.2. PDEδ interference in human colorectal cancer cell lines

We studied the effects of genetic and pharmacological interference with PDEδ solubilizing function in a panel of six human CRC cell lines featuring distinct oncogenic mutations (Table 1). All cell lines were originally derived from CRC patients. SW480 was derived from a primary adenocarcinoma of the colon of a 50 year old Caucasian male (Leibovitz et al. 1976) and the cell line is homozygote for oncogenic KRas (Ahmed et al. 2013). The HCT-116 cell line was derived from a colorectal carcinoma of an adult male (Brattain et al. 1981) and contains one mutant and one wild type KRas allele (S Shirasawa 1993). Both Hke3 and Hkh2 were derived from the HCT-116 cell line by exchanging the oncogenic KRas allele with a non-transcribed KRas allele using homologous recombination (S Shirasawa 1993) to create a panel of isogenic cell lines that presumably only differ in their KRas mutation status. However, the recombination was only successful in Hkh2, while Hke3 cells still harbor the oncogenic KRas allele. However, it is expressed at lower levels in the Hke3 cells (Fasterius et al. 2017). In addition, we studied two wild type KRas expressing CRC cell lines that exhibit other oncogenic mutations. The HT29 cell line, established from a colorectal adenocarcinoma of a 44 year old Caucasian female (Fogh 1975), bears an oncogenic BRaf mutation (V600E) (Di Nicolantonio et al. 2008), an effector of Ras (Marais et al. 1995), whereas DiFi cells, derived from a colorectal carcinoma of a 46 year old female (Olive et al. 1993), harbor an amplification of the EGFR gene accompanied with increased EGFR protein expression levels (Dolf et al. 1991, Gross et al. 1991).

Table 1: Studied human colorectal cancer cell lines including KRas mutation status as well as other relevant oncogenic mutations.

Cell line	KRas status	Other onc. mutations
SW480	G12V//G12V	-
HCT-116	G13D//wt	-
Hke3	G13D//wt	-
Hkh2	-//wt	-
HT29	wt//wt	BRaf (V600E)
DiFi	wt//wt	EGFR overexpression

4.2.1 Generation of stable inducible shRNA-PDEδ cell lines

To investigate, if genetic interference with PDEδ affects cell growth or viability in CRC cells (Table 1), the cell lines within the CRC cell panel were stably transduced with a lentivirus that either encoded a doxycycline-inducible short hairpin RNA (shRNA) against PDEδ (Zimmermann et al. 2013) or a scrambled (scr), non-targeting shRNA as control. Since PDEδ was previously reported to exhibit a low protein turnover (Chandra et al. 2011), shRNA expression was induced by doxycycline over several days and PDEδ protein levels were determined by western blot analysis at different time points. A good knock down efficiency of around 80 % was achieved after 72 h, whereas longer incubation periods showed no significant improvement of the PDEδ knock down level (Figure 11 A).

To evaluate the knock down efficiency in the different CRC cell lines, western blot analysis was performed for all cell lines after 72 h shRNA induction and compared to non-induced samples. All stably transduced shRNA-PDEδ cell lines showed a clear down modulation of PDEδ protein levels upon doxycycline induction compared to the corresponding non-induced controls (Figure 11 B), while the induction of scrambled shRNA expression had no effect on PDEδ protein level (Figure 11 C).

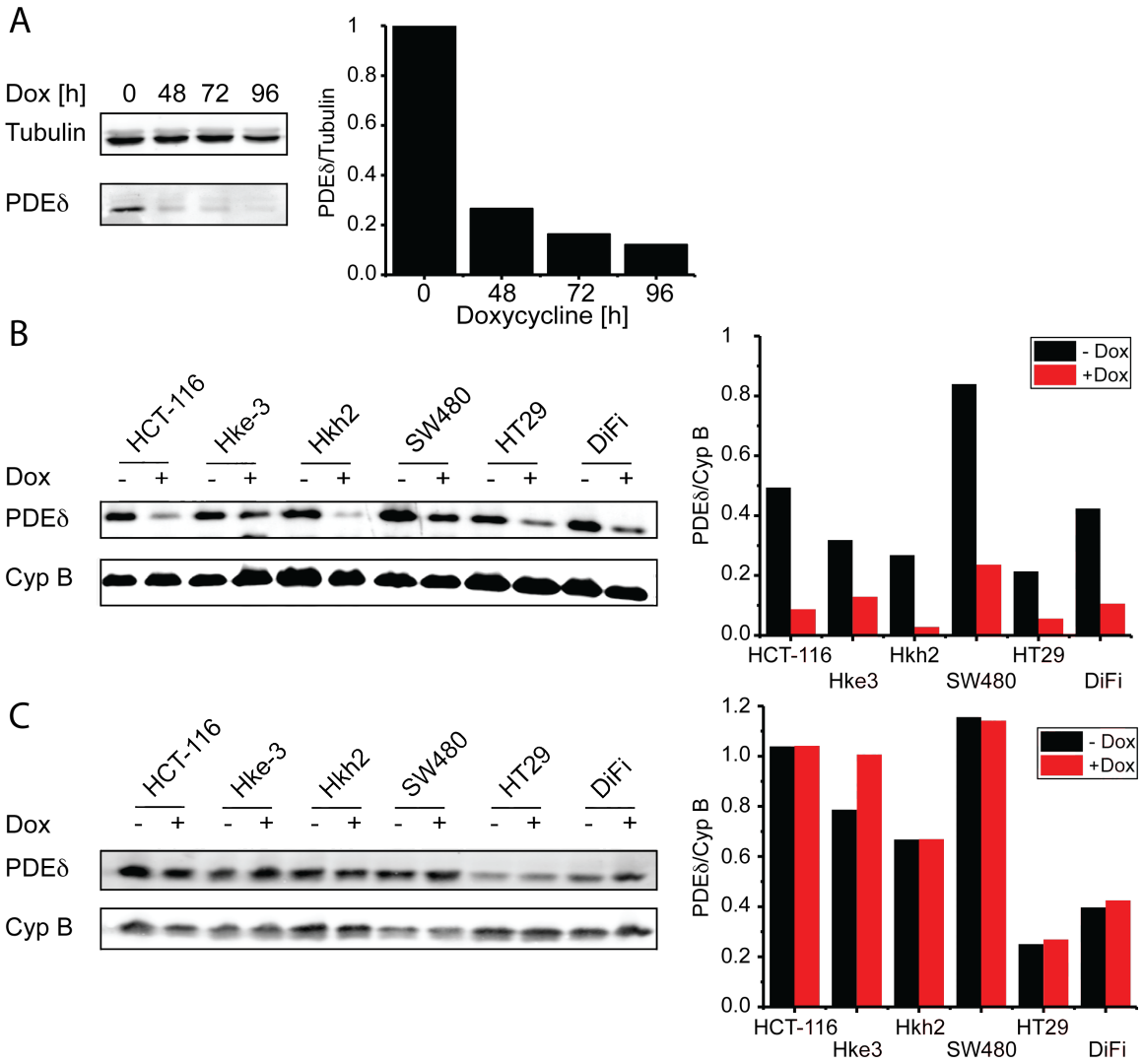

Figure 11: shRNA mediated knock down of PDEδ in distinct CRC cells. A Left: PDEδ protein level in SW480 cells after increasing doxycycline administration periods determined by western blot. Tubulin was used as loading control. Right bar graph: quantification of PDEδ protein levels over time normalized to the untreated control. **B** Left: PDEδ protein level of distinct colorectal cancer cell lines with or without PDEδ shRNA induction by doxycycline for 72 h determined by western blot analysis. Cyclophilin B was used as loading control. Right bar graph: quantification of endogenous PDEδ levels of each cell line with (red) and without (black) doxycycline induction. **C** PDEδ protein level of distinct colorectal cancer cell lines with or without non-targeting (scrambled) shRNA induction by doxycycline after 72 h determined by western blot analysis. Cyclophilin B was used as loading control. Right bar graph: quantification of endogenous PDEδ levels of each cell line with (red) and without (black) doxycycline induced scrambled shRNA expression. Stably transduced HCT-116, Hke3, HT29 and SW480 cell lines were generated by Dr. D.C. Truxius.

Furthermore, comparison of PDEδ expression levels between the non-induced controls revealed that SW480 cells, which are homozygous for $KRas^{G12V}$ exhibited the highest PDEδ expression level, whereas the wild type KRas bearing HT29 cells expressed the lowest amount of PDEδ protein.

4.2.2 Correlation of PDEδ and (oncogenic) Ras protein level

Since PDEδ is necessary to maintain the enrichment of KRas at the PM and thereby its signaling activity (Chandra et al. 2011, Schmick et al. 2014, Schmick et al. 2015), we next investigated if PDEδ expression was correlated to KRas expression levels or Ras activity between the different CRC cell lines.

Since the generation of stably transduced cell lines requires several weeks and involves clonal selection, we correlated the respective expression levels of Ras and PDEδ within the parental cell lines by quantitative western blot analysis. To determine the level of active Ras, cells were serum-starved 24 hours prior to cell lysis and active, GTP-bound Ras was enriched by 3xRBD (Ras binding domain of cRaf) pull-down from whole cell lysates. Here, the amount of pulled down GTP-loaded Ras is a measure of oncogenic Ras due to prior starvation (Figure 12). Pearson's correlation analysis revealed a strong correlation between both PDEδ - Ras protein levels and PDEδ expression and Ras activity within the CRC cell panel (Figure 12 B). CRC cell lines that harbor wild type KRas exhibited overall lower levels of Ras protein expression and no active Ras was enriched in these cell lines following starvation. SW480 cells (homozygote for $KRas^{G12V}$) exhibited the highest PDEδ and Ras expression levels, accompanied with a high amount of active Ras, whereas the oncogenic KRas heterozygote cell lines HCT-116 and Hke3 contained moderate amounts of active Ras.

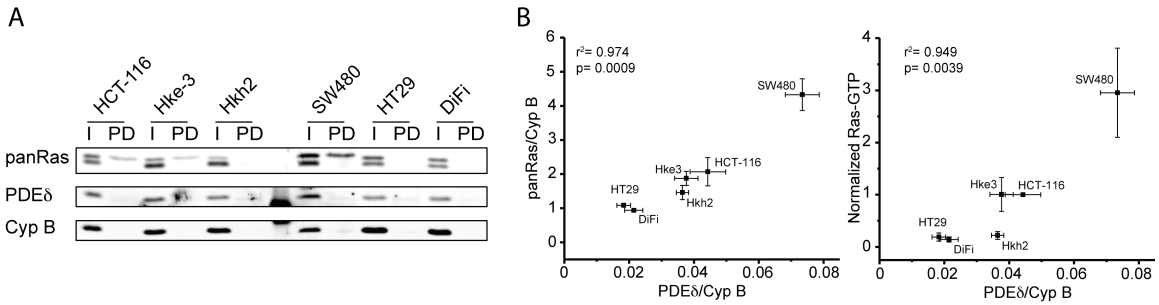

Figure 12: PDEδ and Ras levels in colorectal cancer cell lines. A PDEδ and panRas protein level (I; Input) and Ras-GTP level (PD; pull down) of distinct CRC cell lines determined by western blot analysis. Cells were serum-starved 24 h before lysis and active Ras was enriched by 3xRaf-RBD pull-down. **B** Correlation plots of PDEδ and panRas expression ± s.e.m (N=4) (left) as well as PDEδ and active Ras levels ± s.e.m (N=4; data normalized to HCT-116) (right). Pearson's correlation analysis shows a high correlation of 0.974 and 0.949 between the respective protein expression levels (left) as well as PDEδ expression and Ras activity (right).

4.2.3 Correlation analysis of KRas and PDEδ levels in CRC patients

We next addressed, if the strong correlation between KRas and PDEδ expression could also be observed in tumors of CRC patients and could therefore be of prognostic relevance. The Cancer Genome Atlas (TCGA) research network collected data and case studies for more than 30 cancer types and developed a pipeline for comprehensive data analysis. Since, unfortunately, no protein expression data of CRC patients is available, a dataset containing mRNA expression data of 195 CRC patients was extracted from TCGA (Cancer Genome Atlas 2012) and analyzed instead.

The patient data was first separated by KRas mutational status into KRas wild type (red, n=108) and oncogenic KRas (blue, n=87) cases (Figure 13). Comparison of the mRNA expression between both cohorts revealed that the KRas mRNA expression levels of CRC patient harboring oncogenic KRas mutations were significantly increased. However, the PDE6D mRNA expression was not significantly different between the two groups (Figure 13 A). Furthermore, correlation analysis of PDE6D and KRas mRNA expression showed no correlation within the CRC patient dataset (Figure 13 B).

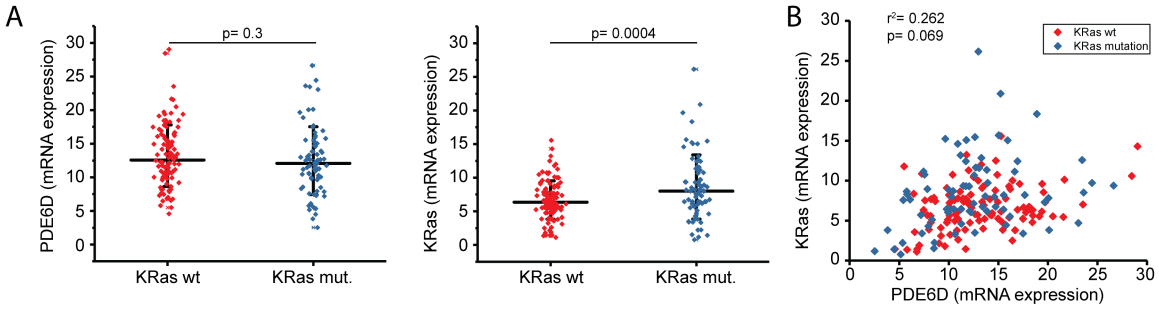

Figure 13: PDE6D and KRas mRNA expression level in CRC patients. A PDE6D (left) and KRas (right) mRNA expression level in cancer cells of 195 CRC patients. The data set was derived from The Cancer Genome Atlas (TCGA). Wild type KRas cases (n= 108) are shown in red, mutant KRas cases (n= 87) are shown in blue. Mean ± s.d are shown by black lines. Significance was calculated using student's t-test. **(B)** Correlation plot of PDE6D versus KRas mRNA expression. Pearson's correlation analysis shows no correlation (r^2 = 0.262).

4.2.4 Determination of PDE6D and KRas mRNA expression in CRC cells

Since the TCGA dataset only contained mRNA expression data, we determined PDE6D and KRas mRNA expression levels within our CRC cell panel by quantitative real-time PCR (RT-qPCR) to examine if the correlation we identified between KRas and PDEδ on the protein level is also present on the mRNA level. The mRNA expression level of the housekeeping gene GAPDH was also determined and used as an internal reference. Consistent with the CRC patient data, PDE6D and KRas mRNA expression were not correlated within the CRC cell panel (r^2 = -0.161) (Figure 14 B). Furthermore, neither PDE6D nor KRas mRNA expression were correlated to their respective protein expression level (Figure 14 A).

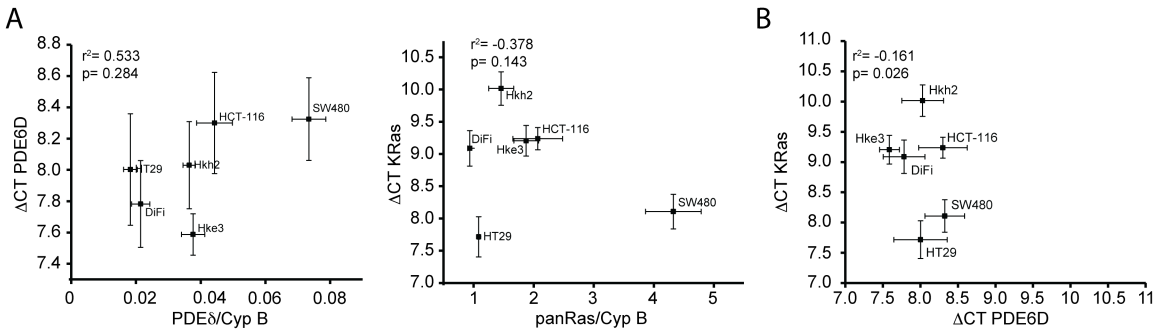

Figure 14: PDE6D and KRas mRNA expression level in the CRC cell panel. A Correlation plots of mRNA versus protein expression for PDEδ (left) and KRas (right), respectively. Error bars depict s.e.m. Pearson's correlation analysis shows a weak positive correlation (r^2 = 0.533) for KRas and no correlation for PDE6D (r^2 = -0.378) between their respective mRNA and protein expression levels. **B** Correlation plot of PDE6D and KRas mRNA expression (N=4) within the CRC cell panel determined by RT-qPCR. Error bars depict s.e.m. GAPDH was used as an internal reference to determine ΔCT values for KRas and PDE6D. Pearson's correlation analysis shows no correlation (r^2 = -0.161).

4.2.5 PDEδ knock down suppresses proliferation in oncogenic KRas harboring CRC cells

We next investigated, if genetic interference with PDEδ affects the growth and viability of CRC cell lines that were stably transduced with doxycycline inducible shRNA against PDEδ. For this, we first performed colony formation assays (Clonogenic assays) (Puck and Marcus 1956, Rafehi et al. 2011) with doxycycline-induced PDEδ knock down in all cell lines and compared them to respective controls after a growth period of ten days (Figure 15 A, C). Here, two proliferative parameters can be extracted. First, the number of colonies that remain after PDEδ knock down, which is a measure of cell viability. Second, the average size of the colonies, which mirrors the proliferation rate. Quantification of both parameters showed clear anti-proliferative effects of PDEδ knock down only in CRC cell lines that harbor an oncogenic KRas mutation. The proliferation and the viability of wild type KRas-bearing CRC cell lines was not significantly reduced besides a minor reduction in growth rate of Hkh2 cells (Figure 15 B, D). Both proliferation and viability reduction were most prominent in SW480 cells that are homozygote for oncogenic KRas. The isogenic HCT-116 and Hke3 cell lines, which are both heterozygote for oncogenic KRas, showed a comparable decrease of proliferation. However, the viability of Hke3

cells, which express lower amounts of oncogenic KRas, was substantially less affected. Correlation of viability and proliferation reduction showed a clear interdependence regarding the KRas mutation status (Figure 15 E) and a strong correlation was apparent from the Pearson's correlation coefficient (r^2 = 0.909).

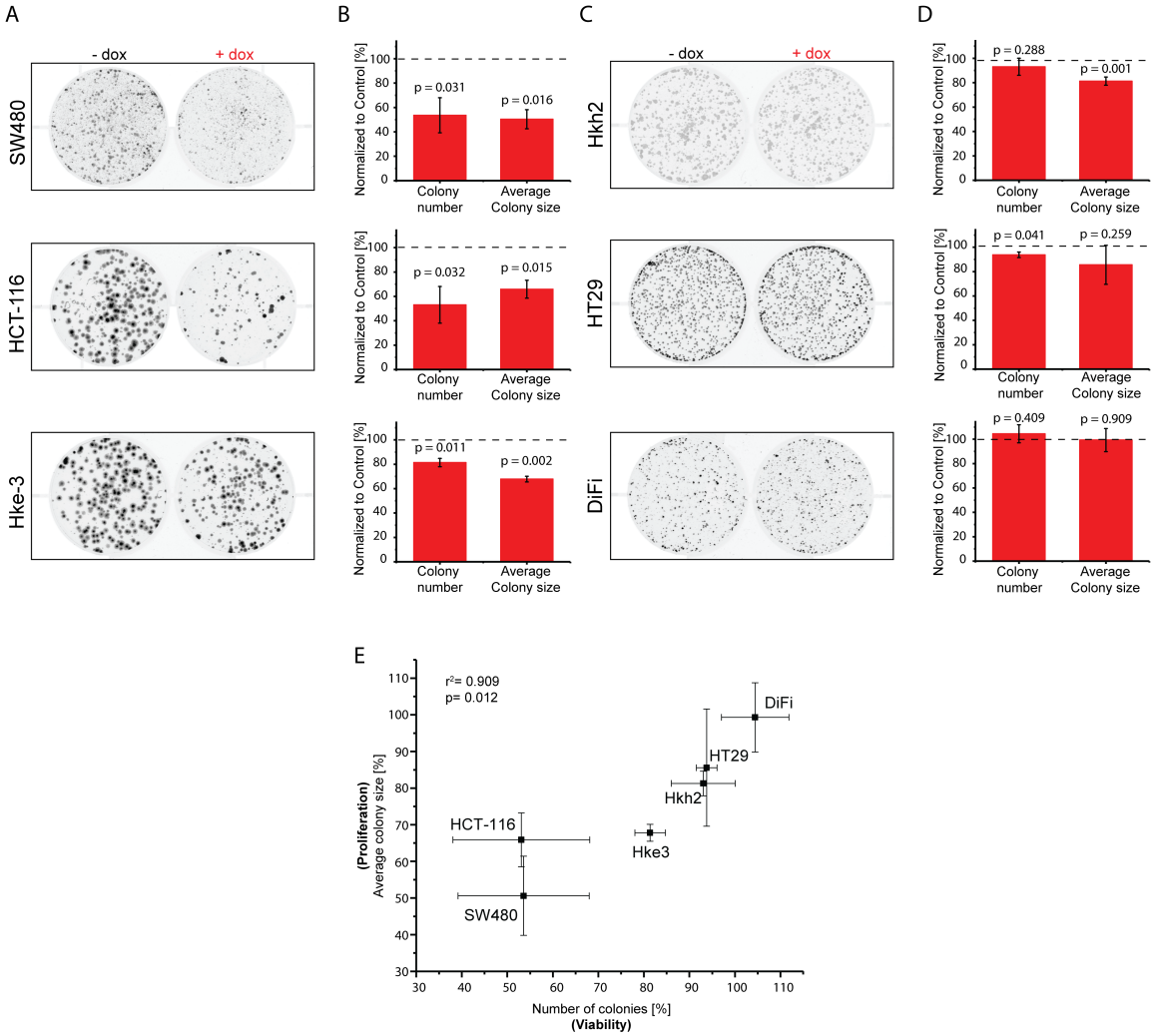

Figure 15: Colony formation assay of doxycycline-inducible PDEδ knock down in CRC cells. A, C Representative colony formation assay experiments (N=3) for cell lines harboring oncogenic KRas (A) or wild type KRas (C). Cells were grown for ten days in the presence (+dox) or absence (-dox) of doxycycline. **B, D** Quantification of colony number and average colony size. Samples, in which PDEδ was knocked down were normalized to the respective untreated controls (dashed line). Significance was calculated using one sample t test. **E** Correlation plot of colony number (Viability) versus average colony size (Proliferation) under PDEδ knock down relative to the corresponding control as determined in (B, D). Pearson's correlation analysis shows a correlation of 0.909. Error bars depict s.d.

The colony formation assay was complemented with an orthogonal proliferation assay in form of real time cell analysis (RTCA). In contrast to the colony formation assay, which is an end-point assay, RTCA measures cell proliferation over time as a function of the impedance on the well-electrode surface (Abassi et al. 2004). As observed in the colony formation assay, PDEδ knock down decreased proliferation in CRC cell lines harboring oncogenic KRas, whereas doxycycline-induced PDEδ knock down had no effect on the proliferation of KRas wild type-bearing cells (Figure 16 A, C). Consistent with the colony formation assay, the strongest growth rate reduction appeared in the homozygote KRasG12V-bearing SW480 cells. After approximately 175 hours, the cell index even started to decrease, indicating cell death. In contrast, in the heterozygote oncogene KRas harboring HCT-116 and Hke3 cells, no cell death became apparent. While the growth rate was affected in both cell lines, the Hke3 cells showed only a delayed proliferation, whereas the proliferation rate in HCT-116 was substantially decreased, resulting in a lower cell number at the end of the measurement. As a control, the proliferation of stably transduced doxycycline-inducible scrambled-shRNA cell lines was also monitored with and without doxycycline induction by RTCA (Figure 16 B, C). As expected, expression of scrambled shRNA had no effect on proliferation of CRC cell lines, independent of their KRas mutation status.

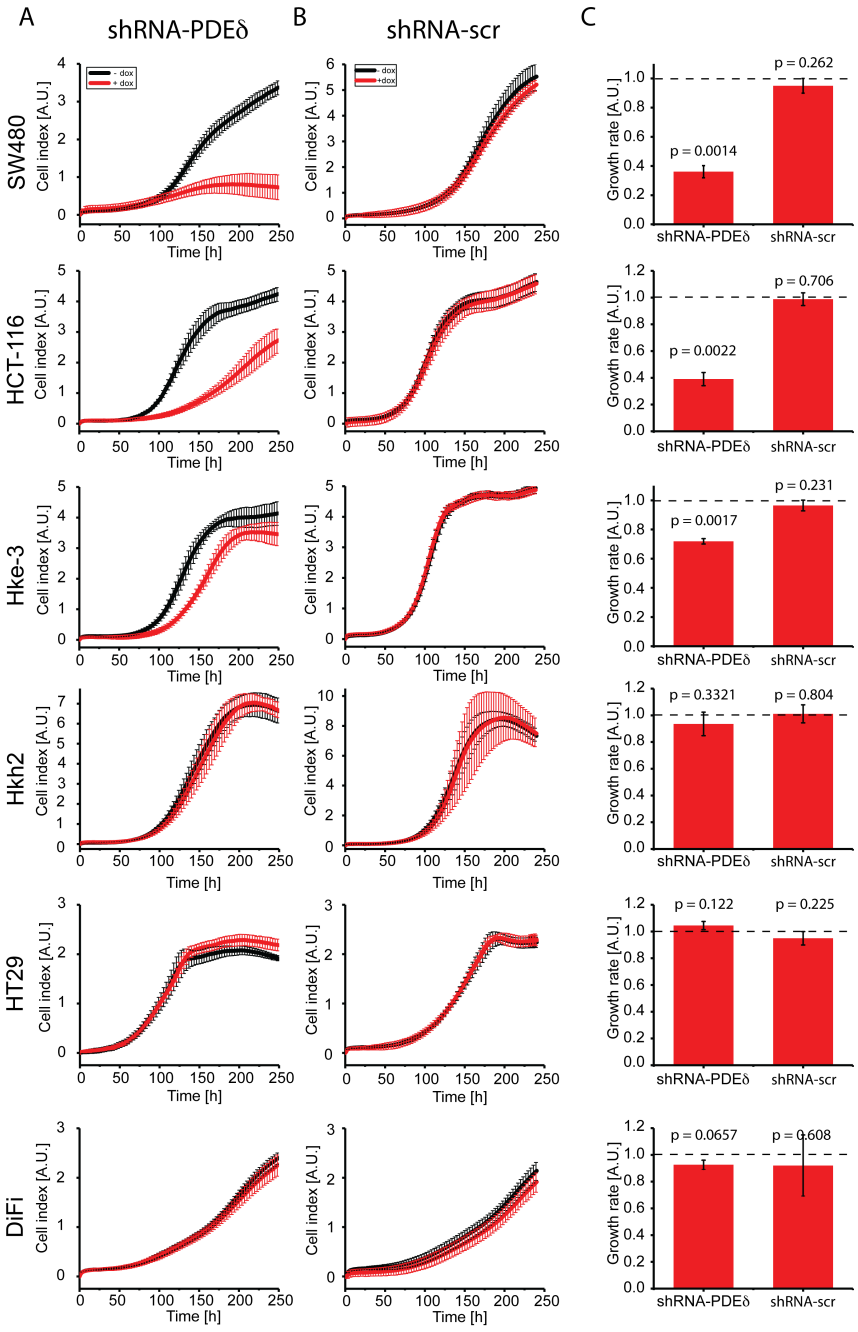

Figure 16: RTCA of CRC cells expressing doxycycline-induced PDEδ or scrambled shRNA. A, B Representative RTCA profiles (N=3) for doxycycline-induced shRNA expression against PDEδ (A) or non-targeting (scr) shRNA (B). Cell indices ± s.d. of four replicates per independent repeat were measured in the presence (red) or absence (black) of doxycycline, which was added at the beginning of the measurement. **C** Growth rates ± s.d. of doxycycline-induced shRNA-PDEδ or scrambled shRNA expression. Growth rates were calculated by integration of the area under the RTCA curve over 240 h and normalized to the respective untreated condition (dashed line). Significance was calculated using one sample t test.

4.2.6 Generation of stable PDEδ-rescue cells

To validate that the observed effects on cell proliferation in the oncogenic KRas-harboring CRC cells are indeed caused by PDEδ knock down and to exclude possible off-target effects, we designed a PDEδ rescue-construct. For this, the region of the PDEδ sequence that is targeted by the shRNA was analyzed in terms of possible positions for synonymous point mutations. While synonymous point mutations may affect the transcription rate of the DNA sequence, the resulting amino acid sequence remains unchanged (Ikemura 1981, Sorensen et al. 1989, Carlini and Stephan 2003). However, since shRNA binding is highly specific, these point mutations should prevent shRNA-mediated degradation of the rescue construct mRNA. To disable shRNA binding capabilities, all eight possible positions were mutated (Figure 17 A). In order to distinguish the endogenous protein from the rescue construct as well as to enable easy selection of stable transfected cells, a N-terminal fused fluorescent protein (mCherry, (Shaner et al. 2004)) was incorporated.

The mCherry-PDEδ rescue construct was then stably transfected into stable shRNA-PDEδ transduced HCT-116 cells. To determine, if the rescue construct resists shRNA-mediated degradation, shRNA-PDEδ expression was induced by doxycycline over several days and endogenous as well as mCherry-rescue PDEδ protein level were determined by quantitative western blot analysis at different time points (Figure 17 B). As apparent from the quantification, the mCherry-PDEδ rescue construct was expressed at a slightly increased level compared to the endogenous protein. Most importantly, the PDEδ rescue construct was indeed highly resistant to shRNA-mediated degradation. Endogenous PDEδ level decreased about 75 %, while only 35 % of the rescue construct was degraded over 72 h (Figure 17 C).

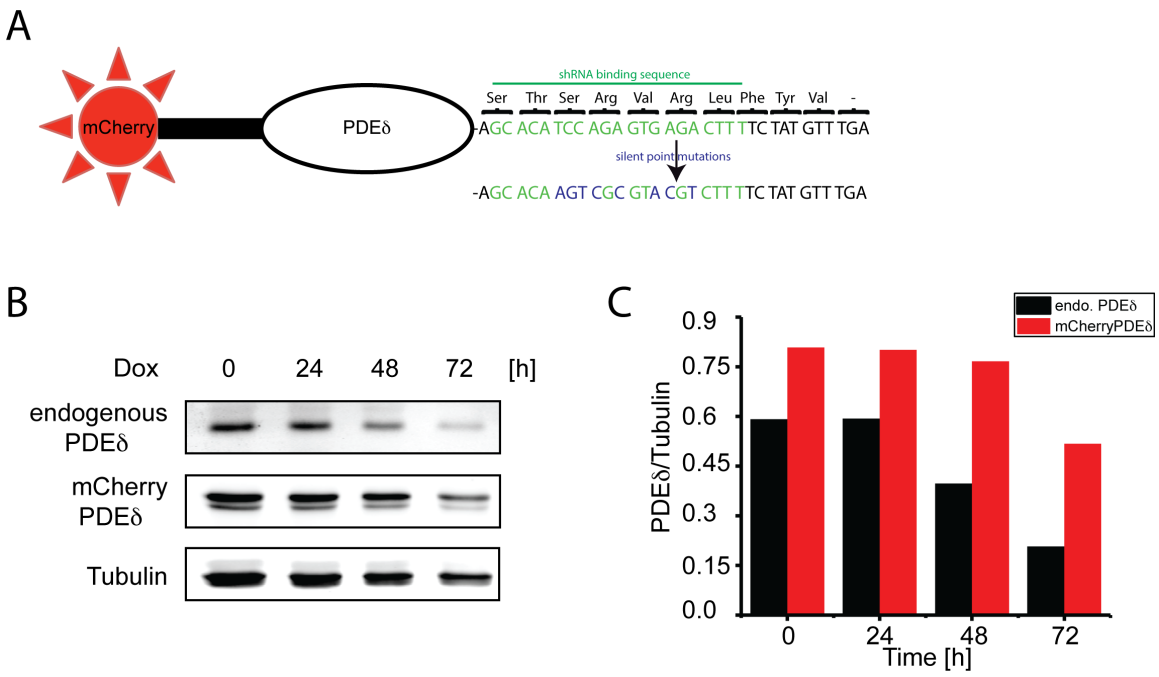

Figure 17: mCherry-PDEδ rescue construct resists shRNA-mediated degradation. A Design of the PDEδ-rescue construct. DNA bases of the shRNA targeted region of PDEδ are shown in green, introduced synonymous point mutations are shown in blue. **B** Endogenous PDEδ and rescue mCherry-PDEδ protein level in HCT-116 after increasing periods of doxycycline administration determined by western blot analysis. Tubulin was used as loading control. **C** Quantification of endogenous PDEδ (black) and mCherry-PDEδ (red) levels after different administration periods. PDEδ expression was normalized to tubulin.

4.2.7 shRNA-resistant PDEδ construct rescues knock down phenotype

After validation that the PDEδ rescue construct resists shRNA-mediated degradation to a great extent, we examined if the rescue construct can counter PDEδ knock down induced growth inhibition in HCT-116 cells. We therefore performed RTCA measurements of both stably transduced shRNA-PDEδ HCT-116 and stable transduced shRNA-PDEδ HCT-116 stably expressing the mCherry-PDEδ rescue construct with and without doxycycline induction, respectively (Figure 18 A). Comparison of both non-induced cell lines showed that the expression of the PDEδ rescue construct did not affect the growth rate. More importantly, the PDEδ rescue was successful as apparent from the growth rate of doxycycline-induced HCT-116 mCherry-PDEδ rescue cells (Figure 18 B). This clearly demonstrated that the

observed growth rate reduction after a PDEδ knock down in oncogenic KRas-bearing CRC cell lines is a specific effect and not caused by side-effects.

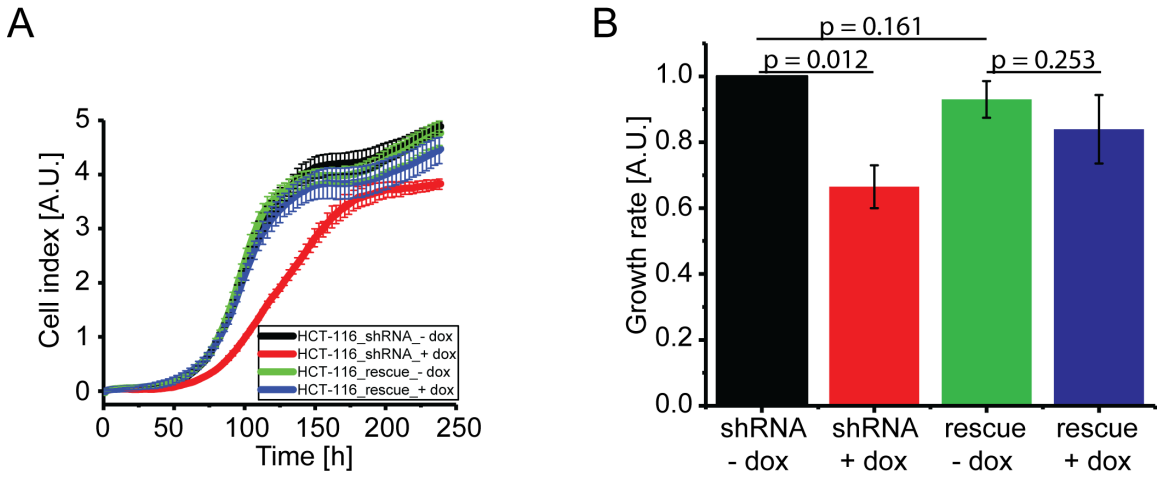

Figure 18: shRNA-resistant PDEδ construct rescues cell growth in HCT-116. A Representative RTCA profiles (N=3) for stable HCT-116 shRNA PDEδ (black, red) and stable HCT-116 shRNA PDEδ stably expressing the rescue mCherry-PDEδ construct (blue, green). Cell indices ± s.d. of four replicates per independent repeat were measured in the presence (red, blue) or absence (black, green) of doxycycline, which was added at the beginning of the measurement. **B** Growth rates ± s.d. of doxycycline-induced shRNA-PDEδ in HCT-116 with and without mCherry-PDEδ rescue construct expression. Growth rates were calculated by the integration of the area under the RTCA curve over 240 h and normalized to the untreated control (black). Significance was calculated using student's *t* test.

4.2.8 Pharmacological PDEδ inhibition affects proliferation and viability of CRC cells harboring oncogenic KRas

We next studied the effects of pharmacological PDEδ inhibition on growth rate and cell viability within the colorectal cancer cell panel, utilizing the small-molecule inhibitors Deltarasin (Zimmermann et al. 2013) and Deltasonamide 2 (Martin-Gago et al. 2017).

To determine effects on cell growth in dependence of the inhibitor dose, we performed RTCA measurements (Figure 19 and 20). Here, Deltarasin treatment resulted in a steep dose-dependent inhibition of cell growth (Figure 19) starting within

a concentration range of 3 - 5 µM in oncogenic KRas-harboring SW480, HCT-116 and Hke3 cell lines. However, the growth rates of the KRas wild type cell lines HT29 and DiFi were only affected at higher inhibitor concentrations.

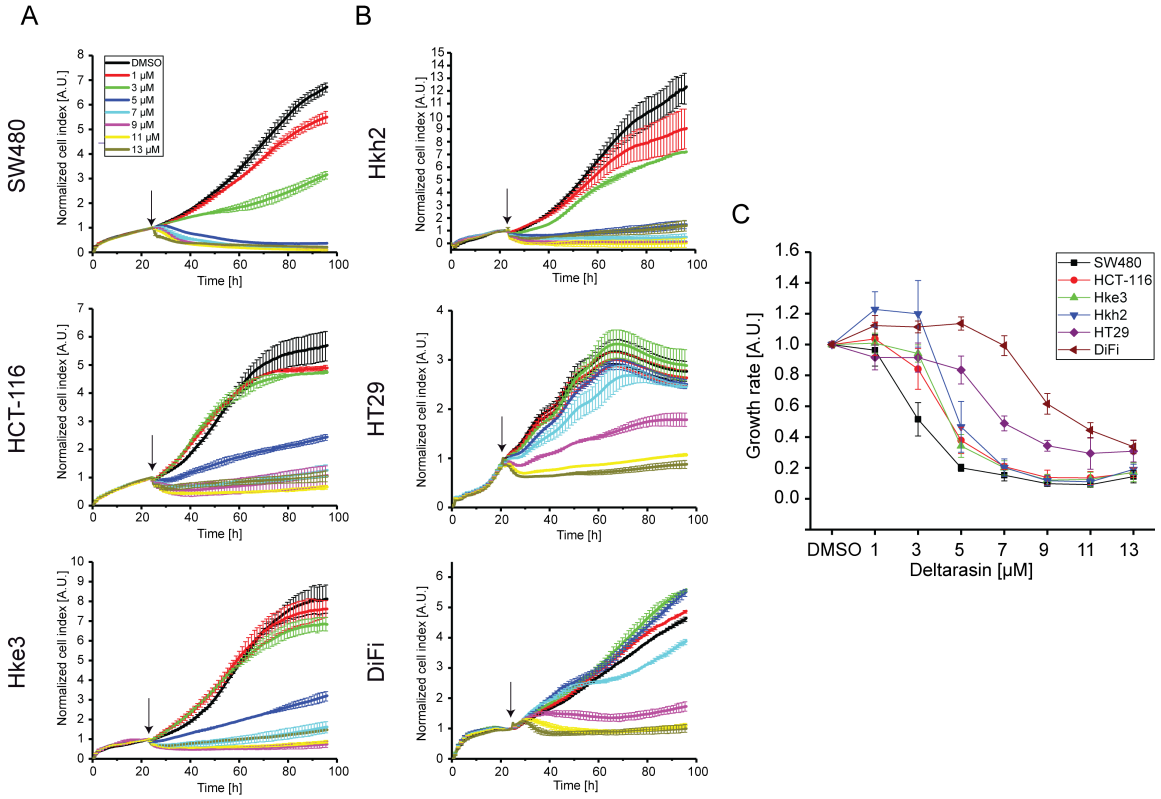

Figure 19: Deltarasin administration affects the growth rate of CRC cell lines. A, B Representative RTCA profiles (N=3) of colorectal cancer cell lines with (A) or without (B) oncogenic KRas mutation treated with different doses of Deltarasin. Cell indices ± s.d. were measured in duplicates per independent repeat and normalized to the time point of Deltarasin administration (arrow). **C** Growth rate ± s.d. in dependence of Deltarasin dose. Growth rates were determined by integration of the area below the RTCA curves over 60 h after drug administration and normalized to the DMSO control.

The to date most potent available small-molecule PDEδ inhibitor Deltasonamide 2 (Figure 20) also exhibited a steep decrease of cell growth in cell lines harboring oncogenic KRas. However, the lowest effective concentration was shifted to lower doses (1.5 - 3 µM). Comparable to Deltarasin treatment, proliferation of KRas wild-type cell lines HT29 and DiFi were affected only at higher Deltasonamide 2

concentrations, whereas the growth rate reduction in Hkh2 cells were comparable to HCT-116 here.

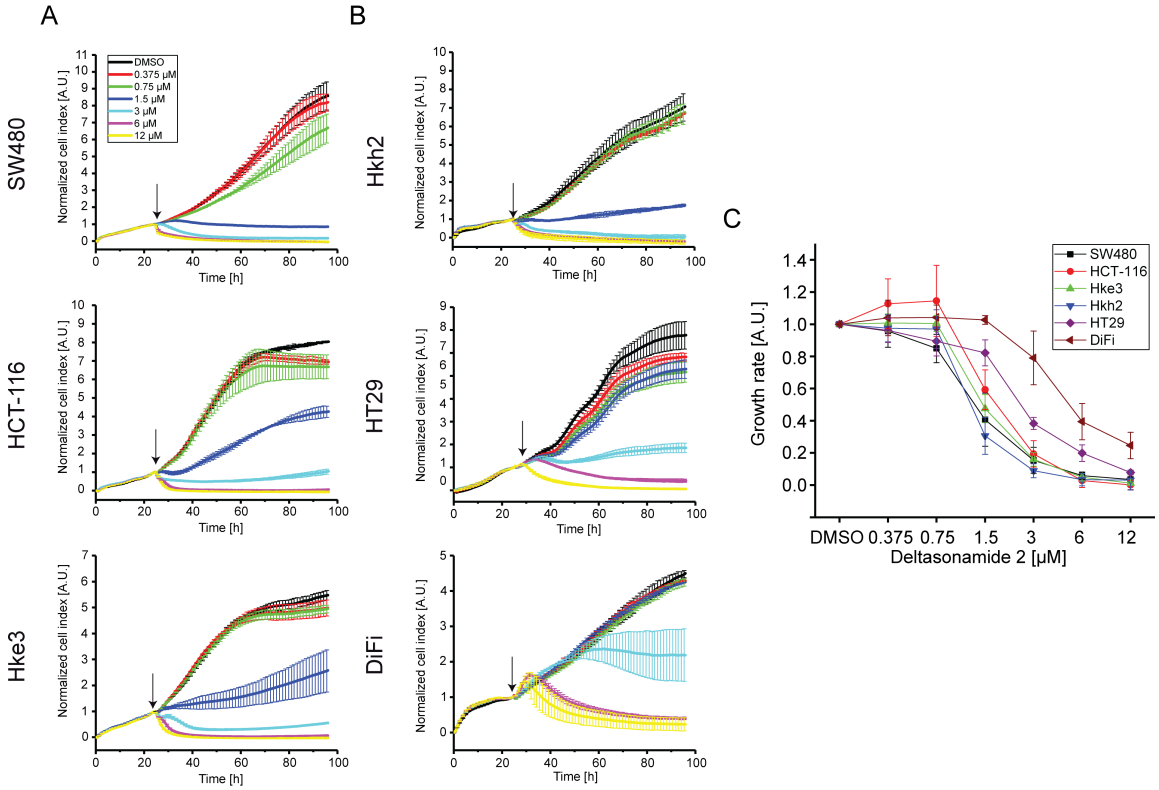

Figure 20: Deltasonamide 2 administration affects the growth rate of CRC cell lines. A, B Representative RTCA profiles (N=3) of colorectal cancer cell lines with (A) or without (B) oncogenic KRas mutation treated with different doses of Deltasonamide 2. Cell indices ± s.d. were measured in duplicates per independent repeat and normalized to the time point of Deltasonamide 2 administration (arrow). **C** Growth rate ± s.d. in dependence of Deltasonamide 2 dose. Growth rates were determined by integration of the area below the RTCA curves over 60 h after drug administration and normalized to the DMSO control.

We further determined cell viability in response to PDEδ inhibitor administration for 24 h by 7-AAD based (7-Aminoactinomycin D) fluorescence assays of single cells in flow through (Figure 21 and 22). 7-AAD is a fluorescent compound that intercalates into double stranded DNA. However, it cannot enter cells with an intact plasma membrane and can therefore be used as a viability stain (Zembruski et al. 2012). Deltarasin administration led to a dose-dependent decrease of cell viability in SW480, HCT-116 and Hke3 cells, starting at a concentration of 5 µM compared to DMSO

control (Figure 21). In the wild-type KRas harboring cell line HT29, no significant increase of cell death was measurable up to a concentration of 7 µM Deltarasin, while the viability of DiFi cells was slightly decreased starting at a concentration of 5 µM.

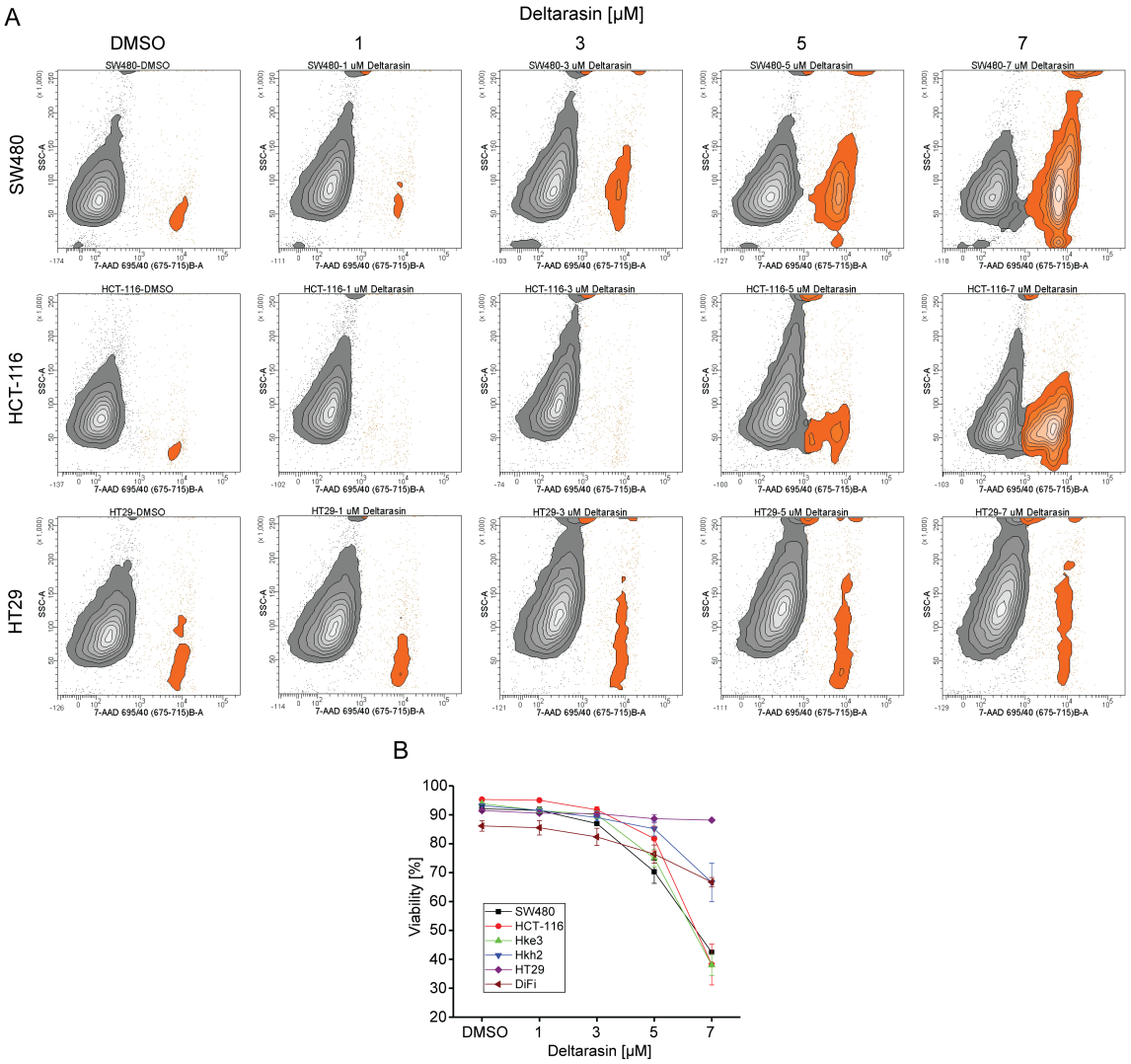

Figure 21: Deltarasin administration reduces viability of CRC cell lines harboring oncogenic KRas. A Representative contour plots (N=3) of side scattering (SSC) versus 7-AAD fluorescence of exemplary CRC cell lines treated with different doses of Deltarasin. 7-AAD negative cells are shown in black, 7-AAD positive cells are shown in orange. Viable, 7-AAD negative cells were gated based on unstained control cells. **B** Cell viability ± s.d. in dependence of Deltarasin dose in CRC cell lines after 24 h of drug administration. Cell death was determined by viability staining using 7-AAD. DMSO was used as vehicle control.

In agreement with the proliferation assays (Figure 19 and 20), treatment with Deltasonamide 2 affected cell viability at lower doses when compared to Deltarasin (Figure 22). Cell death was induced in all oncogenic KRas-harboring cells in a concentration range of 3 - 5 µM. As observed for Deltarasin (Figure 21), HT29 cells showed no dose-dependent increase of cell death compared to the DMSO control and the viability of DiFi cells was only minor affected at higher drug concentrations.

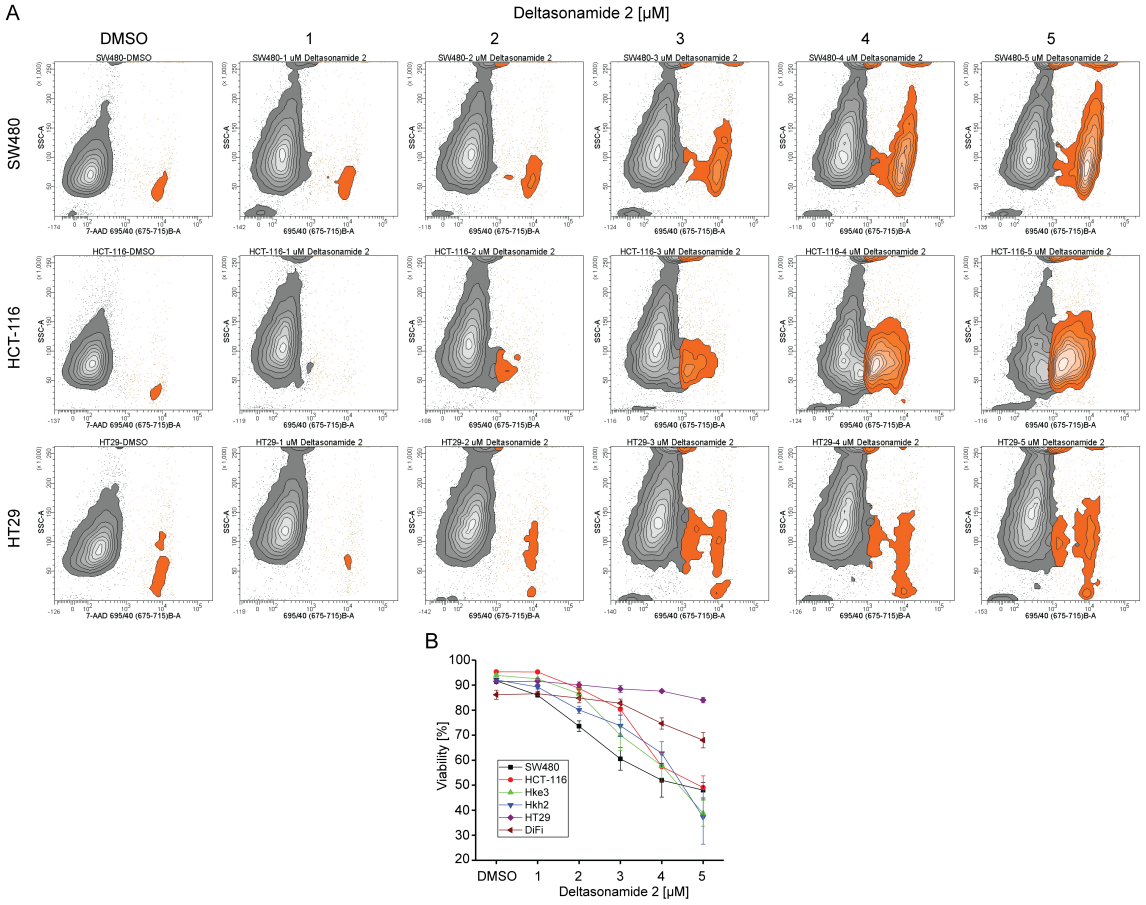

Figure 22: Deltasonamide 2 administration reduces viability of CRC cell lines harboring oncogenic KRas. A Representative contour plots (N=3) of side scattering (SSC) versus 7-AAD fluorescence of exemplary CRC cell lines treated with different doses of Deltasonamide 2. 7-AAD negative cells are shown in black, 7-AAD positive cells are shown in orange. Viable, 7-AAD negative cells were gated based on unstained control cells. **B** Cell viability ± s.d. in dependence of Deltasonamide 2 dose in CRC cell lines after 24 h of drug administration. Cell death was determined by viability staining using 7-AAD. DMSO was used as vehicle control.

To relate both cell growth (RTCA) and viability (7-AAD staining) in dependence of small-molecule PDEδ inhibition, we determined EC_{50} values (RTCA) and Δ cell viability (7-AAD staining) and plotted these against each other (Figure 23 A, C). We opted to determine Δ cell viability here, since survival of wild type KRas-bearing HT29 and DiFi cell lines was barely affected. Therefore, calculation of meaningful EC_{50} values based on the viability assays was impossible. Δ cell viability values were determined as difference in cell viability at highest inhibitor dose (7 µM for Deltarasin and 5 µM for Deltasonamide 2) in comparison to the DMSO control (Figure 21, 22). EC_{50} values for the RTCA were determined by sigmoidal curve fitting of the calculated growth rates from these measurements (Figure 19, 20).

Here, SW480 cells exhibited the lowest EC_{50} in both inhibitor correlation plots (Deltarasin: 2.86 ± 0.31 µM, Deltasonamide2: 1.24 ± 0.06 µM) as well as highly compromised viability. The three isogenic cell lines HCT-116, Hke3 and Hkh2 showed comparable EC_{50} values. However, the cell viability of Hkh2, in which the oncogenic KRas allele was successfully replaced, was significantly less affected by PDEδ inhibition compared to HCT-116 and Hke3. The wild type KRas expressing DiFi and HT29 cells were clearly separated from the cluster of oncogenic KRas harboring cell lines in both correlation plots. The EGFR overexpressing DiFi cells exhibited the highest EC_{50} for both Deltarasin (8.92 ± 0.7 µM) and Deltasonamide 2 (4.02 ± 1 µM), while in case of oncogenic BRaf expressing HT29 cells viability was not affected by inhibitor administration. As already apparent from the determined growth rates (Figure 19, 20), the higher affinity inhibitor Deltasonamide 2 showed a shift to lower EC_{50} values for all CRC cell lines. Apart from that, the correlation plots of both Deltarasin (Figure 23 A) and Deltasonamide 2 (Figure 23 C) were reminiscent in the alignment of the respective cell lines.

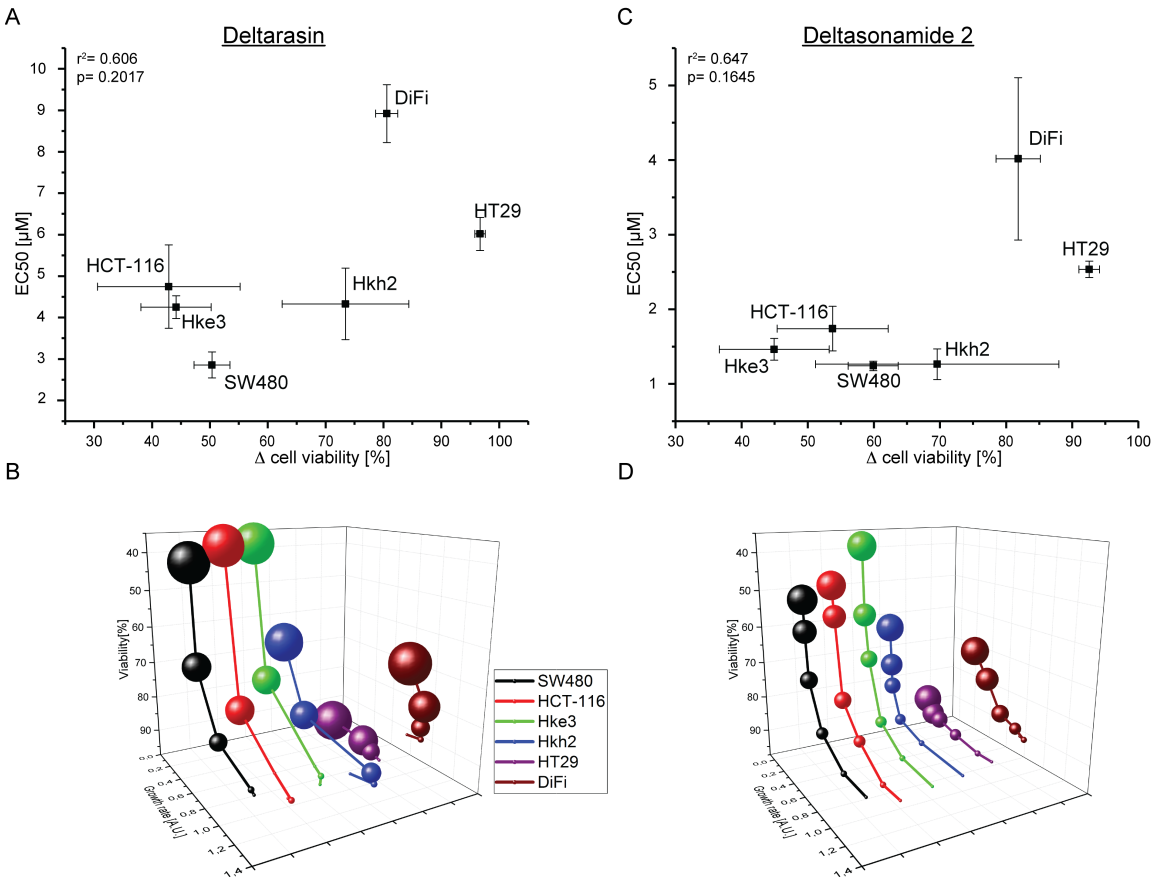

Figure 23: Correlation of growth rate and cell viability upon PDEδ inhibition. A, C Correlation of Δ Cell viability ± s.d. versus EC_{50} ± s.d. for Deltarasin (A) and Deltasonamide 2 (C). Δ cell viability was calculated between the respective used highest inhibitor concentration and the DMSO control (Figure 21, 22). EC_{50} values were determined by sigmoidal curve fit of the growth rates depicted in Figure 19 and 20. **B, D** Four-dimensional correlation of growth rate and cell viability in dependence of inhibitor dose and CRC cell line for Deltarasin (B) and Deltasonamide 2 (D). The dot size is proportional to the applied inhibitor concentration.

To further compare dose-response profiles between Deltarasin and Deltasonamide 2, we plotted viability (as measured by 7-AAD staining) versus growth rate (as measured by RTCA) in dependence of the respective inhibitor dose and cell line (Figure 23 B, D). Again, similar dose-response profiles of the oncogenic KRas-bearing SW480, HCT-116 and Hke3 in form of viability reduction and growth inhibition became apparent for both inhibitors, respectively. The wild type KRas cell lines were

again clearly less affected in both proliferation readouts, whereas the Hkh2 cell line in which the oncogenic KRas allele was replaced by a non-transcribed mutant allele was the most responsive among the KRas wild type cell lines. In case of DiFi cells, mostly cell viability was affected with increasing inhibitor dose, whereas in case of HT29 cells no changes in cell viability were detectable. Instead, both inhibitors primarily affected the growth rate.

4.2.9 PDEδ inhibition affects MAPK signal propagation

To investigate, if the anti-proliferative effects of PDEδ inhibition are caused by impeded Ras signal propagation, we examined the phosphorylation level of the extracellular signal regulated kinase (Erk) (Seger and Krebs 1995, Yoon and Seger 2006) in response to a 5 min EGF stimulus after prior inhibitor treatment for 90 min in SW480 (homozygous KRasG12V mutation) and HT29 (KRas wild type; BRafV600E) cells (Figure 24). Both Deltarasin and Deltasonamide 2 reduced Erk phosphorylation in the oncogenic KRas harboring SW480 cells. Strikingly, the higher affinity inhibitor Deltasonamide 2 was four-times more effective here. In contrast, Deltasonamide 2 did not decrease Erk phosphorylation level in HT29 and Deltarasin administration even led to significantly increased Erk phosphorylation levels. However, this could be a consequence of already known off-target effects (Papke et al. 2016).

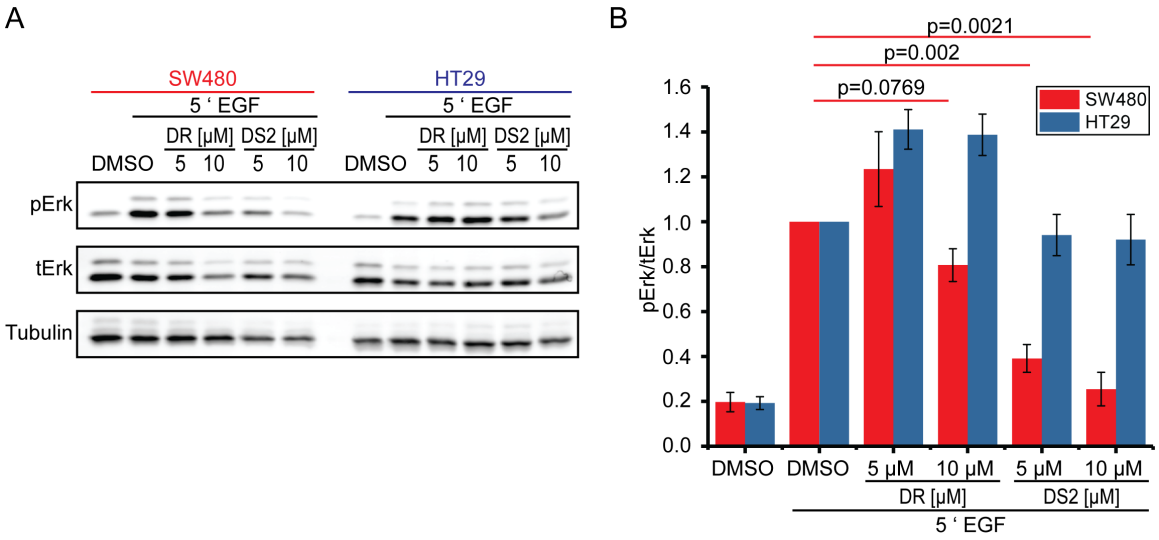

Figure 24: Effects of Deltarasin and Deltasonamide 2 on Erk phosphorylation in CRC. A Total Erk (tErk) and phosphorylated Erk (pErk) protein level in SW480 and HT29 cells determined by western blot analysis. Cells were serum-starved for 16 h and treated with vehicle control (DMSO) or 5 or 10 µM Deltarasin (DR) or Deltasonamide 2 (DS2) for 90 min, respectively. Phosphorylation levels were compared after 5 min stimulation with 100 ng/ml EGF. Tubulin was used as loading control. **B** Quantification of pErk/tErk levels ± s.e.m. (N=4) normalized to the EGF-stimulated DMSO control. Significance was calculated using student's *t* test.

5. Discussion and perspective

5.1 Deltasonamides as new competitive small molecule PDEδ inhibitors

Deltasonamides are the latest chemotype of competitive small molecule PDEδ inhibitors. In contrast to the first- and second-generation inhibitors Deltarasin (Zimmermann et al. 2013) and Deltazinone 1 (Papke et al. 2016), which both exhibit three hydrogen bonds to the farnesyl binding pocket of PDEδ, Deltasonamides engage in a total of seven H-bonds of which two are mediated by water molecules. Due to the improved inhibitor binding, Deltasonamides showed remarkably different properties compared to the former inhibitor classes, which will be discussed in detail below.

5.1.1 Deltasonamides are not displaced from PDEδ by Arl2 activity

The small GTPase Arl2 is essential for the localized release of farnesylated cargo from PDEδ in the perinuclear area. Here, Ras isoforms are kinetically trapped on different endomembrane compartments, depending on their secondary localization motif and from there transported back to the PM via directed vesicular transport ensuring enrichment at the PM (Schmick et al. 2014, Schmick et al. 2015). Arl2-GTP binds to “loaded” PDEδ independent of the cargo carried (Ismail et al. 2011), implying that small molecule inhibitors can also be displaced from the farnesyl binding pocket of PDEδ by allosteric binding of Arl2-GTP to the PDEδ-inhibitor complex. Indeed, fluorescent polarization measurements of fluorescently labeled inhibitor analogues showed that Deltarasin as well as Deltazinone 1 are rapidly displaced from PDEδ *in vitro* in the presence of Arl2-GTP (Martin-Gago et al. 2017). This explains the high difference between measured nano-molar “in cell” K_D’s and micro-molar inhibitor concentrations necessary to affect cell growth for Deltarasin and Deltazinone 1 in oncogenic KRas-dependent hPDAC cell lines (Papke et al. 2016). Because both farnesylated cargo and small molecule inhibitors bind competitively to the hydrophobic binding pocket of PDEδ, the fraction of bound cargo versus inhibitor is dependent on the relative concentrations of both and their corresponding binding affinities. Therefore, some fraction of PDEδ will always bind to farnesylated cargo,

including KRas, leading to enrichment of KRas at the recycling endosome by localized Arl2-mediated release and subsequent vesicular transport back to the PM. Since KRas contains a polybasic stretch in addition to the irreversible farnesylation, which results in a higher affinity to the negatively charged lipids at the inner leaflet of the PM as well as the RE and an corresponding lower dissociation rate ("off-rate"), a small fraction of PDEδ is sufficient to sustain the out-of-equilibrium distribution within the cell (Schmick et al. 2015). In contrast to Deltarasin and Deltazinone 1, the fluorescently labeled Deltasonamide analogue was not displaced from PDEδ *in vitro* even in the presence of 5 µM Arl2 (Martin-Gago et al. 2017). This indicates that the higher number of hydrogen bonds results in an increased affinity of Deltasonamide that overcomes the Arl2-mediated displacement from PDEδ. Thus, lower inhibitor concentrations of Deltasonamide should be sufficient to affect proliferation and survival of oncogenic KRas harboring cells. As apparent from proliferation and viability assays in hPDAC (Figure 9 and 10) as well as human CRC cell lines (Figure 19 to 23), Deltasonamide 2 indeed reduces proliferation and viability at lower doses than Deltarasin. While the effective inhibitor concentrations were still considerably higher than the determined "in cell" K_D's, the required excess of Deltasonamide 2 is 5-fold reduced compared to Deltarasin.

5.1.2 Deltasonamide efficiency is limited by availability rather than affinity

The increased number of hydrogen bonds of Deltasonamide inhibitors does not only decrease Arl2-mediated displacement from PDEδ but also results in lower *in vitro* K_D's of 203 ± 31 pM for Deltasonamide 1 and 385 ± 52 pM for Deltasonamide 2, as determined by competitive fluorescence polarization assays (Martin-Gago et al. 2017). However, the pico-molar affinity that was measured *in vitro* was increased by two orders of magnitude within cells (85 ± 18 nM for Deltasonamide 1 and 61 ± 5 nM for Deltasonamide 2, respectively) and was in the same concentration range as the measured "in-cell" K_D's of Deltarasin (65.6 ± 5.3 nM) and Deltazinone 1 (57.8 ± 16.9 nM). This discrepancy between *in vitro* and "in cell" K_D's for Deltasonamides can be explained by a low availability of inhibitor molecules in the cytoplasm. Assuming that the applied compound concentration to the extracellular environment does not affect

the partitioning of the drug, the partitioning coefficient P can be determined as the ratio of “in cell” and *in vitro* K_D. For Deltasonamide scaffolds this calculation implies that only 0.2 % in case of Deltasonamide 1 and 0.6 % in case of Deltasonamide 2 of the administered inhibitor concentration are available in the cytosol to inhibit the Ras-PDEδ interaction. In contrast, the partitioning of administered Deltarasin as well as Deltazinone 1 into the cytosol is much higher (58.2 % for Deltarasin and 14.5 % for Deltazinone 1). The lower partitioning can be explained by a lower membrane penetration rate of the new chemotype compared to the more lipophilic scaffolds of Deltarasin and Deltazinone 1. This explanation is corroborated from the logP and logD value as predicted with the software platform ACD/Percepta based on the molecular structure (Martin-Gago et al. 2017). The logP values is defined as the concentration ratio of an un-ionized compound between aqueous and organic phase at equilibrium (Kwon 2001), and the logP values of Deltasonamides are comparable to that of Deltazinone 1. In contrast to the logP value, the logD value of a compound additionally takes into account ionization at physiological pH (Kwon 2001). The logD value of Deltasonamides is two times lower compared to Deltarasin and Deltazinone 1. Yet, the “in cell” K_D’s of all compounds lie in a comparable range due to the lower affinity of the first- and second-generation inhibitors. Nevertheless, Deltasonamide 2 showed growth inhibitory effects at 5 – 30-fold lower concentrations compared to Deltarasin or Deltazinone 1 in the oncogenic KRas-dependent hPDAC and hCRC cell lines, implying a higher efficiency despite the lower compound availability within the cell. This means that lower concentrations of Deltasonamide 2 within the cell are sufficient to reduce the fraction of PDEδ molecules available for KRas binding below the threshold that maintains PM enrichment.

The higher efficiency of Deltasonamide 2 was even more prominent on the level of Erk phosphorylation, which we utilized as readout of down-stream signal propagation of oncogenic KRas in response to PDEδ inhibition. 5 µM Deltasonamide 2 led to an approximately 65 % decrease of pErk levels in oncogenic KRas harboring SW480 cells following stimulation with 100 ng/ml EGF for 5 min. In contrast, 10 µM Deltarasin were necessary to reduce pErk by 20 % (Figure 24).

Altogether, this marks Deltasonamide 2 as the most potent inhibitor of the KRas-PDEδ interaction so far. However, the discussed problems need to be solved to promote the development of clinical relevant inhibitors. For this, different strategies could be applied which are discussed in depth below.

5.1.3 Future perspective of PDEδ inhibitors

The previous development of non-covalent small molecule PDEδ inhibitors was based on the Alpha Screen technology (Zimmermann et al. 2013) utilizing an in-house compound library with over 150,000 compounds. Positive hits out of the Alpha Screen were analyzed and promising chemotypes were optimized to enhance affinity while considering solubility and availability (Zimmermann et al. 2013, Papke et al. 2016, Martin-Gago et al. 2017). While the latest inhibitor chemotype Deltasonamide exhibits a high affinity and overcomes the displacement from PDEδ by Arl2-GTP due to a total of seven hydrogen bonds formed, the bioavailability of the drug was remarkably reduced compared to former inhibitors. If the partitioning into cells is already low in two-dimensional cell culture model systems, this availability problem will be amplified in *in vivo* applications. For example, it has already been shown that the heterogeneity of a tumor *in vivo* as well as the corresponding microenvironment (hypoxia, low pH) can negatively influence drug delivery (Feig et al. 2012, Stylianopoulos et al. 2018). However, proliferation and viability assays *in vitro* showed that Deltasonamide 2 is nevertheless the most potent inhibitor of the KRas-PDEδ interaction thus far, indicating that the increased affinity can compensate for the lower availability to some degree. Still, further inhibitor development should completely focus on an enhanced bioavailability of the drug, because Deltasonamides exhibit already a pico-molar affinity *in vitro*.

In case the bioavailability cannot be sufficiently increased without sacrificing too much potency of the drug, other approaches of efficient drug delivery could be investigated. For instance, existing encapsulation techniques that are already explored for other drugs (Singh et al. 2010, Kumari et al. 2014) could be investigated. This could allow the use of compound classes that would otherwise be disregarded due to their poor

bioavailability. However, this approach is a recent development and not yet in depth explored.

Another perspective of future PDEδ inhibitor design could be the switch to covalent inhibitors. Covalent inhibitors are appealing in the first place because lower inhibitor concentration should be sufficient to interfere with spatial Ras localization due to the zero off-rate. However, covalent inhibitors commonly exhibit other difficulties compared to drugs featuring a competitive binding mode. For instance, off-target effects are much more crucial due to the irreversible nature of the interaction. Commonly, covalent inhibitors are designed to target reactive cysteine and lysine residues of the protein of interest (Baillie 2016, Martin-Gago et al. 2017). In case of the farnesyl binding pocket of PDEδ, no such residue is exposed. However, it has been already shown that a covalent modification in the PDEδ farnesyl binding pocket is possible by targeting the glutamic acid at position 88 (Martin-Gago et al. 2017). Still, the advantage of a covalently binding inhibitor over Deltasonamide 2 remains to be shown, since the Arl2-GTP mediated displacement of Deltasonamide 2 from PDEδ is already remarkably low (k_{off} = 0.8 ± 0.1 $s^{-1} \cdot 10^{-3}$) (Martin-Gago et al. 2017).

5.2 PDEδ interference as new strategy for colorectal cancer treatment

Previous studies regarding PDEδ inhibition as new opportunity to target aberrant KRas signaling were restricted to pancreatic ductal adenocarcinoma cell models. This was reasoned by the high abundance (> 90 %) of oncogenic KRas mutation in PDAC (Cox et al. 2014). However, the described therapy approach is not limited to PDAC since other tumor types also frequently harbor oncogenic KRas mutations. One of this other tumor types are colorectal adenocarcinoma, where activating KRas mutations are present in 45 % of all reported cases (Cox et al. 2014). Standard therapy for CRC patients nowadays involves treatment with monoclonal antibodies against EGFR as alternative to systemic cytotoxic chemotherapy (Humblet 2004). Strikingly, EGFR inhibition reduces growth of CRC tumors independent of the EGFR mutation status. However, tumors expressing either oncogenic KRas or BRaf are unresponsive to anti-EGFR therapy approaches (Benvenuti et al. 2007, Di Nicolantonio et al. 2008, Misale et al. 2012). This is not astonishing, since both KRas and BRaf are downstream effectors of EGFR within the MAPK signaling network (Seger and Krebs 1995) and therefore render signal propagation independent of EGFR input within the network in case of oncogenic mutations of either protein. Thus, alternative therapy approaches for oncogenic KRas harboring CRC are desperately needed.

5.2.1 PDEδ interference selectively impedes proliferation and survival of oncogenic KRas harboring CRC

In this study, we explored the applicability of PDEδ interference in CRC by utilizing six CRC cell lines that feature distinct oncogenic mutations and that were all originally derived from patients. Phenotypic effects of PDEδ interference on growth and viability of these cells were investigated using both genetic down regulation by inducible knock down and acute pharmacological interference by small molecule inhibitors. Inducible knock down harbors less unspecific off-target effects compared to most small molecule inhibitors. However, knock down approaches are limited to target validation and cannot be applied for therapy. Here, inhibitors are more beneficial because the used concentrations and the field of application are more controllable.

Both PDEδ knock down and small molecule inhibition by Deltarasin as well as Deltasonamide 2 selectively reduced growth rate and viability of cell lines harboring oncogenic KRas within the CRC cell panel. This emphasizes that the observed effects are a specific result of PDEδ interference. The probability that shRNA-mediated knock down and the administration of two structural unrelated small molecule inhibitors exhibit off-target effects with comparable phenotypic responses only in selected cell lines is rather unlikely.

Both PDEδ knock down and small molecule inhibition were most effective in SW480, a cell line that harbors an oncogenic G12V mutation on both KRas alleles. This indicates that these cells are dependent on oncogenic KRas signaling and thereby on the solubilizing PDEδ functionality and cannot compensate for loss of PDEδ function. Moreover, growth rate and viability of both HCT-116 and Hke3, which are both heterozygote for oncogenic KRas, were clearly reduced upon PDEδ interference. However, the survival and proliferation were less reduced compared to SW480 cells. Among the KRas wild type bearing cell lines, Hkh2 (HCT-116-derived) showed the clearest response to PDEδ knock down and inhibition. The possible reasoning for this will be discussed in chapter 5.2.3.

In contrast, neither HT29 cells nor DiFi cells were affected by PDEδ interference. For HT29 cells, which harbor an oncogenic BRaf (V600E) mutation, this is anticipated, since BRaf is an effector of active Ras in the MAPK network (Moodie et al. 1993, Seger and Krebs 1995). Therefore, oncogenic mutations of BRaf should render cells independent of Ras signal propagation. This became also evident from the fraction of phosphorylated Erk in response to EGF stimulation after prior inhibitor treatment (Figure 24). The pErk level remained unchanged in HT29 cells even after treatment with 10 µM Deltasonamide 2, whereas the fraction of pErk decreased in oncogenic KRas harboring SW480 cells in a dose-dependent manner.

In case of the DiFi cell line, which exhibits increased EGFR expression level, PDEδ inhibition should affect KRas-mediated signal propagation since EGFR is located

upstream of Ras. However, as apparent from our quantitative western blot analysis, DiFi cells express comparable low amounts of Ras protein (Figure 12). Considering further that signal propagation within the cell is not at all a linear process and distinct signaling networks are interconnected by means of cross talk and positive and/or negative feedbacks (Dobrzynski et al. 2014, Koseska and Bastiaens 2017), it is reasonable to assume that the proliferative and survival signals that originate from elevated EGFR levels can be processed independently of Ras proteins.

5.2.2 Interdependence of oncogenic KRas and PDEδ

The wild type KRas-bearing HT29 and DiFi cell lines were not only the least sensitive to PDEδ interference but also expressed the lowest amount of PDEδ protein. In contrast, the oncogenic KRas homozygote SW480 cell line exhibited amplified PDEδ level in agreement with the highest sensitivity to PDEδ interference. As apparent from Figure 12, the PDEδ expression was correlated to both total Ras protein level as well as Ras activity within the CRC cell panel. This strongly implies an interdependence of PDEδ expression and corresponding KRas activity, rendering PDEδ an even more tempting target to interfere with aberrant Ras signaling. The interdependence is based on the solubilizing PDEδ function and the amount of Ras-GTP. However, the interdependence is only manifested on the protein level, whereas corresponding mRNA expression level were completely uncorrelated (Figure 14 B). Furthermore, the PDE6D and KRAS mRNA expression level were not correlated to the respective protein levels within the CRC cell lines (Figure 14 A). That is unsurprising, since many regulatory processes can interfere between mRNA transcription and protein translation.

A different PDEδ expression as well as correlated Ras expression/activity was even present between the three oncogenic KRas harboring cell lines (SW480, HCT-116, Hke3). This correlation was also mirrored in the varying survivability in response to PDEδ interference, at least for the genetic PDEδ knock down (Figure 15). As expected, the viability after PDEδ knock down anti-correlated with the amount of

expressed oncogene, which is the consequence of the interdependence of PDEδ expression and oncogenic KRas activity.

5.2.3 Exploiting oncogene addiction

The above described interdependence of oncogenic KRas activity and PDEδ expression, which peaks in the so-called oncogene addiction (Weinstein and Joe 2006, Sharma and Settleman 2007, Weinstein and Joe 2008), can be exploited to selectively kill oncogenic KRas harboring cancer cells. Oncogene addiction means that cells which express an oncogene can become dependent on the survival signal originating from this oncogene, while other signaling branches are more and more abounded. Consequently, oncogene addiction, which is initially beneficial for the cancer cells, can be exploited to selectively kill cells harboring the oncogene, while cells without the oncogene will still be affected in their growth but survive the treatment.

This feature was also present within our CRC panel. Between KRas wt and oncogenic KRas bearing cell lines, the differences in cell viability were much more pronounced compared to the differences in anti-proliferative effects (Figure 23). Furthermore, our clonogenic assay results after PDEδ knock down suggests that the commitment of oncogene addiction is connected to the expression level of the respective oncogene: Comparison of viability and cell growth of HCT-116 and Hke3 cells, which were derived from HCT-116 and express lower amounts of oncogenic KRas (Fasterius et al. 2017), showed that the viability of Hke3 cells was significantly less affected compared to HCT-116, whereas the proliferation in both cell lines was equally reduced. The concept that oncogene addiction is correlated to the respective protein expression level is further substantiated by a statistic paper reporting a strong correlation of increased Ras expression and oncogenic KRas mutations in patient data derived from The Cancer Genome Atlas (Stephens et al. 2017).

While oncogene addiction can be exploited to selectively kill cancer cells, decreased cell proliferation independent of the mutational status of the targeted oncogene is

somehow expected. Since KRas is a central effector of intracellular proliferative signaling, one would expect that the depletion of a large amount of the KRas fraction from the PM as a consequence of PDEδ inhibition negatively affects cell growth. This is substantiated by the different effects on proliferation concerning the wild type KRas bearing cell lines within our cell panel. Between these three cell lines (Hkh2, HT29, DiFi) PDEδ interference was most effective in Hkh2, the cell line that was derived from HCT-116 by replacing the oncogenic KRas allele with a non-transcribed one (Fasterius et al. 2017). In contrast to the other two KRas wild type cell lines, Hkh2 cells do not, to our knowledge, bear another oncogenic mutation. This renders Hkh2 more dependent on “normal” KRas signal propagation compared to HT29 (oncogenic BRaf mutation) or DiFi (EGFR overexpression), which is well mirrored in our proliferation assays. However, the anti-proliferative effect is still remarkably lower compared to oncogenic KRas bearing cell lines (Figure 15 and 23). This is consistent with the fact that the residual fraction of KRas that remains at the PM after PDEδ interference is sufficient for signal propagation of “normal” cells but not for cells dependent on oncogenic KRas signaling (Schmick et al. 2015).

Together, this implies that cancer treatment should be more focused on exploiting oncogene addiction. Thereby, tumor relapse rates could be reduced because more tumor cells are actually killed, whereas normal cells receive less splash damage. However, tumor relapse can also be a consequence of tumor heterogeneity (Fidler and Hart 1982, Heppner 1984). Even after treatment with drugs that selectively kill the respective cancer cells, chances are high that a sub-population of tumor cells, even one cell could be enough, featured additional oncogenic mutations or became resistant to the first therapy approach. To overcome such relapse problems, combinatorial therapy strategies could be applied.

5.2.4 Combined anti-KRas and anti-EGFR therapy

In combinatorial drug treatment strategies, distinct drugs are either administered in parallel or sequentially. The idea here is to simultaneously interfere with two independent proliferative networks to both effectively target several subpopulations

within the tumor and reduce chances of later tumor relapse. For CRC tumors harboring oncogenic KRas mutations it would therefore be reasonable to explore combinatorial anti-KRas and anti-EGFR therapy, since antibody-treatment against EGFR is already approved and, more importantly, efficient in the cure of colorectal cancer if neither oncogenic KRas nor BRaf mutations are present (Benvenuti et al. 2007, Di Nicolantonio et al. 2008, Misale et al. 2012). Furthermore, a possible heterogeneity problem could be also overcome by this strategy. By first treating the CRC patient with a PDEδ inhibitor, the cancer cells harboring an oncogenic KRas mutation should become sensitized for sequential anti-EGFR treatment. The order of drug administration may have a big influence here, as it was already reported in previous studies that explored combinatorial drug treatment strategies (Lee et al. 2012).

However, one of the biggest challenges in basic research of combining anti-EGFR therapy approaches with other drugs is the ineffectiveness of the anti-EGFR antibodies in 2D cell culture models. One explanation for this is the missing immune response or the heterogenic cellular environment *in vivo*, which cannot be resembled in 2D cell culture. The DiFi cell line is one of the few available cell culture model systems that is responsive to anti-EGFR antibody treatment (Moroni et al. 2005), most likely because they harbor a highly amplified EGFR expression level (Gross et al. 1991, Moroni et al. 2005). One possibility to explore combinatorial treatment of PDEδ inhibition and anti-EGFR antibodies could be the use DiFi cells that were engineered to express oncogenic KRas (Misale et al. 2012), yet one would still miss the cellular context-dependent influences. Another alternative would be to utilize 3D organoid culture as model system, which would more closely mirror the environment *in vivo (Sato et al. 2009, Sato et al. 2011)*. It is anyway the next necessary step to investigate the effectiveness of PDEδ inhibitors in organoid model systems, since most tested inhibitors in 2D *in vitro* model systems fail in later preclinical stages (Zeeberg et al. 2016).

5.2.5 Small intestine organoids as advanced model system

As described above, organoids, in contrast to classical 2D cell culture, more closely reassemble the environment *in* vivo. For instance, small intestinal organoids, which can be grown from single stem cells that were isolated from the intestine of a mouse, resemble the *in vivo* structure of intestine tissue in a self-organized process. In the presence of essential stemness maintenance factors, they can be grown as a 3D culture utilizing a matrigel matrix and can be indefinitely maintained (Sato et al. 2009, Sato et al. 2011). Therefore, 3D organoid culture is a valuable alternative to tumor xenografts model in nude mice.

First pilot experiments in small intestine organoids, either isolated from a wt mouse or a mouse that was engineered to exhibit an endogenous oncogenic KRas allele, showed that small molecule PDEδ inhibition selectively affected proliferation and survival of oncogenic KRas harboring organoids over time. This is another evidence that small molecule PDEδ inhibitors could indeed be effective *in vivo*. The first generation small molecule inhibitor Deltarasin was already successfully tested in xenografted tumor models in nude mice, resulting in stalled tumor volume increase (Zimmermann et al. 2013). However, more experiments in organoids are necessary to assess the role of oncogenic mutations in a heterogenic system featuring stem cells and a multitude of partly to fully differentiated cells.

6. Materials and Methods

6.1 Materials

6.1.1 Buffers and media

1x PBS (phosphate buffered saline)	138 mM NaCl, 2.7 mM KCl, 10 mM Na_2HPO_4, 1.8 mM KH_2PO_4 (adjust to pH 7.4)
1x TBS (tris buffered saline)	100 mM Tris-HCl (pH 7.5), 150 mM NaCl
1x TBS-T	100 mM Tris-HCl (pH 7.5), 150 mM NaCl, 0.1 % (v/v) Tween-20
RIPA buffer	20mM Tris (pH 7.5), 150 mM NaCl, 0.5mM Na_2-EDTA, 1 % sodium deoxycholate, 0.1 % sodium dodecyl sulfate, 1 % IGEPAL, supplemented with Complete Mini EDTA-free protease inhibitor (Roche Applied Science) and 1 % phosphatase inhibitor cocktail 2 and 3 (P5726 and P0044, Sigma Aldrich)
Bacterial lysis buffer	50 mM Tris-HCl (pH 7.5), 400 mM NaCl, 1mM DTT, 1 % Triton X-100, 1mM EDTA, supplemented with Complete Mini EDTA-free protease inhibitor (Roche Applied Science)
RBD pull down wash buffer	50 mM Tris-HCl (pH 7.5), 50 mM NaCl, 20 % Glycerol, 1 mM EDTA, 1 mM DTT, supplemented with Complete Mini EDTA-free protease inhibitor (Roche Applied Science)
RBD pull down cell lysis buffer	50 mM Tris-HCl (pH 7.5), 200 mM NaCl, 10 % Glycerol, 2.5 mM $MgCl_2$, 1 % Triton X-100, supplemented with Complete Mini EDTA-free protease inhibitor (Roche Applied Science)
1x separating gel buffer	1.5 M Tris-HCl (pH 8.8)
1x stacking gel buffer	0.5 M Tris-HCl (pH 6.8)
1x SDS Running buffer	25 mM Tris-base, 192 mM glycine, 0.1 % SDS
2x SDS sample buffer	150 mM Tris-HCl (pH 6.8), 1.2 % SDS, 30 % Glycerol, 2.1 M β-mercaptoethanol, 0.1 % bromophenolblue
5x SDS sample buffer	60 mM Tris-HCl (pH 6.8), 2 % SDS, 25 % Glycerol, 14.4 mM β-mercaptoethanol, 0.1 % bromophenolblue
1x Transfer buffer	25 mM Tris-base, 192 mM glycine, 20 % (v/v) methanol
SOC (super optimal broth) medium	2 % (20 g/l) trypton, 0.5 % (5 g/l) yeast-extract, 10 mM NaCl, 2.5 mM KCl, 10 mM $MgCl_2$, 20 mM glucose

TB (terrific broth) medium	1.2 % (12 g/l) trypton, 2.4 % (24 g/l) yeast-extract, 17 mM KH_2PO_4, 72 mM K_2HPO_4, 0.4 % (4 ml/l) glycerol
LB (lysogeny broth) medium	1 % (10 g/l) tryptone, 0.5 % (5 g/l) yeast-extract, 1 % (10 g/l) NaCl
LB agar plates with respective selection antibiotics	LB medium with 15 g/l agar, supplemented with respective antibiotics (Ampicillin: 100 µg/ml, Kanamycin: 50 µg/ml)
TAE (Tris-acetate-EDTA) buffer	40 mM Tris (pH 7.5), 20 mM NaOAc, 1 mM EDTA
DNA sample buffer (10x)	50 % Glycerol, 0.1 % Orange G, 100 mM EDTA

6.1.2 Commercial kits and reagents

Name	**Supplier**
Accutase™	EMD Millipore Corporation
DNA 2-log Ladder	NEB
DNA Clean & Concentrator™ kit	Zymo research
Dulbecco's Modified Eagle's Medium (DMEM)	PAN Biotech GmbH
Effectene transfection kit	Qiagen
Fetal calf serum (FCS)	PAN Biotech GmbH
FuGene® 6 transfection reagent	Promega
High Capacity cDNA Reverse Transcription Kit	Thermo Fisher Scientific
L-Glutamine	PAN Biotech GmbH
Lipofectamine 2000 transfection kit	Invitrogen
Micro BCA™ Protein Assay kit	Thermo Fisher Scientific
Non-essential amino acids (NEAA)	PAN Biotech GmbH
Odyssey® Blocking Buffer (TBS)	LI-COR
Pierce™ Glutathione Magnetic Agarose Beads	Thermo Fisher Scientific
Precision Plus Protein™ Dual Color	Bio-Rad
Q5® High-Fidelity DNA Polymerase	New England Biolabs

Q5® Site-Directed Mutagenesis Kit	New England Biolabs
QIAprep® Spin Miniprep kit	Qiagen
RedSafe Nucleic Acid Staining Solution	JH Science
RNA isolation kit	Zymo research
T4 DNA-Ligase	Invitrogen
TaqMan® gene expression master mix	Thermo Fisher Scientific
TaqMan®-assays: PDE6D (Hs01062025_m1) KRas (Hs00364282_m1) GAPDH (Hs02758991_g1)	Thermo Fisher Scientific
Trypsin/EDTA solution	PAN Biotech GmbH
Zymoclean™ Gel DNA recovery kit	Zymo research

6.1.3 Chemicals

Name	**Supplier**
2-Mercapto-ethanol	SERVA Electrophoresis GmbH
7-Aminoactinomycin D (7-AAD)	BD Bioscience
Acetic acid	Sigma-Aldrich
Bovin serum albumin, fraction V, pH 7.0 (BSA)	SERVA Electrophoresis GmbH
Ammonium persulfate (APS)	SERVA Electrophoresis GmbH
Ampicillin sodium salt	SERVA Electrophoresis GmbH
Bromophenolblue	Sigma-Aldrich
Crystal violet	Sigma-Aldrich
Deltarasin	Chemietek
Dimethyl sulfoxide (DMSO)	SERVA Electrophoresis GmbH
Dithiothreitol (DTT)	Fluka® Analytical
Doxycycline	Sigma-Aldrich
Epidermal growth factor	Sigma-Aldrich
Ethanol	J.T.Baker
Ethylenediaminetetracetic acid (EDTA)	Fluka® Analytical
Glycerol	GERBU Biotechnik GmbH
Glycine	Carl Roth GmbH
Isopropanol	J.T.Baker

Isopropyl β-D-1-thiogalactopyranoside (IPTG)	Applichem
Kanamycin sulfate	GERBU Biotechnik GmbH
Magnesium chloride ($MgCl_2$)	Merck KG
Methanol	Sigma-Aldrich
N,N,N',N'-Tetramethylene-diamine (TEMED)	Carl Roth GmbH
Phosphatase inhibitor cocktail 2 & 3	Sigma-Aldrich
Potassium-dihydrogenphosphate (KH_2PO_4)	Carl Roth GmbH
Puromycin	Sigma-Aldrich
Sodium chloride (NaCl)	Fluka® Analytical
Sodium dodecyl sulfate (SDS)	Carl Roth GmbH
Tris-base	Carl Roth GmbH
Tris-HCl	J.T.Baker
Triton X-100	SERVA Electrophoresis GmbH
Tween 20	SERVA Electrophoresis GmbH

6.1.4 Antibodies

Antibody	Dilution	Supplier
anti-PDE6D (sc-50260)	1:200	Santa Cruz
anti-Cyclophylin-B (Ab16045)	1:3,000	Abcam
anti-panRas (OP40)	1:1,000	Calbiochem
anti-mCherry (Ab1674453)	1:1,000	Abcam
anti-α-tubulin (T6074)	1:3,000	Sigma
anti-Erk1/2 (Ab36991)	1:1,000	Abcam
anti-phospho-p44/42 (Thr202/Tyr204) (#4370)	1:1,000	Cell Signaling Technology
IRDye 680 d@rb IgG	1:10,000	LI-COR
IRDye 800 d@ms IgG	1:10,000	LI-COR
IRDye 800 d@gt IgG	1:10,000	LI-COR

6.2 Cell biology

6.2.1 Mammalian cell culture

The pancreatic ductal adenocarcinoma cell lines PANC-1, PANC-Tu-1, MiaPaCa2 and BxPc-3 (all cell lines were a kind gift from Prof. Dr. Stephan Hahn) as well as colorectal cancer cell lines HCT-116 (ATCC American Type Culture Collection), Hke3 (kind gift from Dr. Owen Sansom), Hkh2 (kind gift from Prof. Dr. Walter Kolch), DiFi (kind gift from Dr. Clara Montagut) and SW480 (ATCC) were maintained in DMEM (Dulbecco's modified Eagle medium) supplemented with 10 % FCS (fetal calf serum), 2 mM L-glutamine and 1 % NEAA (non-essential amino acids), at 37°C and 5 % CO_2 in a humidified incubator. HT29 cells (ATCC) were maintained in Ham's medium, supplemented with 10 % FCS and 1 mM L-glutamine, at 37°C and 5 % CO_2 in a humidified incubator.

Cell line identity was validated by STR-profiling (DSMZ, Braunschweig, Germany) and all cell lines were routinely tested for mycoplasma.

6.2.2 Cell line maintenance and cryo preservation

To ensure optimal growth conditions, adherent cells have to be passaged on a regular basis. Otherwise, confluency and resulting contact inhibition could lead to a perturbation. For passaging, the growth medium was removed and the cells were washed with 1x PBS. Subsequently, a trypsin/EDTA solution was applied for 5 to 10 min at 37 °C to detach the cells. Due to the short incubation time, only extracellular proteins are cleaved by the digestion enzyme, while the cellular integrity is not affected. Detached cells were resuspended in fresh growth medium and seeded at the proper density after determining the cell number with a cell counter (Vi-Cell XR, Beckman Coulter). For long time storage, cells were stored at -150 °C in "freezing" medium, containing 10 % DMSO as cryo-protectant to prevent ice crystal formation. For this, cells were collected by centrifugation at 200 g for 5 min. The resulting cell pellet was resuspended in "freezing" medium with a concentration of 1 - $2 \cdot 10^6$ cells per ml and divided into CryoPure screw cap tubes. Subsequently, the cells were

frozen down with a constant cooling rate of -1 °C per min in a CoolCell® cell freezing container placed first into a -80 °C freezer overnight and then transferred to a -150 °C freezer for longtime storage.

6.2.3 Generation of stable shRNA expressing cell lines

Lentiviruses were produced by transfecting packaging cells (HEK293T) with a three plasmid system. For transfections 6 µg pCMVΔR8.2, 2 µg pHIT G and 4 µg plasmid DNA, either encoding PDEδ-targeting or non-targeting shRNA (all plasmids were kind gifts from Prof. Dr. Stephan Hahn), were combined with 32 µl of FuGene transfection reagent in a final volume of 600 µl serum-free medium and incubated for 30 min at RT. Subsequently, the transfection mixture was added to 50 % confluent HEK293T cells in a 10 cm dish. Cells were incubated for 16 h (37 °C and 5% CO_2), before the medium was exchanged to remove remaining transfection reagent. 48 h post transfection, lentivirus-containing supernatants were collected and filtered (0.2 µm pore size) for subsequent infection of target cells. 0.5 – 2 ml viral supernatant containing 10 µg/ml polybrene was immediately used to infect target cells in 6-well plates at 50% confluency. After an initial incubation period of 24 h, all lentivirus containing supernatants were removed and the cells were supplied with fresh medium, containing the appropriate amount of puromycin for selection. Puromycin tolerance was tested for all target cell lines prior to shRNA transduction (Table 2).

Table 2: Puromycin concentration used for selection of stable cell lines

Cell line	Puromycin [µg/ml]
SW480	2
HCT-116	1
Hke3	1
Hkh2	1
HT29	1.5
DiFi	1

6.2.4 Transient transfection

For transient transfection of plasmid DNA, either Effectene for MDCK cells or Lipofectamine 2000 for MiaPaCa-2 cells were used as transfection reagents according to the manufacturers' protocol. To transfect an 8-well Lab-Tek chamber with Effectene, 1 µg plasmid DNA was mixed with 8 µl Enhancer in 360 µl Buffer EC. After 5 min incubation at RT, 10 µl Effectene were added and the mixture incubated for another 15 min at RT. Afterwards, 640 µl of complete growth medium were added and the mixture equally added to all wells in a drop-wise manner.

To transfect an 8-well Lab-Tek chamber with Lipofectamine 2000, 4 µg plasmid DNA were added to 240 µl serum free medium (OptiMEM) and 10 µl Lipofectamine 2000 were added to additional 240 µl OptiMEM. After 5 min incubation at RT, both mixtures were combined and incubated for another 20 min. Finally, 60 µl of transfection master mix were applied to each well. After six hours, medium was exchanged to fresh growth medium.

6.2.5 Generation of stable PDEδ-rescue construct expressing cell line

To generate a PDEδ construct that resists shRNA-mediated degradation, eight synonymous point mutations were introduced into the targeting region of the PDEδ shRNA of a previously published mCherry-PDEδ construct (Chandra et al. 2011) using Q5® Site-Directed Mutagenesis Kit according to the manufacturer's protocol (see 6.3.5). After sequence validation, the mutated mCherry-PDEδ construct was cloned into a PiggyBac vector (System Bioscience) utilizing the restriction enzymes SpeI and NotI (NEB). Afterwards, HCT-116 cells were co-transfected with the above described construct and a PiggyBac transposase (System Bioscience, ratio 1:1) to enable genome integration (Wilson et al. 2007, Zhao et al. 2016). Stably transfected cells were selected by fluorescence activated cell sorting (FACS; (Herzenberg et al. 1976)) based on mCherry fluorescence one week after transfection.

6.2.6 Real-time cell analysis

RTCA measurements were performed using 16-well E-plates on a Dual Plate xCELLigence instrument (Roche Applied Science) in a humidified incubator (37°C, 5 % CO_2). RTCA measures the impedance-based cell index (CI), which is a dimensionless parameter that evaluates the ionic environment at the electrode/solution interface. This information is further integrated into the cell number (Abassi et al. 2004). Continuous impedance measurements every 15 min were monitored for up to 300 hours. Before the cells were seeded into the chambers, blank measurements were performed with growth medium without cells. The number of seeded cells was depended on the cell line. Accordingly, 1 - $2 \cdot 10^4$ cells were plated in each well of the 16-well plates for inhibitor dose-response measurements (~96 h) and 0.75 - $2 \cdot 10^3$ cells per well for shRNA-mediated knock down measurements (~ 240 h). After seeding, cells were allowed to grow for one day to allow them to reach steady growth before small-molecule inhibitor administration. In contrast, for cells that stably expressed the inducible shRNA against PDEδ or non-targeting shRNA, doxycycline was directly applied to the wells at the beginning of the experiment. For the dose-dependent inhibitor measurements, the amount of DMSO was kept constant between the individual conditions and did not exceed 0.24 %. Cell indices were normalized to the time point of drug administration. For shRNA experiments no normalization was applied.

6.2.7 Clonogenic assays

Sparsely seeded cells (1 – $2 \cdot 10^3$ per well) were maintained in 6-well plates in the presence or absence of 200 ng/ml doxycycline that was applied one day after seeding. Fresh growth medium, supplemented with fresh doxycycline, was supplied every two to three days. After ten days, cells were fixed with 4 % PFA for 20 min and subsequently incubated with 0.05 % (v/v) crystal violet for 20 min to stain the individual colonies. The “analyze particle” plug-in of ImageJ was used for quantification of the total cell number and the average colony size. Because overlapping colonies were apparent for some cell lines and conditions, a cell profiler

pipeline was utilized to separate these overlapping colonies. The suitable pipeline was programed by Dr. Jana Harizanova.

6.2.8 Apoptosis assay

Apoptosis assays were performed on a LSR II flow cytometer (BD Bioscience). For this, cells were seeded in 6-well plates at a density of $2 \cdot 10^5$ cells per well and treated with different concentrations of small-molecule inhibitors (Deltarasin or Deltasonamide 2) for 24 h. DMSO was used as a vehicle control. Subsequently, the supernatant was collected in FACS vials and the cells were washed with 1 ml PBS. Afterwards, cells were detached with 0.5 ml Accutase™. The detached cells were re-suspended in 1 ml PBS and transferred to the respective FACS vials and centrifuged at 200 g for 5 min. The supernatant was discarded and the cells were washed twice with PBS. Afterwards, cell pellets were re-suspended in 100 µl PBS containing 5 µl of 7-AAD (BD Bioscience) to stain for dead cells. Samples were vortexed and incubated in the dark for 15 min at ambient temperature. Afterwards, 200 µl PBS was added and the samples were transferred to fresh FACS vials through filter lids. Single cell fluorescence was measured in flow through within one hour after transfer using 488 nm as excitation wave length and the emission filter 695/40. Measurements were acquired and gated with the BD FACSDiva™ software.

6.2.9 Small molecule inhibitor treatment

Deltarasin (Lot. No. 1) was purchased from Chemietek. Deltasonamide 1 and 2 were synthesized in-house as described in (Martin-Gago et al. 2017). For RTCA, Deltarasin was used in a concentration range of 1 to 13 µM and Deltasonamide 1 and 2 were used in a concentration range of 0.375 to 12 µM. For apoptosis assays, inhibitors were used in a concentration range of 1 to 7 µM (Deltarasin) and 1 to 5 µM (Deltasonamide 2), respectively. For the KRas re-localization study, Deltasonamide 2 was used at a concentration of 5 µM.

6.3 Molecular biology

6.3.1 Transformation of chemical competent *E. coli*

Mammalian plasmid DNA can be amplified using chemical competent bacteria strains (here: E. *coli* XL10Gold). For transformation, 100 µl bacteria suspension were thawed on ice and mixed gently with 3.5 µl 2.25 M DTT (dithiothreitol) to enhance transformation efficiency. Either, 10 µl ligation-mix (see 6.3.3) or 1 µl plasmid DNA were gently added and incubated on ice for 30 min. Subsequently, the bacteria were heat-shocked at 42 °C in a water bath for 45 seconds and incubated on ice for at least two min. Afterwards, 400 µl SOC medium were added and the bacteria incubated at 37 °C for 1 h on a shaker (200 rpm). 100 µl bacteria suspension were plated on an agar plate containing the appropriate antibiotic for selection and incubated overnight at 37 °C. On the next day, single colonies were used to inoculate a 5 ml overnight culture in TB medium. To harvest the plasmid DNA, 2 ml of the overnight culture were purified using the DNA preperation QIAprep® Spin Miniprep kit (Qiagen) according to the manufacturer's protocol.

6.3.2 Polymerase chain reaction

Polymerase chain reaction (PCR) (Mullis et al. 1986) can be used, among other things, to exponentially amplify the coding region of a desired protein out of a plasmid vector for sub-cloning into another backbone. For this, amplification primers were designed that also introduced restriction endonuclease enzyme recognition sequences on both sites. DNA of interest was amplified by Q5® High-Fidelity DNA Polymerase (Table 3 and 4):

Table 3: Pipetting schema for PCR reaction

Components	50 µl reaction	Final concentration
5x Q5 reaction buffer	10 µl	1x
10 mM dNTPs	1 µl	200 µM
10 µM forward primer	2.5 µl	0.5 µM
10 µM reverse primer	2.5 µl	0.5 µM
Template DNA	1 ng	
Q5 Polymerase	0.5 µl	0.02 U/µl
Nulease-free water	To 50 µl	

Table 4: Cycling conditions for Q5 polymerase PCR

Step	Temperatur [°C]	Time [s]
Initial denaturation	98	30
35 Cycles	98	10
	50 – 72	30
	72	30 per kb
Final extension	72	120
Hold	4	∞

After PCR amplification, the DNA was purified using the Zymo DNA Clean & Concentrator™ kit (Zymo research) according to the manufacturer's protocol.

6.3.3 Restriction- Ligation

Restriction-ligation is a convenient method to insert a DNA sequence of interest into a plasmid backbone. In a first step, both insert and vector were cut with restriction endonucleases (NEB), which recognize specific DNA sequences, under conditions according to the free online tool "NEB double digest finder". The vector was further incubated with 1 U CIAP (calf intestinal alkaline phosphatase) for an additional hour to dephosphorylate free 5' DNA-ends and thereby prevent self-ligation. To separate and purify cut vector and insert, agarose gel electrophorese was performed (see 6.3.4). Afterwards, the insert could be incorporated into the vector between the

complementary DNA overhangs utilizing the enzyme DNA T4 ligase. For this, 100 ng vector were ligated with an amount of insert, used in a fourfold molar excess, according to the following equation (1):

$$\text{Amount insert [ng]} = \frac{100\ \text{ng vector} \cdot [\text{bp}]\ \text{insert} \cdot 4}{[bp]\ vector} \quad (1)$$

Ligated DNA was then amplified in E. *coli* as described in 6.3.1.

6.3.4 Agarose gel electrophorese

Agarose gel electrophorese enables the separation and thereby purification of DNA fragments of different molecular weights. Depending on the size of the DNA fragments of interest, 1 – 2 g low-melting agarose were melted in 100 ml 1x TAE buffer supplemented with 5 µl RedSafe Nucleic Acid Staining Solution to visualize DNA under UV light. After solidification of the gel, DNA samples, mixed with 10x DNA sample buffer, were size-separated by applying a constant voltage of 120 V for 30 min. 2-log ladder (NEB) was used as molecular weight marker. Afterwards, DNA fragments of interest were cut out of the gel under an UV-lamp. Subsequently, the DNA was purified with the Zymoclean Gel DNA recovery kit (Zymo research) according to the manufacture's protocol.

6.3.5 Site-directed mutagenesis

Site-directed mutagenesis is a convenient form of PCR that is used, among others, to introduce point mutations into a given sequence. For this, the Q5 Site-directed mutagenesis kit (NEB) was utilized according to the manufacturer's protocol. Mutagenesis primers were designed with the free online tool "NEBaseChanger" (NEB) and the recommended annealing temperatures were used for the PCR protocol (Table 5).

Table 5: Cycling conditions for Q5 mutagenesis PCR

Step	Temperature [°C]	Time [s]
Initial denaturation	98	30
25 Cycles	98	10
	50 – 72	30
	72	30 per kb
Final extension	72	120
Hold	4	∞

6.3.6 Quantitative real-time PCR

To determine PDE6D and KRas mRNA level in CRC cell lines, RNA was isolated using a RNA extraction kit (Zymo Research) according to the manufacturer's protocol. In short, $1 \cdot 10^5$ cells were seeded into a 6-well plate and grown for one day. Growth medium was discarded and cells were lysed in 300 µl RNA lysis buffer and mixed 1:1 (v/v) with ethanol. RNA and DNA were concentrated in a Zymo-Spin™ IC column and DNA removed by DNase I treatment. After subsequent washing steps, RNA is eluted with RNase-free water. 2 µg of the isolated RNA of each cell lysate were used to perform RT-PCR according to the manufacturer's protocol (High Capacity cDNA Reverse Transcription Kit; Thermo Fisher Scientific), yielding 2 µg cDNA. In short, RNA was mixed with dNTPs and RT random Primers and MultiScribe™ Reverse Transcriptase was used to convert RNA to corresponding cDNA in a one-cycle reaction. For quantitative PCR, commercial available TaqMan®-assays (Thermo Fisher Scientific) for PDE6D (Hs01062025_m1), KRas (Hs00364282_m1) and GAPDH (Hs02758991_g1) were utilized according to the manufacturer's protocol. The qPCR was performed on a 20 µl scale in 96-well fast plate setup. ΔCT-values were calculated by subtracting the CT values of the used housekeeping gene GAPDH from either KRas CT or PDE6D CT values.

6.4 Biochemistry

6.4.1 Whole cell lysates

Cells were washed once with ice-cold 1x PBS and lysed using RIPA-buffer for 10 min on ice. Afterwards, lysates were scraped off the plate and thoroughly homogenized by a 26G syringe and subsequently centrifuged at 14,000g for 20 min at 4 ° C and the supernatant transferred to fresh tubes.

For PDEδ protein level analysis, whole cell lysates were prepared after 72 h of doxycycline induction.
For EGF-induced phospho-Erk response analysis in SW480 and HT29, cells were starved for 16 h prior to incubation for 90 min with 5 or 10 µM of Deltarasin or Deltasonamide 2, respectively. Afterwards, cells were stimulated with 100 ng/ml EGF for 5 min and subsequently washed with ice-cold PBS and lysed in 100 µl ice-cold RIPA buffer. Lysates were further processed as described above.

To enable equal protein loading for the following quantitative western blot analysis, protein concentration of each lysate was determined by BCA (bicinchoninic acid) assay utilizing BSA (bovine serum albumin) in a concentration range from 0.25 to 4 µg as standard. After protein concentration was determined, proteins were denatured in 5x SDS sample buffer for 10 min at 95 °C.

6.4.2 Raf-RBD pull-down

For enrichment of Ras-GTP, 3xRaf-RBD pull down was executed. Recombinant GST-3xRafRBD (Chandra et al. 2011) was expressed in E. Coli BL21DE3 by induction with 0.1 mM IPTG for 5 h after the culture reached an OD_{600} of 0.8. Afterwards, bacteria were harvested and lysed with bacterial lysis buffer and bacterial lysates were stored at – 20°C. For the pull down, 700 µg crude bacterial lysate was incubated with magnetic GSH sepharose 4B beads for 2 h at 4 °C on a rotating wheel. Afterwards, beads were washed three times with washing buffer and subsequently re-equilibrated in cell lysis buffer. Whole cell lysates were prepared after overnight starvation in cell

lysis buffer. Cells were therefore washed with ice-cold PBS and incubated on ice in cell lysis buffer for 10 min. Afterwards, cells were scraped off the plate and the lysates were thoroughly homogenized by a 26G syringe. 25 µg of WCL were used as “input control” to determine panRas, PDEδ and Cyclophilin B level, whereas 400 µg of WCL was subjected to GST-3xRaf-RBD, bound onto GSH sepharose 4B (GE) beads, pull down. After incubation for 30 min at 4 °C on a rotating wheel, beads were washed three times with cell lysis buffer. Then, bound Ras-GTP was eluted with 50 µl 2x SDS sample buffer for 10 min at 95 °C. Afterwards, SDS–polyacrylamide gel electrophoresis was carried out.

6.4.3 SDS polyacrylamide gel electrophorese

SDS polyacrylamide gel electrophoresis is performed to separate proteins of whole cell lysates by their molecular weight, here under denaturing conditions. Depending on the molecular weight of the proteins of interest, separating gels contained 12 – 15 % acrylamide, while the overlaid stacking gel always contained 4 % acrylamide. Equal amounts of protein were loaded on a gel in an electrophoresis chamber filled with SDS running buffer. Precision Plus Protein™ Dual Color was used as marker to determine molecular weights. Electrophoresis was performed at constant voltage of 130 V for 120 min.

6.4.4 Western blot

Gels were blotted onto polyvinylidene fluoride (PVDF) membrane (Immobilon, Millipore). For this, the PVDF membrane was activated in methanol for 1 min and placed onto the SDS-gel in transfer buffer. By applying a constant voltage of 40 V for one hour, the size-separated proteins were transferred through the electric field onto the PVDF membrane. Subsequently, the membrane is blocked for 1 h at room temperature with Odyssey blocking buffer. The following incubation with primary antibodies against the proteins of interest was carried out overnight at 4 °C on a shaker. Afterwards, blots were washed three times with TBS-T (0.1 % Tween-20 in 1x TBS) and incubated with secondary antibodies for 45 min at RT on a shaker and

subsequently washed three times with TBS-T. The used antibodies and corresponding dilutions are noted in 6.1.4. Blots were scanned on a LI-COR Odyssey imaging system. Western blots were quantified using the Gel profiler plugin of ImageJ.

6.5 Microscopy and data acquisition

6.5.1 Confocal laser scanning microscopy

Confocal images were acquired with a confocal laser-scanning microscope (FV1000, Olympus). For detection of mCitrine-Rheb and mCitrine-KRas, samples were excited using the 488 nm wavelength of an argon laser. Fluorescence signal was collected through an oil immersion objective (×60/1.35 UPlanSApo, Olympus) and spectrally filtered by a band pass filter from 500 nm to 550 nm. For excitation of mCherry-PDEδ, a 561 nm diode laser was used. The fluorescence emission was spectrally filtered by a band pass filter from 600 to 700 nm.

6.5.2 FLIM-FRET

Fluorescence lifetime images were acquired using a confocal laser-scanning microscope (FV1000, Olympus) equipped with a time-correlated single-photon counting module (LSM Upgrade Kit, Picoquant). For detection of the donor (mCitrine), the sample was excited using a 507-nm diode laser (Picoquant) at a 40-MHz repetition frequency. Fluorescence signal was collected through an oil immersion objective (×60/1.35 UPlanSApo, Olympus) and spectrally filtered using a narrow-band emission filter (HQ 530/11, Chroma). Photons were detected using a single-photon counting avalanche photodiode (PDM Series, MPD) and timed using a single-photon counting module (PicoHarp 300, Picoquant).

6.6 Data analysis

6.6.1 Cell segmentation

Cell segmentation was performed with an in-house developed software package programed in Python, called “Segmentor”. Confocal images of cells were used to generate whole cell masks as well as nuclear masks, which were loaded into Segmentor together with the fluorescence images. In Segmentor, the distance of each pixel to the center of the nucleus (NC) as well as to the closest part of the PM is calculated. To normalize the distance of each pixel within each cell, the normalized distance *d* is calculated (2):

$$d = \frac{\mathrm{dPM}}{\mathrm{dPM+dNC}} \quad (2)$$

Afterwards, all pixels are segmented into three concentric rings with equal radius, based on their normalized distance, and the mean fluorescence intensity of each segment is calculated (Konitsiotis et al. 2017). The outer segment depicted the mean intensity at the plasma membrane and the two inner segments were averaged to determine the mean intensity of the inner cell (cytosol). The mean intensity of plasma membrane and cytosol were normalized to the total mean intensity of each cell at each time point, yielding the fractions of protein of interest at the PM and in the cytosol, respectively.

6.6.2 Global analysis of FLIM data

Intensity thresholds were applied to segment the cells from the background fluorescence. Data were further analyzed via global analysis (Grecco et al. 2009) to obtain the molecular fraction α of interacting mCitrine-Rheb and mCherry-PDEδ molecules. During global analysis, the acquired time-domain FLIM data is Fourier-transformed into frequency domain data, whereby all higher harmonics information is lost. Thus, only the first harmonic, which contains the lifetime information, is used for analysis. The corresponding lifetimes of donor and donor-acceptor are calculated as a function of the demodulation and the phase-shift and can be represented as clouds on a half-circle. While the two lifetime values are global values (constant), the molecular fraction α differs in each pixel. The resulting α-maps were further

processed by multiplying them pixel-wise with the FLIM intensity image and dividing them by the average intensity to calculate intensity-weighted α values. The resulting α-maps were binned by a factor of two to reduce noise.

The dependence of the molecular interacting fraction α on the inhibitor concentration was determined through sequential addition of Deltasonamide 1 or Deltasonamide 2 followed by incubation periods of 10 min before FLIM data acquisition. Dose–response relationships were calculated by plotting obtained α per concentration of the respective compound, using the equation (Papke et al. 2016) (3):

$$\alpha = A_0 \cdot \frac{A \cdot [X]}{[X] + KD} \quad (3)$$

where A_0 is α in absence of the inhibitor, A an asymptotic offset and [X] is the concentration of inhibitor in the medium. A_0 was normalized to 0.2.

6.6.3 *In silico* analysis of PDE6D and KRas mRNA expression in CRC patient data

For the in silico analysis of available patient data, a dataset containing KRas and PDE6D mRNA expression data of 195 CRC patients, including mutation status of the KRas gene, was downloaded from The Cancer Genome Atlas (TCGA) (Cancer Genome Atlas 2012). Patient data was separated into wild type KRas (n=108) and mutant KRas (n=87) cases and compared with regard to differences in their mRNA expression levels of KRas and PDE6D. For correlation analysis KRas mRNA expression levels were plotted versus corresponding PDE6D mRNA expression levels and Pearson's correlation coefficient was determined.

6.6.4 Statistics

For samples that were normalized and compared to a control, significance was calculated using one sample Student's *t*-test. If the resulting *p*-values were smaller than 0.05, the sample was assumed to be significantly different to the control case.

For multiple sample comparison between each other, one-way ANOVA, utilizing Fischer's LSD for mean value comparison, was applied. Again, for *p*-values smaller than 0.05, the samples were assumed to be significantly different from each other.

To determine, if parameters in a given data set were correlated, Pearson's correlation analysis was applied, testing for a linear dependence between both parameters. Here, a high positive Pearson p value indicates a positive correlation of both parameters, while a negative *p* value implies an anti-correlation.

7. References

Abassi, Y. A., J. A. Jackson, J. Zhu, J. O'Connell, X. Wang and X. Xu (2004). "Label-free, real-time monitoring of IgE-mediated mast cell activation on microelectronic cell sensor arrays." J Immunol Methods **292**(1-2): 195-205.

Ahmed, D., P. W. Eide, I. A. Eilertsen, S. A. Danielsen, M. Eknaes, M. Hektoen, G. E. Lind and R. A. Lothe (2013). "Epigenetic and genetic features of 24 colon cancer cell lines." Oncogenesis **2**: e71.

Babij, C., Y. Zhang, R. J. Kurzeja, A. Munzli, A. Shehabeldin, M. Fernando, K. Quon, P. D. Kassner, A. A. Ruefli-Brasse, V. J. Watson, F. Fajardo, A. Jackson, J. Zondlo, Y. Sun, A. R. Ellison, C. A. Plewa, M. T. San, J. Robinson, J. McCarter, R. Schwandner, T. Judd, J. Carnahan and I. Dussault (2011). "STK33 kinase activity is nonessential in KRAS-dependent cancer cells." Cancer Res **71**(17): 5818-5826.

Baillie, T. A. (2016). "Targeted Covalent Inhibitors for Drug Design." Angew Chem Int Ed Engl **55**(43): 13408-13421.

Basso, A. D., P. Kirschmeier and W. R. Bishop (2006). "Lipid posttranslational modifications. Farnesyl transferase inhibitors." J Lipid Res **47**(1): 15-31.

Batzer, A. G., D. Rotin, J. M. Urena, E. Y. Skolnik and J. Schlessinger (1994). "Hierarchy of binding sites for Grb2 and Shc on the epidermal growth factor receptor." Mol Cell Biol **14**(8): 5192-5201.

Benvenuti, S., A. Sartore-Bianchi, F. Di Nicolantonio, C. Zanon, M. Moroni, S. Veronese, S. Siena and A. Bardelli (2007). "Oncogenic activation of the RAS/RAF signaling pathway impairs the response of metastatic colorectal cancers to anti-epidermal growth factor receptor antibody therapies." Cancer Res **67**(6): 2643-2648.

Bishop, W. R., R. Bond, J. Petrin, L. Wang, R. Patton, R. Doll, G. Njoroge, J. Catino, J. Schwartz, W. Windsor and et al. (1995). "Novel tricyclic inhibitors of farnesyl protein transferase. Biochemical characterization and inhibition of Ras modification in transfected Cos cells." J Biol Chem **270**(51): 30611-30618.

Bos, J. L., H. Rehmann and A. Wittinghofer (2007). "GEFs and GAPs: critical elements in the control of small G proteins." Cell **129**(5): 865-877.

Bowtell, D., P. Fu, M. Simon and P. Senior (1992). "Identification of murine homologues of the Drosophila son of sevenless gene: potential activators of ras." Proc Natl Acad Sci U S A **89**(14): 6511-6515.

Brattain, M. G., W. D. Fine, F. M. Khaled, J. Thompson and D. E. Brattain (1981). "Heterogeneity of malignant cells from a human colonic carcinoma." Cancer Res **41**(5): 1751-1756.

Canagarajah, B. J., A. Khokhlatchev, M. H. Cobb and E. J. Goldsmith (1997). "Activation mechanism of the MAP kinase ERK2 by dual phosphorylation." Cell **90**(5): 859-869.

Cancer Genome Atlas, N. (2012). "Comprehensive molecular characterization of human colon and rectal cancer." Nature **487**(7407): 330-337.

Capon, D. J., P. H. Seeburg, J. P. McGrath, J. S. Hayflick, U. Edman, A. D. Levinson and D. V. Goeddel (1983). "Activation of Ki-ras2 gene in human colon and lung carcinomas by two different point mutations." Nature **304**(5926): 507-513.

Carlini, D. B. and W. Stephan (2003). "In vivo introduction of unpreferred synonymous codons into the Drosophila Adh gene results in reduced levels of ADH protein." Genetics **163**(1): 239-243.

Chandra, A., H. E. Grecco, V. Pisupati, D. Perera, L. Cassidy, F. Skoulidis, S. A. Ismail, C. Hedberg, M. Hanzal-Bayer, A. R. Venkitaraman, A. Wittinghofer and P. I. Bastiaens (2011). "The GDI-like solubilizing factor PDEdelta sustains the spatial organization and signalling of Ras family proteins." Nat Cell Biol **14**(2): 148-158.

Cox, A. D., S. W. Fesik, A. C. Kimmelman, J. Luo and C. J. Der (2014). "Drugging the undruggable RAS: Mission possible?" Nat Rev Drug Discov **13**(11): 828-851.

Der, C. J., T. G. Krontiris and G. M. Cooper (1982). "Transforming genes of human bladder and lung carcinoma cell lines are homologous to the ras genes of Harvey and Kirsten sarcoma viruses." Proc Natl Acad Sci U S A **79**(11): 3637-3640.

Di Nicolantonio, F., M. Martini, F. Molinari, A. Sartore-Bianchi, S. Arena, P. Saletti, S. De Dosso, L. Mazzucchelli, M. Frattini, S. Siena and A. Bardelli (2008). "Wild-type BRAF is required for response to panitumumab or cetuximab in metastatic colorectal cancer." J Clin Oncol **26**(35): 5705-5712.

Dobrzynski, M., L. K. Nguyen, M. R. Birtwistle, A. von Kriegsheim, A. Blanco Fernandez, A. Cheong, W. Kolch and B. N. Kholodenko (2014). "Nonlinear signalling networks and cell-to-cell variability transform external signals into broadly distributed or bimodal responses." J R Soc Interface **11**(98): 20140383.

Dolf, G., R. E. Meyn, D. Curley, N. Prather, M. D. Story, B. M. Boman, M. J. Siciliano and R. R. Hewitt (1991). "Extrachromosomal amplification of the epidermal growth factor receptor gene in a human colon carcinoma cell line." Genes Chromosomes Cancer **3**(1): 48-54.

Elsasser, H. P., U. Lehr, B. Agricola and H. F. Kern (1993). "Structural analysis of a new highly metastatic cell line PaTu 8902 from a primary human pancreatic adenocarcinoma." Virchows Arch B Cell Pathol Incl Mol Pathol **64**(4): 201-207.

Fasterius, E., C. Raso, S. Kennedy, N. Rauch, P. Lundin, W. Kolch, M. Uhlen and C. Al-Khalili Szigyarto (2017). "A novel RNA sequencing data analysis method for cell line authentication." PLoS One **12**(2): e0171435.

Feig, C., A. Gopinathan, A. Neesse, D. S. Chan, N. Cook and D. A. Tuveson (2012). "The pancreas cancer microenvironment." Clin Cancer Res **18**(16): 4266-4276.

Fidler, I. J. and I. R. Hart (1982). "Biological diversity in metastatic neoplasms: origins and implications." Science **217**(4564): 998-1003.

Fodde, R. (2002). "The APC gene in colorectal cancer." Eur J Cancer **38**(7): 867-871.

Fogh, J. (1975). Human tumor cells in vitro. New York, Plenum Press.

Forbes, S. A., N. Bindal, S. Bamford, C. Cole, C. Y. Kok, D. Beare, M. Jia, R. Shepherd, K. Leung, A. Menzies, J. W. Teague, P. J. Campbell, M. R. Stratton and P. A. Futreal (2011). "COSMIC: mining complete cancer genomes in the Catalogue of Somatic Mutations in Cancer." Nucleic Acids Res **39**(Database issue): D945-950.

Gideon, P., J. John, M. Frech, A. Lautwein, R. Clark, J. E. Scheffler and A. Wittinghofer (1992). "Mutational and kinetic analyses of the GTPase-activating protein (GAP)-p21 interaction: the C-terminal domain of GAP is not sufficient for full activity." Mol Cell Biol **12**(5): 2050-2056.

Grecco, H. E., P. Roda-Navarro and P. J. Verveer (2009). "Global analysis of time correlated single photon counting FRET-FLIM data." Opt Express **17**(8): 6493-6508.

Gross, M. E., M. A. Zorbas, Y. J. Danels, R. Garcia, G. E. Gallick, M. Olive, M. G. Brattain, B. M. Boman and L. C. Yeoman (1991). "Cellular growth response to epidermal growth factor in colon carcinoma cells with an amplified epidermal growth

factor receptor derived from a familial adenomatous polyposis patient." Cancer Res **51**(5): 1452-1459.

Gunes, C. and K. L. Rudolph (2013). "The role of telomeres in stem cells and cancer." Cell **152**(3): 390-393.

Hanahan, D. and R. A. Weinberg (2011). "Hallmarks of cancer: the next generation." Cell **144**(5): 646-674.

Hancock, J. F., A. I. Magee, J. E. Childs and C. J. Marshall (1989). "All ras proteins are polyisoprenylated but only some are palmitoylated." Cell **57**(7): 1167-1177.

Hancock, J. F., H. Paterson and C. J. Marshall (1990). "A polybasic domain or palmitoylation is required in addition to the CAAX motif to localize p21ras to the plasma membrane." Cell **63**(1): 133-139.

Hanzal-Bayer, M., L. Renault, P. Roversi, A. Wittinghofer and R. C. Hillig (2002). "The complex of Arl2-GTP and PDE delta: from structure to function." EMBO J **21**(9): 2095-2106.

Heppner, G. H. (1984). "Tumor heterogeneity." Cancer Res **44**(6): 2259-2265.

Herzenberg, L. A., R. G. Sweet and L. A. Herzenberg (1976). "Fluorescence-activated cell sorting." Sci Am **234**(3): 108-117.

Hingorani, S. R., L. Wang, A. S. Multani, C. Combs, T. B. Deramaudt, R. H. Hruban, A. K. Rustgi, S. Chang and D. A. Tuveson (2005). "Trp53R172H and KrasG12D cooperate to promote chromosomal instability and widely metastatic pancreatic ductal adenocarcinoma in mice." Cancer Cell **7**(5): 469-483.

Humblet, Y. (2004). "Cetuximab: an IgG(1) monoclonal antibody for the treatment of epidermal growth factor receptor-expressing tumours." Expert Opin Pharmacother **5**(7): 1621-1633.

Ikemura, T. (1981). "Correlation between the abundance of Escherichia coli transfer RNAs and the occurrence of the respective codons in its protein genes: a proposal for a synonymous codon choice that is optimal for the E. coli translational system." J Mol Biol **151**(3): 389-409.

Ismail, S. A., Y. X. Chen, A. Rusinova, A. Chandra, M. Bierbaum, L. Gremer, G. Triola, H. Waldmann, P. I. Bastiaens and A. Wittinghofer (2011). "Arl2-GTP and Arl3-GTP regulate a GDI-like transport system for farnesylated cargo." Nat Chem Biol **7**(12): 942-949.

Iversen, L., H. L. Tu, W. C. Lin, S. M. Christensen, S. M. Abel, J. Iwig, H. J. Wu, J. Gureasko, C. Rhodes, R. S. Petit, S. D. Hansen, P. Thill, C. H. Yu, D. Stamou, A. K. Chakraborty, J. Kuriyan and J. T. Groves (2014). "Molecular kinetics. Ras activation by SOS: allosteric regulation by altered fluctuation dynamics." Science **345**(6192): 50-54.

Jackson, J. H., C. G. Cochrane, J. R. Bourne, P. A. Solski, J. E. Buss and C. J. Der (1990). "Farnesol modification of Kirsten-ras exon 4B protein is essential for transformation." Proc Natl Acad Sci U S A **87**(8): 3042-3046.

John, J., R. Sohmen, J. Feuerstein, R. Linke, A. Wittinghofer and R. S. Goody (1990). "Kinetics of interaction of nucleotides with nucleotide-free H-ras p21." Biochemistry **29**(25): 6058-6065.

Karnoub, A. E. and R. A. Weinberg (2008). "Ras oncogenes: split personalities." Nat Rev Mol Cell Biol **9**(7): 517-531.

Khokhlatchev, A. V., B. Canagarajah, J. Wilsbacher, M. Robinson, M. Atkinson, E. Goldsmith and M. H. Cobb (1998). "Phosphorylation of the MAP kinase ERK2 promotes its homodimerization and nuclear translocation." Cell **93**(4): 605-615.

Kholodenko, B. N., J. B. Hoek and H. V. Westerhoff (2000). "Why cytoplasmic signalling proteins should be recruited to cell membranes." Trends Cell Biol **10**(5): 173-178.

Konitsiotis, A. D., L. Rossmannek, A. Stanoev, M. Schmick and P. I. H. Bastiaens (2017). "Spatial cycles mediated by UNC119 solubilisation maintain Src family kinases plasma membrane localisation." Nat Commun **8**(1): 114.

Koseska, A. and P. I. Bastiaens (2017). "Cell signaling as a cognitive process." EMBO J **36**(5): 568-582.

Kumari, A., R. Singla, A. Guliani and S. K. Yadav (2014). "Nanoencapsulation for drug delivery." EXCLI J **13**: 265-286.

Kwon, Y. (2001). Handbook of essential pharmacokinetics, pharmacodynamics, and drug metabolism for industrial scientists. New York, Kluwer Academic/Plenum Publishers.

Lee, M. J., A. S. Ye, A. K. Gardino, A. M. Heijink, P. K. Sorger, G. MacBeath and M. B. Yaffe (2012). "Sequential application of anticancer drugs enhances cell death by rewiring apoptotic signaling networks." Cell **149**(4): 780-794.

Leibovitz, A., J. C. Stinson, W. B. McCombs, 3rd, C. E. McCoy, K. C. Mazur and N. D. Mabry (1976). "Classification of human colorectal adenocarcinoma cell lines." Cancer Res **36**(12): 4562-4569.

Lemmon, M. A. and J. Schlessinger (2010). "Cell signaling by receptor tyrosine kinases." Cell **141**(7): 1117-1134.

Lieber, M., J. Mazzetta, W. Nelson-Rees, M. Kaplan and G. Todaro (1975). "Establishment of a continuous tumor-cell line (panc-1) from a human carcinoma of the exocrine pancreas." Int J Cancer **15**(5): 741-747.

Lin, D. T. S., N. G. Davis and E. Conibear (2017). "Targeting the Ras palmitoylation/depalmitoylation cycle in cancer." Biochem Soc Trans **45**(4): 913-921.

Lorentzen, A., A. Kinkhabwala, O. Rocks, N. Vartak and P. I. Bastiaens (2010). "Regulation of Ras localization by acylation enables a mode of intracellular signal propagation." Sci Signal **3**(140): ra68.

Luo, J., M. J. Emanuele, D. Li, C. J. Creighton, M. R. Schlabach, T. F. Westbrook, K. K. Wong and S. J. Elledge (2009). "A genome-wide RNAi screen identifies multiple synthetic lethal interactions with the Ras oncogene." Cell **137**(5): 835-848.

Marais, R., Y. Light, H. F. Paterson and C. J. Marshall (1995). "Ras recruits Raf-1 to the plasma membrane for activation by tyrosine phosphorylation." EMBO J **14**(13): 3136-3145.

Martin-Gago, P., E. K. Fansa, C. H. Klein, S. Murarka, P. Janning, M. Schurmann, M. Metz, S. Ismail, C. Schultz-Fademrecht, M. Baumann, P. I. Bastiaens, A. Wittinghofer and H. Waldmann (2017). "A PDE6delta-KRas Inhibitor Chemotype with up to Seven H-Bonds and Picomolar Affinity that Prevents Efficient Inhibitor Release by Arl2." Angew Chem Int Ed Engl **56**(9): 2423-2428.

Martin-Gago, P., E. K. Fansa, M. Winzker, S. Murarka, P. Janning, C. Schultz-Fademrecht, M. Baumann, A. Wittinghofer and H. Waldmann (2017). "Covalent Protein Labeling at Glutamic Acids." Cell Chem Biol **24**(5): 589-597 e585.

Mendoza, M. C., E. E. Er and J. Blenis (2011). "The Ras-ERK and PI3K-mTOR pathways: cross-talk and compensation." Trends Biochem Sci **36**(6): 320-328.

Misale, S., R. Yaeger, S. Hobor, E. Scala, M. Janakiraman, D. Liska, E. Valtorta, R. Schiavo, M. Buscarino, G. Siravegna, K. Bencardino, A. Cercek, C. T. Chen, S. Veronese, C. Zanon, A. Sartore-Bianchi, M. Gambacorta, M. Gallicchio, E. Vakiani, V. Boscaro, E. Medico, M. Weiser, S. Siena, F. Di Nicolantonio, D. Solit and A. Bardelli (2012). "Emergence of KRAS mutations and acquired resistance to anti-EGFR therapy in colorectal cancer." Nature **486**(7404): 532-536.

Moodie, S. A., B. M. Willumsen, M. J. Weber and A. Wolfman (1993). "Complexes of Ras.GTP with Raf-1 and mitogen-activated protein kinase kinase." Science **260**(5114): 1658-1661.

Moroni, M., S. Veronese, S. Benvenuti, G. Marrapese, A. Sartore-Bianchi, F. Di Nicolantonio, M. Gambacorta, S. Siena and A. Bardelli (2005). "Gene copy number for epidermal growth factor receptor (EGFR) and clinical response to antiEGFR treatment in colorectal cancer: a cohort study." Lancet Oncol **6**(5): 279-286.

Morton, J. P., P. Timpson, S. A. Karim, R. A. Ridgway, D. Athineos, B. Doyle, N. B. Jamieson, K. A. Oien, A. M. Lowy, V. G. Brunton, M. C. Frame, T. R. Evans and O. J. Sansom (2010). "Mutant p53 drives metastasis and overcomes growth arrest/senescence in pancreatic cancer." Proc Natl Acad Sci U S A **107**(1): 246-251.

Mullis, K., F. Faloona, S. Scharf, R. Saiki, G. Horn and H. Erlich (1986). "Specific enzymatic amplification of DNA in vitro: the polymerase chain reaction." Cold Spring Harb Symp Quant Biol **51 Pt 1**: 263-273.

Nancy, V., I. Callebaut, A. El Marjou and J. de Gunzburg (2002). "The delta subunit of retinal rod cGMP phosphodiesterase regulates the membrane association of Ras and Rap GTPases." J Biol Chem **277**(17): 15076-15084.

Olive, K. P., D. A. Tuveson, Z. C. Ruhe, B. Yin, N. A. Willis, R. T. Bronson, D. Crowley and T. Jacks (2004). "Mutant p53 gain of function in two mouse models of Li-Fraumeni syndrome." Cell **119**(6): 847-860.

Olive, M., S. Untawale, R. J. Coffey, M. J. Siciliano, D. M. Wildrick, H. Fritsche, S. Pathak, L. M. Cherry, M. Blick, P. Lointier and et al. (1993). "Characterization of the DiFi rectal carcinoma cell line derived from a familial adenomatous polyposis patient." In Vitro Cell Dev Biol **29A**(3 Pt 1): 239-248.

Papke, B. and C. J. Der (2017). "Drugging RAS: Know the enemy." Science **355**(6330): 1158-1163.

Papke, B., S. Murarka, H. A. Vogel, P. Martin-Gago, M. Kovacevic, D. C. Truxius, E. K. Fansa, S. Ismail, G. Zimmermann, K. Heinelt, C. Schultz-Fademrecht, A. Al Saabi, M. Baumann, P. Nussbaumer, A. Wittinghofer, H. Waldmann and P. I. Bastiaens (2016). "Identification of pyrazolopyridazinones as PDEdelta inhibitors." Nat Commun **7**: 11360.

Parada, L. F., C. J. Tabin, C. Shih and R. A. Weinberg (1982). "Human EJ bladder carcinoma oncogene is homologue of Harvey sarcoma virus ras gene." Nature **297**(5866): 474-478.

Prior, I. A., P. D. Lewis and C. Mattos (2012). "A comprehensive survey of Ras mutations in cancer." Cancer Res **72**(10): 2457-2467.

Puck, T. T. and P. I. Marcus (1956). "Action of x-rays on mammalian cells." J Exp Med **103**(5): 653-666.

Rafehi, H., C. Orlowski, G. T. Georgiadis, K. Ververis, A. El-Osta and T. C. Karagiannis (2011). "Clonogenic assay: adherent cells." J Vis Exp(49).

Rocks, O., A. Peyker, M. Kahms, P. J. Verveer, C. Koerner, M. Lumbierres, J. Kuhlmann, H. Waldmann, A. Wittinghofer and P. I. Bastiaens (2005). "An acylation cycle regulates localization and activity of palmitoylated Ras isoforms." Science **307**(5716): 1746-1752.

Rozenblum, E., M. Schutte, M. Goggins, S. A. Hahn, S. Panzer, M. Zahurak, S. N. Goodman, T. A. Sohn, R. H. Hruban, C. J. Yeo and S. E. Kern (1997). "Tumor-suppressive pathways in pancreatic carcinoma." Cancer Res **57**(9): 1731-1734.

S Shirasawa, M. F., N Yokoyama, T Sasazuki (1993). "Altered growth of human colon cancer cell lines disrupted at activated Ki-ras." Science **260**(5104): 85-88.

Sato, T., D. E. Stange, M. Ferrante, R. G. Vries, J. H. Van Es, S. Van den Brink, W. J. Van Houdt, A. Pronk, J. Van Gorp, P. D. Siersema and H. Clevers (2011). "Long-term expansion of epithelial organoids from human colon, adenoma, adenocarcinoma, and Barrett's epithelium." Gastroenterology **141**(5): 1762-1772.

Sato, T., R. G. Vries, H. J. Snippert, M. van de Wetering, N. Barker, D. E. Stange, J. H. van Es, A. Abo, P. Kujala, P. J. Peters and H. Clevers (2009). "Single Lgr5 stem cells build crypt-villus structures in vitro without a mesenchymal niche." Nature **459**(7244): 262-265.

Schmick, M., A. Kraemer and P. I. Bastiaens (2015). "Ras moves to stay in place." Trends Cell Biol **25**(4): 190-197.

Schmick, M., N. Vartak, B. Papke, M. Kovacevic, D. C. Truxius, L. Rossmannek and P. I. H. Bastiaens (2014). "KRas localizes to the plasma membrane by spatial cycles of solubilization, trapping and vesicular transport." Cell **157**(2): 459-471.

Seger, R. and E. G. Krebs (1995). "The MAPK signaling cascade." FASEB J **9**(9): 726-735.

Shaner, N. C., R. E. Campbell, P. A. Steinbach, B. N. Giepmans, A. E. Palmer and R. Y. Tsien (2004). "Improved monomeric red, orange and yellow fluorescent proteins derived from Discosoma sp. red fluorescent protein." Nat Biotechnol **22**(12): 1567-1572.

Sharma, S. V. and J. Settleman (2007). "Oncogene addiction: setting the stage for molecularly targeted cancer therapy." Genes Dev **21**(24): 3214-3231.

Singh, A., P. Greninger, D. Rhodes, L. Koopman, S. Violette, N. Bardeesy and J. Settleman (2009). "A gene expression signature associated with "K-Ras addiction" reveals regulators of EMT and tumor cell survival." Cancer Cell **15**(6): 489-500.

Singh, A., M. F. Sweeney, M. Yu, A. Burger, P. Greninger, C. Benes, D. A. Haber and J. Settleman (2012). "TAK1 inhibition promotes apoptosis in KRAS-dependent colon cancers." Cell **148**(4): 639-650.

Singh, M. N., K. S. Hemant, M. Ram and H. G. Shivakumar (2010). "Microencapsulation: A promising technique for controlled drug delivery." Res Pharm Sci **5**(2): 65-77.

Sorensen, M. A., C. G. Kurland and S. Pedersen (1989). "Codon usage determines translation rate in Escherichia coli." J Mol Biol **207**(2): 365-377.

Stylianopoulos, T., L. L. Munn and R. K. Jain (2018). "Reengineering the Physical Microenvironment of Tumors to Improve Drug Delivery and Efficacy: From Mathematical Modeling to Bench to Bedside." Trends Cancer **4**(4): 292-319.

Tan, M. H., N. J. Nowak, R. Loor, H. Ochi, A. A. Sandberg, C. Lopez, J. W. Pickren, R. Berjian, H. O. Douglass, Jr. and T. M. Chu (1986). "Characterization of a new primary human pancreatic tumor line." Cancer Invest **4**(1): 15-23.

Traut, T. W. (1994). "Physiological concentrations of purines and pyrimidines." Mol Cell Biochem **140**(1): 1-22.

van der Geer, P., S. Wiley, G. D. Gish and T. Pawson (1996). "The Shc adaptor protein is highly phosphorylated at conserved, twin tyrosine residues (Y239/240) that mediate protein-protein interactions." Curr Biol **6**(11): 1435-1444.

Vetter, I. R. and A. Wittinghofer (2001). "The guanine nucleotide-binding switch in three dimensions." Science **294**(5545): 1299-1304.

Vigil, D., J. Cherfils, K. L. Rossman and C. J. Der (2010). "Ras superfamily GEFs and GAPs: validated and tractable targets for cancer therapy?" Nat Rev Cancer **10**(12): 842-857.

Weinberg, R. A. (1994). "Oncogenes and tumor suppressor genes." CA Cancer J Clin **44**(3): 160-170.

Weinstein, I. B. and A. Joe (2008). "Oncogene addiction." Cancer Res **68**(9): 3077-3080; discussion 3080.

Weinstein, I. B. and A. K. Joe (2006). "Mechanisms of disease: Oncogene addiction--a rationale for molecular targeting in cancer therapy." Nat Clin Pract Oncol **3**(8): 448-457.

Welch, J. S., T. J. Ley, D. C. Link, C. A. Miller, D. E. Larson, D. C. Koboldt, L. D. Wartman, T. L. Lamprecht, F. Liu, J. Xia, C. Kandoth, R. S. Fulton, M. D. McLellan, D. J. Dooling, J. W. Wallis, K. Chen, C. C. Harris, H. K. Schmidt, J. M. Kalicki-Veizer, C. Lu, Q. Zhang, L. Lin, M. D. O'Laughlin, J. F. McMichael, K. D. Delehaunty, L. A. Fulton, V. J. Magrini, S. D. McGrath, R. T. Demeter, T. L. Vickery, J. Hundal, L. L. Cook, G. W. Swift, J. P. Reed, P. A. Alldredge, T. N. Wylie, J. R. Walker, M. A. Watson, S. E. Heath, W. D. Shannon, N. Varghese, R. Nagarajan, J. E. Payton, J. D.

Baty, S. Kulkarni, J. M. Klco, M. H. Tomasson, P. Westervelt, M. J. Walter, T. A. Graubert, J. F. DiPersio, L. Ding, E. R. Mardis and R. K. Wilson (2012). "The origin and evolution of mutations in acute myeloid leukemia." Cell **150**(2): 264-278.

Wennerberg, K., K. L. Rossman and C. J. Der (2005). "The Ras superfamily at a glance." J Cell Sci **118**(Pt 5): 843-846.

Whyte, D. B., P. Kirschmeier, T. N. Hockenberry, I. Nunez-Oliva, L. James, J. J. Catino, W. R. Bishop and J. K. Pai (1997). "K- and N-Ras are geranylgeranylated in cells treated with farnesyl protein transferase inhibitors." J Biol Chem **272**(22): 14459-14464.

Wilson, M. H., C. J. Coates and A. L. George, Jr. (2007). "PiggyBac transposon-mediated gene transfer in human cells." Mol Ther **15**(1): 139-145.

Wittinghofer, F. (1998). "Ras signalling. Caught in the act of the switch-on." Nature **394**(6691): 317, 319-320.

Wright, L. P. and M. R. Philips (2006). "Thematic review series: lipid posttranslational modifications. CAAX modification and membrane targeting of Ras." J Lipid Res **47**(5): 883-891.

Yarden, Y. and J. Schlessinger (1987). "Self-phosphorylation of epidermal growth factor receptor: evidence for a model of intermolecular allosteric activation." Biochemistry **26**(5): 1434-1442.

Yoon, S. and R. Seger (2006). "The extracellular signal-regulated kinase: multiple substrates regulate diverse cellular functions." Growth Factors **24**(1): 21-44.
Yunis, A. A., G. K. Arimura and D. J. Russin (1977). "Human pancreatic carcinoma (MIA PaCa-2) in continuous culture: sensitivity to asparaginase." Int J Cancer **19**(1): 128-135.

Zeeberg, K., R. A. Cardone, M. R. Greco, M. Saccomano, A. Nohr-Nielsen, F. Alves, S. F. Pedersen and S. J. Reshkin (2016). "Assessment of different 3D culture systems to study tumor phenotype and chemosensitivity in pancreatic ductal adenocarcinoma." Int J Oncol **49**(1): 243-252.

Zembruski, N. C., V. Stache, W. E. Haefeli and J. Weiss (2012). "7-Aminoactinomycin D for apoptosis staining in flow cytometry." Anal Biochem **429**(1): 79-81.

Zhao, S., E. Jiang, S. Chen, Y. Gu, A. J. Shangguan, T. Lv, L. Luo and Z. Yu (2016). "PiggyBac transposon vectors: the tools of the human gene encoding." Transl Lung Cancer Res **5**(1): 120-125.

Zimmermann, G., B. Papke, S. Ismail, N. Vartak, A. Chandra, M. Hoffmann, S. A. Hahn, G. Triola, A. Wittinghofer, P. I. Bastiaens and H. Waldmann (2013). "Small molecule inhibition of the KRAS-PDEdelta interaction impairs oncogenic KRAS signalling." Nature **497**(7451): 638-642.

8. Publications

Results and methods presented in this thesis have contributed to the following publications:

Martin-Gago, P.*, Fansa, E. K.*, Klein, C. H.*, Murarka, S.*, Janning, P., Schurmann, M., Metz, M., Ismail, S., Schultz-Fademrecht, C., Baumann, M., Bastiaens, P. I., Wittinghofer, A. and Waldmann, H. (2017). "A PDE6delta-KRas Inhibitor Chemotype with up to Seven H-Bonds and Picomolar Affinity that Prevents Efficient Inhibitor Release by Arl2." Angew Chem Int Ed Engl **56**(9): 2423-2428. doi:10.1002/anie.201610957

Koos, B., Christmann, J., Plettenberg, S., Käding, D., Becker, J., Keteku, M., Klein, C. H., Imtiaz, S., Janning, P., Bastiaens, P. I. and Wehner, F. (2018), Hypertonicity-induced cation channels in HepG2 cells: architecture and role in proliferation vs. apoptosis. J Physiol, 596: 1227-1241. doi:10.1113/JP275827

Klein, C. H., Truxius, D. C., Vogel, H. A., Harizanova, J., Murarka, S., Martín-Gago, P. and Bastiaens, P. I. (2018), PDEδ inhibition impedes the proliferation and survival of human colorectal cancer cell lines harboring oncogenic KRas. Int. J. Cancer. (In press). doi:10.1002/ijc.31859

Kovacevic, M.*, Klein, C. H.*, Rossmannek, L., Konitsiotis, A.D., Stanoev, A., Kraemer, A.U. and Bastiaens, P. I., A spatially regulated GTPase cycle of Rheb controls growth factor signaling to mTORC1 (under consideration). bioRxiv 472241; doi: https://doi.org/10.1101/472241

Garivet, G.*, Hofer, W.*, Konitsiotis, A. D.*, Klein, C. H.*, Kaiser, N., Mejuch, T., Fansa, E. K., Wittinghofer, A., Bastiaens, P. I. and Waldmann, H., Small molecule inhibition of the UNC-Src interaction impairs dynamic Src localization in cells (in review).

* = Contributed equally

9. Acknowledgement

First of all, I want to thank Prof. Dr. Philippe Bastiaens for his mentoring and guidance through a fascinating project, for his inspiring vision of science and for pushing me out of my comfort zone, thereby helping me to evolve.

Second, I want to thank PD. Dr. Leif Dehmelt for being my second examiner as well as for all his valuable input as member of my thesis advisory committee.

I want to thank Dr. Astrid Krämer and Tanja Forck for all their help, especially with administrative work.

I further want to thank our technicians and engineers for all their help in the lab and/ or with equipment. Thank you: Lisa, Micha, Hendrike, Jutta, Kirsten, Manu, Sven and Michael.

I want to thank all current and former members of department II for all their help, scientific discussions and most importantly for providing a nice and stimulating working atmosphere.

Außerdem möchte ich meiner Familie danken, allen voran meinen Eltern: Danke für eure anhaltende Unterstützung in sämtlichen Lebensbereichen und dafür, dass ihr immer an mich geglaubt habt!

Abschließend gilt mein Dank meiner Frau Mandy: Danke, dass du in den letzten neun Jahren immer an meiner Seite warst. Egal, wie schwierig/turbulent manche Abschnitte auch waren, konnte ich mich stets auf deine Unterstützung verlassen!